THE UNIVERSITY
OF MICHIGAN
OCT 21 1959
ENGINEERING
LIBRARY

The Canadian Journal of Chemical Engineering

formerly

CANADIAN JOURNAL OF TECHNOLOGY

CONTENTS

Fundamental Aspects of Solids-Gas Flow. Part II: The Sphere Wake in Steady Laminar Fluids	*L. B. Torobin* *W. H. Gauvin*	**167**
Development of Design Criteria for Biological Treatment of an Industrial Effluent Containing 2,4-D Waste Water	*R. E. Mills*	**177**
An Analysis of Air and Solid Flow in a Spouted Wheat Bed	*B. Thorley* *J. B. Saunby* *K. B. Mathur* *G. L. Osberg*	**184**
Heats of Mixing and Vapor-Liquid Equilibrium Calculations	*Benjamin C.-Y. Lu*	**193**
Removal of a Mist in a Fluidized Bed	*D. S. Scott* *D. A. Guthrie*	**200**
Note on Fluidization in Beds of Rice and Wheat	*Liang-Tseng Fan* *Charles J. Schwartz*	**204**

OPPORTUNITY FOR INQUIRING MINDS

Each year C-I-L provides fellowships for promising young scientists doing post-graduate research at Canadian universities. Through this program, now in its eighteenth year, over 200 students have had the opportunity to carry out original work under university direction thus adding to their own, and Canada's, store of scientific knowledge.

Grants to endow chairs of science and to expand facilities further support the development of inquiring minds. C-I-L's own activities, so dependent on constant development and research, also provide scope and a congenial atmosphere for many trained talents, working together in the ever-new world of chemistry.

SOME OF THE RESEARCH PROJECTS CARRIED ON BY HOLDERS OF C-I-L FELLOWSHIPS:

isotopes produced in nuclear fission • chemistry of wood carbohydrates • wood pulping with liquid ammonia • soil fertility • electrically activated oxygen • gas engineering • nitrogen derivatives of steroids • the use of gaseous ammonia as a plant nutrient • mechanisms of organic reactions using radioactive carbon • spectral analysis of molecules • reactions of active nitrogen • waterfowl habits.

CANADIAN INDUSTRIES LIMITED

Serving Canadians Through Chemistry

C-I-L

AGRICULTURAL CHEMICALS • AMMUNITION • COATED FABRICS • INDUSTRIAL CHEMICALS • COMMERCIAL EXPLOSIVES • PAINTS • PLASTICS • TEXTILE FIBRES

The Canadian Journal of Chemical Engineering

formerly

Canadian Journal of Technology

VOLUME 37 OCTOBER, 1959 NUMBER 5

Editor
A. Cholette
Faculty of Science, Laval University
Quebec, Que.

Managing Editor
T. H. G. Michael

Publishing Editor
D. W. Emmerson

Assistant Publishing Editors
R. G. Watson
R. N. Callaghan

Circulation Manager
M. M. Lockey

EDITORIAL BOARD

Chairman
W. M. CAMPBELL, Atomic Energy of Canada Limited,
Chalk River, Ont.

L. D. DOUGAN, Polymer Corp. Limited,
Sarnia, Ont.

W. H. GAUVIN, McGill University,
Montreal, Que.

G. W. GOVIER, University of Alberta,
Edmonton, Alta.

J. W. HODGINS, McMaster University,
Hamilton, Ont.

A. I. JOHNSON, University of Toronto,
Toronto, Ont.

E. B. LUSBY, Imperial Oil Limited,
Toronto, Ont.

LEO MARION, National Research Council,
Ottawa, Ont.

R. R. McLAUGHLIN, University of Toronto,
Toronto, Ont.

G. L. OSBERG, National Research Council,
Ottawa, Ont.

J. H. SHIPLEY, Canadian Industries Limited,
Montreal, Que.

H. R. L. STREIGHT, Du Pont of Canada Limited,
Montreal, Que.

EX-OFFICIO

E. GORDON YOUNG, President, The Chemical Institute of Canada.

H. BORDEN MARSHALL, Chairman of the Board of Directors.

H. S. SUTHERLAND, Director of Publications.

Authorized as second class mail, Post Office Department, Ottawa. Printed in Canada

Manuscripts for publication should be submitted to the Editor: Dr. A. Cholette, Faculty of Science, Laval University, Boulevard de l'Entente, Quebec, Que. (Instructions to authors are on the next page).

Editorial, Production and Circulation Offices: 18 Rideau Street, Ottawa 2, Ont.

Advertising Office: C. N. McCuaig, manager of advertising sales, *The Canadian Journal of Chemical Engineering*, Room 601, 217 Bay Street, Toronto, Ont. Telephone—EMpire 3-3871.

Plates and Advertising Copy: Send to *The Canadian Journal of Chemical Engineering*, 18 Rideau Street, Ottawa 2, Ont.

Subscription Rates: In Canada—$3.00 per year and 75c per single copy; U.S. and U.K.—$4.00; Foreign—$4.50.

Change of Address: Advise Circulation Department in advance of change of address, providing old as well as new address. Enclose address label if possible.

The Canadian Journal of Chemical Engineering is published by The Chemical Institute of Canada every two months.

Unless it is specifically stated to the contrary, the Institute assumes no responsibility for the statements and opinions expressed in *The Canadian Journal of Chemical Engineering*. Views expressed in the editorials do not necessarily represent the official position of the Institute.

The Canadian Journal of Chemical Engineering

INSTRUCTIONS TO AUTHORS

Manuscript Requirements for Articles

1. The manuscript should be in English or French.
2. The original and two copies of the manuscript should be supplied. These are to be on 8½ x 11 inch sheets, typewritten, and double spaced. Each page should be numbered.
3. Symbols should conform to American Standards Association. An abridged set of acceptable symbols is found in the third edition of Perry's Chemical Engineers' Handbook. Greek letters and subscripts and superscripts should be carefully made.
4. Abstracts of not more than 200 words in English indicating the scope of the work and the principal findings should accompany all technical papers.
5. References should be listed in the order in which they occur in the paper, after the text, using the form shown here: "Othmer, D. F., Jacobs, Jr., J. J., and Levy, J. F., Ind. Eng. Chem. **34**, 286 (1942). Abbreviations of journal names should conform to the "List of Periodicals Abstracted by Chemical Abstracts". Abbreviations of the common journals are to be found in Perry's Handbook also. All references should be carefully checked with the original article.
6. Tables should be numbered in Arabic numerals. They should have brief descriptive titles and should be appended to the paper. Column headings should be brief. Tables should contain a minimum of descriptive material.
7. All figures should be numbered from 1 up, in Arabic numerals. Drawings should be carefully made with India ink on white drawing paper or tracing linen. All lines should be of sufficient thickness to reproduce well, especially if the figure is to be reduced. Letters and numerals should be carefully and neatly made, with a stencil. Generally speaking, originals should not be more than twice the size of the desired reproduction; final engravings being 3¼ in. or 7 in. wide depending on whether one column or two is used.
8. Photographs should be made on glossy paper with strong contrasts. Photographs or groups of photographs should not be larger than three times the size of the desired reproduction.
9. All tables and figures should be referred to in the text.

Submission of Manuscripts

1. The three copies of the manuscript, including figures and tables, should be sent directly to:
   DR. A. CHOLETTE, editor,
   The Canadian Journal of Chemical Engineering,
   Faculty of Science, Laval University,
   Boulevard de l'Entente,
   Quebec, Que.
2. The authors addresses and titles should be submitted with the manuscript.
3. The author may suggest names of reviewers for his article, but the selection of the reviewers will be the responsibility of the editor. Each paper or article is to be reviewed by two chemical engineers familiar with the topic. Reviewers will remain anonymous.
4. All correspondence regarding reviews should be directed to the editor.

Reprints

1. At least 50 free "tear sheets" of each paper will be supplied.
2. Additional reprints may be purchased at cost. An estimated cost of reprints, with an attached order form, will be sent to the author with the galley proofs.
3. Orders for reprints must be made before the paper has appeared in the Journal.

Communications, Letters and Notes to the Editor

Short papers, as described below, will be considered for publication in this Journal. Their total length should not exceed 600 words, or its equivalent.

Communications

A communication is a prompt preliminary report of observations made which are judged to be sufficiently important to warrant expedited publication. It usually calls for a more expanded paper in which the original matter is republished with more details.

Letters

A letter consists of comments or remarks submitted by readers or authors in connection with previously published material. It may deal with various forms of discussion arising out of a publication or it may simply report and correct inadvertent errors.

Notes

A note is a short paper which describes a piece of work not sufficiently important or complete to make it worth a full article. It may refer to a study or piece of research which, while it is not finished and may not be finished, offers interesting aspects or facts. As in the case of an article a note is a final publication.

* * *

Fundamental Aspects of Solids-Gas Flow

Part II. The Sphere Wake in Steady Laminar Fluids[1]

L. B. TOROBIN[2] *and W. H. GAUVIN*[2]

A review is made of the experimental evidence and theoretical considerations evolving from studies of the wake formed by an aerodynamically-smooth sphere moving in steady rectilinear motion through a turbulence-free stream. The roles of complex fluid dynamic phenomena which include boundary layer separation, vorticity transfer and those characterized by the Strouhal Number, as well as less evident fine scale processes are presented, with reference being made to pertinent two-dimensional cylinder studies.

CURRENT studies of the various aspects of solids-gas flow are characterized by a growing attention to the fundamental approach—a trend which is in many respects typical of the changes which are occurring on a broader front in all phases of chemical engineering. One by one, older concepts of the science are being re-examined in the light of the recent experimental evidence. Undeniably useful as these concepts have been in the past some of them obviously require complete reappraisal, as they no longer appear to account adequately for the increasing complexities of modern technology. Similarly, the continued usefulness of friction factors, mass transfer coefficients and countless other semi-empirical proportionalities may in many cases be questioned, since they certainly fail to provide a proper appreciation of the underlying mechanisms. In extreme cases, particularly when coincident with ill use of the methods of dimensional analysis, such an approach has been known to result in serious misconceptions.

Increasing use of the principles of fluid mechanics in the interpretation of chemical engineering operations is doing much to improve the understanding of the basic phenomena. The necessity of introducing large numbers of simplifying assumptions for the solution of complex problems is being minimized by the wide-spread availability of computing devices, while new mathematical methods of approximation provide at least tentative solutions to even the most intractable of non-linear differential equations. Finally, better instrumentation and the development of powerful experimental methods are contributing greatly to the refinement of the physical measurements.

Nowhere are the beneficial effects of these various improvements felt more strongly than in the field of solids-gas flow. There remains, however, the necessity of re-assessing the old experimental evidence in the light of the recent findings. The function of this series of articles is to present a critical analysis of the more significant studies concerned with the various individual phenomena which, in total, constitute the multiparticle solids-gas system. Starting with idealized single-particle behavior, each additional complexity will be considered in turn, laying the groundwork for a subsequent discussion of the complete problem. In Part I [1], introductory concepts of fluid mechanics were reviewed and the aerodynamics of a single smooth sphere moving in a very slow steady motion in an infinite, turbulence-free stream were described. As the particle velocity relative to the fluid is increased, the momentum transfer becomes dependent on the very complex phenomena in the region of wake, and these are discussed in the present article.

IV. PROPERTIES OF THE WAKE

Sphere Wake Configuration and Shedding Frequency

The observation of the wake of a sphere is fraught with difficulty, and very often phenomena seemingly clearly established by one observer will be contradicted by an equally legitimate work. It is only too easy to misinterpret even the stereoscopic photographs of this region, and the results appear to be susceptible to such factors as the geometry of the equipment and the turbulence of the stream.

An illustration of the conflicting evidence is afforded by the reports of the first appearance of the vortex ring which ushers in the wake regime, and which probably comes into being in the sphere boundary layer at the rear stagnation point—i.e. the most downstream point of the body—in the vicinity of a Reynolds Number of ten. Careful observations of this region convinced Williams [2] that this did not occur even at a Reynolds Number of 720, but Nisi and Porter [3] clearly showed this to occur at Re = 8.14 by photographing the smoke-filled flow of air about

[1]*Manuscript received July 23, 1959.*
[2]*McGill University and Pulp and Paper Research Institute of Canada, Montreal, Que.*

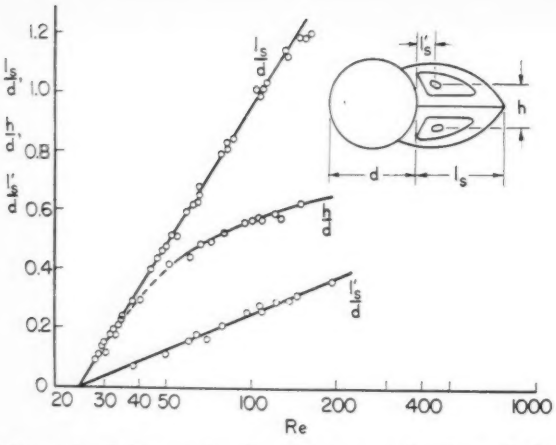

Figure 1—Sphere wake dimensions as a function of the Reynolds Number (Taneda).

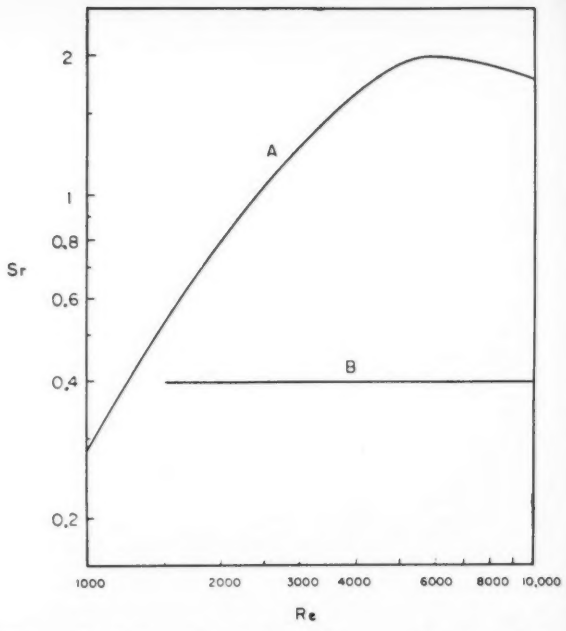

Figure 2—Sphere Strouhal numbers as a function of the Reynolds Number (Möller).

a supported sphere illuminated with a powerful plane beam of light. A similar but possibly more refined technique adapted to a water system was recently employed by Taneda [4] which showed the initial wake formation to occur at Re = 24. Great care was taken to eliminate the possible effect of the wall, and Taneda felt that the sphere support rod, which can never be done away with in studies of this type, exerted only a minor influence on the wake properties. The excellence of the photographs obtained allows confident measurement of the dimensions of the wake and its development for the region $5 < Re < 300$. and the results, which are important for multiparticle studies, are given in Figure 1. They could not be compared with the measurements of Nisi and Porter, since the latter have failed to mention the sphere size corresponding to the plots of eddy position which they had given.

As the Reynolds Number increases, the fixed ring vortex grows in size and decreases in stability and at a Reynolds value of about 130 its downstream portion begins to oscillate. The oscillations become more severe until at a Reynolds value referred to as the lower critical Reynolds Number it detaches from the fluid system adhering to the body of the sphere and streams away at a velocity which is less than the fluid relative velocity.

Some feel that this occurs at a Reynolds Number of 200 [5] and others at 1000 [6], but it more likely first occurs at a value of approximately 500 for a smooth sphere moving in a steady motion through a turbulence-free and essentially infinite fluid. A new ring forms as the unstable one detaches, so that there is a periodicity injected into the wake flow in this Reynolds Number region [7]. Lunnon [8] remarks that there should be periodic increases and decreases in the drag coefficient corresponding to the alternate growth and slipping away of the rings, thus explaining the fluctuating fall velocities of a sphere noted by Schmidt [7] and Liebster [9].

There is no unanimity as to the fate of the ring following detachment, but it probably changes as the flow is increased. Schmiedel [10] observed that periodic shedding of vortex rings existed only within the Reynolds Number range of 500 to 1000, and Winny [11] recorded photographically the formation of intertwining helical vortex filaments in the range 2000 to 8000. Ernish [12] at a Reynolds Number of 8400 reported the formation of two vortex lines trailing to the rear of the sphere forming interlaced spirals. Von Karman [13, 14] noted that at approximately 10,000 there existed two vortex filaments which were displaced 180° from each other, and whose position of generation alternated irregularly. Lunnon [6] points out that if two such spirial threads do indeed exist, they must act on the sphere to cause it to move in a slightly curved and spiral path.

Perhaps the best observations on wake formation are those given by Möller [15] who employed stereoscopic cinematography to record the fluid movement behind a sphere being drawn in steady motion through water with Reynolds Numbers of 150 to 10,000. The vortex ring formation and shedding were obvious at 450, and, these vortices moved askew giving the impression of being linked together in a "vortex chain" ("Wirbelkette"). At a Reynolds Number of about 1000 there occasionally appeared discrete vortices which with increasing values took the upper hand over the vortex chain until 1500. From this value upwards only discrete vortices—referred to by Möller as "vortex streets"—were noted. These vortices—not to be confused with the Von Karman vortex street occurring in the wake of a cylinder—were unstable, and they joined together to form periodic balls of vorticity, or "Wirbelvolken".

The rhythmical and therefore non-turbulent component of the cyclic vortex phenomenon is usually described by the Strouhal Number $Sr = Fd/U_o$, where F is the frequency of shedding, and Möller presented two Strouhal Number curves which are reproduced in Figure 2. Curve A gives the variation of frequency of vortex shedding with increasing flow, while curve B indicates the frequency of formation of the "Wirbelvolken". Winny [11] reported Strouhal Numbers considerably lower than those given by Möller, but his results do not seem to be as reliable. Schmiedel's results for freely-falling spheres [10] indicated Strouhal Numbers of 0.327 and 0.389 at Re = 690 and 955 respectively, which are not excessively higher than Möller's curve, in view of the experimental difficulties.

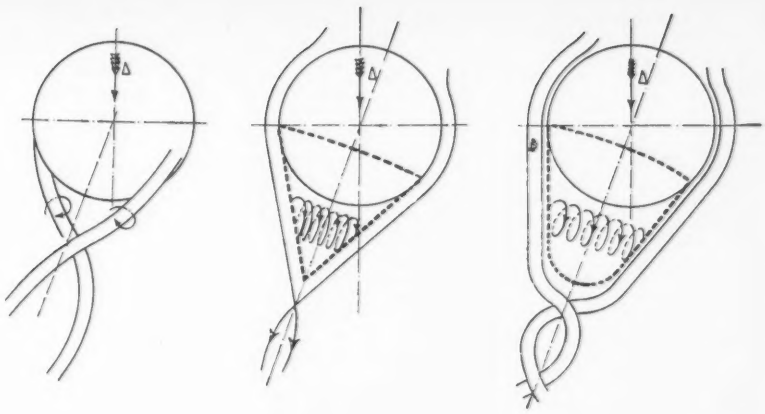

Figure 3—Sphere wake configurations below, at, and above the upper critical Reynolds Number (Foch and Chartier).

Foch and Chartier [16, 17] developed an ingenious stereoscopic method for obtaining a quantitative survey of the fluid movement in the wake of a sphere in an air current, by the time-lapse photography of tracer particles injected into the flow. Figure 3 a, b, and c, were obtained from the results for Reynolds Numbers below, at, and above the higher critical value. In the subcritical region, the wake clearly consisted of two intertwining vortex filaments whose points of separation from the sphere moved about the latter's surface. The axis of symmetry of the wake spun about the sphere axis parallel to the flow, sweeping out of a cone of half-angle Δ as indicated in the diagrams. Figure 3b was obtained at the higher critical value, and here the wake had an inner "dead water" core demarcated by the dotted line, in which the tracer particles moved in a coil-like direction transverse to the wake axis of symmetry. At higher Reynolds Numbers, the flow –which is probably representative of sphere systems in which there has been a laminar-turbulent transition in the attached boundary layer–seemed to generate a spiral wake as given in Figure 3c.

A surprising result was recently reported by Cometta [18] in the course of a hot-wire investigation of the unsteady flow pattern in air of the wake of spheres of 1.9, 2.2, 3.7 and 5.7 cm. diameter. In contradiction to the smooth Sr-vs-Re curve obtained by Möller, Cometta's results showed an abrupt change in the Strouhal Number at a Reynolds Number of 7,400. Although he makes no mention of Möller's detailed results, some of his limited data seem to fall on the curve given by Möller for the "Wirbelkette" and others obtained with larger spheres near the curve for the "Wirbelvolken". Cometta is at a loss to explain this apparent effect of sphere size, but a comparison with Möller's curves suggests that he may be measuring the fluctuations at different regions of the wake in the two cases. Cometta is also of the opinion that a helical wake movement never appears, although this argument is difficult to uphold in the light of Foch and Chartier's detailed measurements.

Sphere Wake Separation Circle and Pressure Distribution

The position of the circle formed by the separation of the boundary layer from the sphere surface changes with the Reynolds Number, and this phenomenon exerts a dominant influence on the vortex formation and the overall momentum transfer problem. Taneda [4] studied the separation position variation up to a Reynolds value of 450. Data obtained with different sphere diameters all fell on a smooth logarithmic curve which showed the angle α between the rear stagnation point and the separation circle to increase steadily from a value of zero at $Re = 24$ to 72° at $Re = 450$. This subject was investigated at the same time by Garner [19] whose technique implies that the boundary layer for mass transfer is coincident with the velocity boundary layer so that the minimum rate of solution of a soluble sphere marks out the separation circle. The results differ from those of Taneda below $Re = 100$, Garner's values of α being higher; but above 100 the results are almost coincident. Garner's data show α to remain constant above $Re = 500$, but this is contradicted by an earlier work of Ermish [12] who found, by means of pressure measurements at the sphere surface in the range $800 < Re < 26{,}000$, that α increases steadily throughout the range. The discrepancy may be due to the deformation of the dissolving sphere surface in the vicinity of the separation point. Ermish felt that the increase of α may account for the gradual and moderate increase of wake cross-section accompanying the increase of C_D in this region. This drag coefficient increase may also be caused by a shifting towards the sphere of the laminar-turbulent transition point in the *separated* boundary layer [20]. The normal pressure on the sphere surface is a maximum at the front stagnation point and falls smoothly to a minimum at the separation point; it then rises to an amount which is inversely proportional to the drag coefficient, and then remains roughly constant across most of the width of the wake. The form drag may be measured directly from the graphical integration of the pressure distribution in the vicinity of the sphere [21, 22], and Flachsbart [23] used this method to obtain a value of 0.460 for the drag coefficient at relatively high Reynolds Numbers, which agreed exactly with the resistance obtained from force measurements–thus illustrating the negligible role played by frictional resistance in this region.

Theoretical Studies of the Sphere Wake

The theoretical problems resulting from the separation, pressure distribution, and wake shedding phenomena are fundamental, and of such complexity that they remain to be properly developed for systems far less complex than that of the sphere. The application of what has resulted from investigations of simpler flow systems is hampered by insufficient experimental evidence as to the nature and characteristics of the sphere ambient flow. The results made available by present measuring techniques are difficult to interpret, being ambiguous and often contradictory.

Theoreticians have attempted to provide a crutch for the experimentalists who work in the wake region by predicting – from "reductio ad absurdum" reasoning – what type of vortex existence would be very difficult to justify. The studies, some of which were initiated by Karman and Rubach [24], deal with the stability of different vortex systems to mathematically-expressed disturbances. Rosenhead [25], however, cautions that the mathematical form of these disturbances may not correspond to those which exist in nature, and that the results may thus be quite misleading. (The stability of boundary layer systems to infinitesimal and finite perturbations will be discussed in detail in a following paper dealing with the effects of free stream vorticity).

There are many possible types of vortex systems which can be investigated, but the accent has been on those which had seemed to be detected by experiment. The most obvious system would be one made up of a series of separated rings moving parallel to their axis of symmetry. Levy and Forsdyke [26, 27] proved that such a system composed of equal vortex rings in parallel planes was only partially stable and inferred that their production will occur only at a transition stage to more stable systems.

For low Reynolds Numbers the wake of a cylinder consists of two stationary and symmetrical eddies; in the range 70 to 10^5, asymmetry sets in and eddying is formed alternatively from side to side, approximated by Karman's classical "vortex street" which he proved to be stable for one configuration only. The striking success achieved for the cylinder aroused hope that it could be extended somehow to the sphere, which is after all its axisymmetric analogue; however, Rosenhead [28] has shown that the Karman vortex street is three-dimensionally unstable when allowance is made for the finite thickness of the vortex filaments. Jeffreys [29] points out that the instability is slight when the vortices are thin, as they are initially. The conclusion is, however, that there is no simple extension of the Karman vortex street to three dimensions.

Levy [30] suggested a quasi-steady motion, consisting of two interlocking helical vortices, but Jeffreys [29] showed that it would be very difficult to maintain such a central vortex system. The latter also erroneously concluded that the actual motion in the wake was probably completely turbulent, i.e. there was no periodicity associated with it. Lampariello [31] demonstrated the instability of a helical vortex filament, but Levy and Forsdyke [32] countered by showing that the helices are stable above a certain pitch. In a communication to Marshall and Stanton [33] Rosenhead pointed out theoretical reasons against a helical vortex as proposed by Levy, and indeed photographs obtained by the former of the wake of a flat circular plate which had originally seemed to indicate a helical vortex showed on closer inspection to be made up of periodic discharges of a series of rings of vorticity from the disc.

Obviously there is much occurring in the sphere wake flow that is not presently discerned, let alone understood. There have been suggestions that some of the conflicting results may be due to a weakness of the law of dynamic similarity–according to which the Reynolds Number inter-relates phenomena occurring in fluids with different properties–when applied to fluids of greatly different densities. Nisi and Porter [3] feel that "the approximate law that may have been found sufficiently good for one case, may be inapplicable to another" and interesting differences between mechanism of turbulence in a liquid and in a gas are discussed in a recent provocative paper by Evans [34].

There are indications that acoustic phenomena resulting from the high-frequency oscillation of shed vortices may produce beat frequencies which will dictate the value of the Strouhal Number [35, 36] and through it the value of the drag coefficient. Experiment will have to bring out the finer details of the system which will include the *fluctuating* components of the pressures and drag forces on the sphere.

The Two-Dimensional Wake—Experimental Observations

The quantitative characteristics of the flow perpendicular to an infinitely-long cylinder can at times serve as a useful first approximation of the flow about a sphere, even though the field of the latter is not a general axisymmetric analogue of the former. The variation of the flow patterns as well as the drag coefficients of the cylinder with increasing Reynolds Numbers is similar to the sphere and the lower and higher critical Reynolds Numbers occur at approximately 40 and 5×10^5, respectively. Since the cylinder represents a considerably simpler system than the sphere, it has received more theoretical and experimental attention. Indeed some work done with cylinders may never be repeated with spheres without the introduction of invalidating effects resulting from the perforation of the flow field and the restraining action of the supporting apparatus. The problem of the cylinder is therefore a vital and immediate antecedent to the more difficult sphere system.

Studies of the wake of a cylinder may be grouped into two classes: the first deals with the wake in the immediate vicinity of the body, while the second is concerned with the downstream development at approximately 50 diameters or more. The latter class, which has been the subject of work by Townsend [37], Kobashi [38], Grant [39] and others, is related, but not of immediate importance to the problem of the evaluation of the drag coefficient, since the fluid pressure in this region is not far removed from that of the free stream.

Papers given by Ahlborn [40] in 1902 and Bernard [41] in 1908 were among the first to give photographic evidence of periodic arrangement of vortices in the wake of a cylinder, although a knowledge of this had already been demonstrated by Leonardo da Vinci. Karman's classical treatment of the vortex street which was presented in 1911 [42] initiated an extensive series of theoretical investigations of the alternate system of vortices which has as yet failed to relate properly the downstream flow in the wake to the initial conditions at the surface of the body. The fascinating geometry of the periodic flow and the theoretical foot-in-the-door provided by Karman attracted many workers to its study. The Strouhal Number-vs-Reynolds Number relationship for cylinders – an effect which cannot be accounted for by the Karman theory since the latter assumes a perfect fluid–is much better established than for spheres, and this is due in part to the work of Carmichael, Dupin and Tessie-Solier [43], Fage [44], Fage and Johansen [45], Fage and Falkner [46], Relf [47], Relf and Owen [48], Simmons [49], Rosenhead and Schwabe [50], Richardson [51], Blenk [52], Link [53], Thom [54], Lock [55], Lehnert [56], Kruger and Lauth [57], Tyler [58], Kovasznay [59], and most recently Drescher [60], Etkin, Korbacher and Keefe [61], Roshko [62], Taneda [63], Hama [64], Richardson [65] and Cometta [18].

The flow in the immediate vicinity of the front of the cylinder, i.e. the front "stagnation point", has always been assumed to be free from fluctuation, and this seems to be confirmed by all photographs of the region, although some fluctuations can be observed in cinematographic studies. Piercy and Richardson [66] studied the flow very close to the surface of a cylinder by means of a hot-wire anemometer, and their very precise velocity fluctuation contours reproduced in Figure 4 underline the great complexity of the flow. Surprisingly, there are large velocity fluctuations very close to the front stagnation point, and the disturbance seems to be damped out and then disappears into the boundary layer as it moves towards the wake. There has been very little comment in the literature regarding this phenomenon, although it may be an important precursor of the wake generation. The results also indicate that in the vicinity of the separation point there arises a "funnel of vorticity" whose very large-amplitude fluctuations may have been fed by the agglomeration of smaller vibrations occurring in the separating boundary layer. The funnel seems to be the starting point of the large vortices in the rear.

The fate of the boundary layer after it separates from the cylinder has received far better attention than its sphere analogue. Fage and Johansen [67] recognized that the river of vorticity emanating from the separation point and flowing into the heart of the wake represented one of the key phenomena which must be incorporated into the understanding of the overall momentum transfer. They investigated carefully the structure of the separated layers springing from the surface of a cylinder and various other two-dimensional bodies by measuring their velocity profiles and then calculating their vorticity content from this information in the following manner: at a given point in a two-dimensional flow, the vorticity is given by the expression:

$$(\delta v/\delta x - \delta u/\delta y) \quad \ldots\ldots(1)$$

where u and v are the instantaneous velocities in the mutually perpendicular x and y directions respectively. If the flow in the separated layer were free from fluctuations, then the total vorticity K passing through its cross-section per unit time would be given by:

$$K = \int_{y_1}^{y_2} (\delta v/\delta x - \delta u/\delta y)u dy \quad \ldots\ldots(2)$$

where y_1 and y_2 are respectively the inner and outer limits of the separated layer. By convention the vorticity is usually expressed as a dimensionless term λ obtained by dividing K by the square of the free stream velocity; i.e.

$$\lambda = K/U_o^2 \quad \ldots\ldots(3)$$

As the vorticity moves deeper into the wake it is acted on by viscous forces and turbulent mixing and it is gradually annihilated by vorticities of opposite sign [68]; therefore at a given point x downstream from the separation point the flow is characterized by the vorticity survival fraction β_x defined by

$$\beta_x = \lambda_x/\lambda_s \quad \ldots\ldots(4)$$

the subscripts x and s referring to values at x and at the separation point respectively. For the cylinder, Fage and Johansen found that $\lambda_s = 1.01$ and that β_x falls steadily to a value of 0.93 at one-half the cylinder diameter distance from the separation point. It has been suggested that at the point of formation of the vortex centres, β_x drops to a value of approximately 0.5 but there are as yet no detailed measurements of the variations of this parameter with position in the wake and which the flow Reynolds Number—the latter dictating the average ratio of the turbulent vorticity to the total.

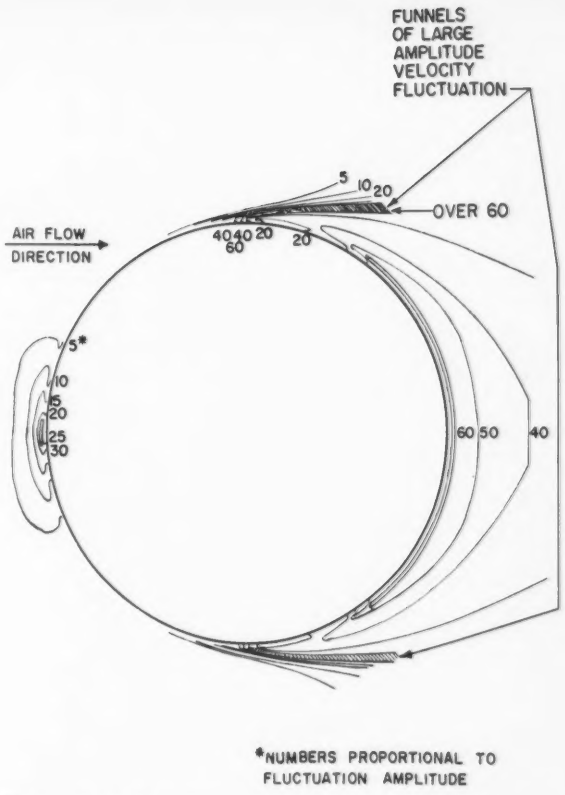

Figure 4—Velocity fluctuations in vicinity of cylinder surface (Piercy and Richardson).

It should be noted that the foregoing treatment completely ignores the vorticity associated with the non-steady component of the flow. Fage and Johansen felt that this was justified in that the velocity fluctuations in the separated flow—which they measured with a relatively large and uncompensated hot-wire and recorded with a string galvanometer—were sufficiently small to allow Equation (2) to be applied. Even if correct, this should not be a generalization, since large scale velocity fluctuations can be present as shown by the work of Piercy and Richardson [66].

The results of Schiller and Linke [20] and of Kovasznay [59] show that the free boundary layer of the cylinder will remain laminar up to a distance which diminishes with increasing Reynolds Numbers and free stream turbulence, but the mechanism for this behavior is obscure. A better understanding of the separated boundary layer is vital to the solution of the overall momentum transfer problem and a long range program directed toward this end is reported by Sato [69]: preliminary observations deal with the stability of a boundary layer separating from a sudden discontinuity on a flat plate. Eventually effects such as that of surface curvature, pressure distribution and free stream turbulence will be investigated. Similar observations by Maekawa and Atsumi [70] reiterate the need for the investigation of the effect of surface curvature on the separated layer behavior.

The separated boundary layer and its development into the cylinder wake were studied by Roshko [62] in a detailed survey with a hot-wire anemometer. Three regions were evident: at a Reynolds Number of 40 there was the start of a "stable" range in which could be discerned a change from stable viscous flow in the attached rear vortices to the alternate breaking-away forming the vortex street, but there was no laminar-turbulent instability present in the entire system. From Re = 150 to 300 (called the transition range) there was a laminar-turbulent instability, but this occurred in the separated boundary layer, the transition approaching the separation point with increasing Reynolds Numbers. Above 300 (referred to as the irregular range) transition occurred at the separation point, and the velocity fluctuations had both periodic and truly turbulent components, which would correspond to the wakes shown in Schmiedel's photographs for falling spheres at Reynolds Numbers above 1000 [10]. Roshko terms the fluctuation intensities observed at a particular point $\overline{u'^2}$ as being given by:

$$\overline{u'^2} = \overline{u_t'^2} + \overline{u_1'^2} + \overline{u_2'^2} \quad \ldots\ldots\ldots\ldots\ldots\ldots\ldots\ldots\ldots\ldots (5)$$

where $\overline{u_t'^2}$ results from the truly turbulent fluctuations, $\overline{u_1'^2}$ is the fluctuation contributed by the shedding frequency N and $\overline{u_2'^2}$ is the fluctuation resulting from the interaction of both vortices and corresponds to the frequency $N_2 = 2N$. The higher harmonics were found to be negligible. The wake energy E is therefore the sum of $E_R + E_1 + E_2$, corresponding to the above velocity intensities. The energy spectrum, i.e. the energy variation with frequency, was shown by the hot-wire anemometer exploration not to be a smooth one at the beginning of the wake, and exhibited "bumps" at N and N_2. There was, however, a strong tendency for the spectrum to smooth out as it moved downstream by a transfer of energy from the high energy spectral bands to the lower ones. Preliminary measurements with a microphone probe of the wake *pressure* fluctuations reported by Strasberg and Cooper [71] have revealed energy spectra which correspond in shape with those obtained by Roshko. The "irregular" range characterized by a fluctuating but non-turbulent component of the wake energy has been recently shown by Cometta [25] to extend up to at least a Reynolds Number of 10^6, and corresponding Strouhal Numbers are measurable up to that region. Further mention of the wake energy spectrum will be made in the section dealing with the effect of high relative free-stream turbulence intensities.

A very detailed study of the "stable" and "transition" stages of development of the separated boundary layer of the cylinder has been made by Taneda [72] which corresponds to the work which he did on the sphere wake. Unlike earlier investigations, the results obtained by his refined photographic technique for the range Re = 0.1 to 1000, are sufficiently quantitative to establish the dimensions of the various components of the flow field. This was compared with a theoretically calculated flow for a Reynolds Number of 40 resulting from a numerical solution given by Kawaguti [73] similar to, but more complete than the one which he gave for the sphere, and which has already been discussed. Here the agreement is excellent. The boundary layer separation point was observed to be at 53° from the forward stagnation point comparing with Kawaguti's calculated value of 52.2°, and the ratio of the downstream lengths of the stationary wake vortex, s, to the cylinder diameter d, was measured at 2.1, compared to the calculated value of 1.9. A plot of s/d vs Re for the stable stationary vortex region was qualitatively similar to the results for the sphere given in Figure 1, but they show that at a given Reynolds Number, the cylinder wake is more elongated than its sphere counterpart.

Taneda found what he termed a remarkable fine scale phenomenon in the region of Re = 35 to 45. Very small disturbances seemed to appear at the rear centre of the cylinder, moving downstream at the interface of the two stationary vortices, at the end of which they trembled for a short time and died away. At Reynolds Numbers above 45 they passed on downstream and may have seeded the periodic shedding. Although not mentioned by Taneda, there is some possibility that this phenomenon is linked with the instability noticed just above the front stagnation point by Piercy and Richardson [66].

Acoustic Phenomena

There is good reason to believe that fine scale phenomena in the flow which have yet to be fully discovered may play a dominating role in determining the properties of the wake. These are probably linked with the acoustic radiation which accompanies fluctuations in velocity, i.e. the aerodynamic sound as differentiated from that resulting from bodily vibrations. Richardson [74] recently presented an eloquent plea for a reunion of efforts dealing with turbulence and acoustic phenomena, emphasizing the aspects common to both subjects; the importance of the relationship of the acoustic radiation resulting from isotropic turbulence to the general problem of a universal turbulence theory is underlined in an interesting paper by Meecham and Ford [75].

Of immediate importance to the wake problem is a theory developed by Lighthill [76, 77] in 1952 which indicates that the velocity fluctuations in a turbulent wake and the fluctuating stresses at the body surface act as acoustic sources generating sound whose intensity varies exponentially with the relative fluid velocity. The difficult measurement of the acoustic intensities for different locations in the cylinder flow field has been the subject of recent investigations by Bingham, Weimer and Griffith [78], Gerrard [79], Phillips [80], Etkin, Korbacher and Keefe [81], Richardson [65] and McGregor [81]. It has been found that small fluctuating pressures caused by the shedding vortices occur all along the cylinder surface, the intensities of which rise from the front stagnation point to a maximum at the sides. The results, which include the evaluation of the fluctuating component of the drag coefficient, are promising but as yet incomplete. They may also be expected to explain the rather marked effects of sound fields noted on the mass and momentum transfer [82] and the shedding frequency [83] of blunt bodies.

Theoretical Treatment of the Cylinder Wake

Although the evolution of a theoretical description of the wake phenomena of the cylinder is as yet in the embryonic state, the work that has been done is valuable towards the eventual solution of the sphere system. There are three conventional avenues of approach to the problem which are due to Kirchhoff [84], Karman [85] and Crocco and Lees [86].

Kirchhoff notes that the flow about a cylinder immersed in an "ideal" or frictionless fluid i.e. the potential flow, can readily be calculated by the methods of classical hydrodynamics; however, this would predict a pressure distribution in which the force on the upstream portion of the body is the mirror image of that on the down-

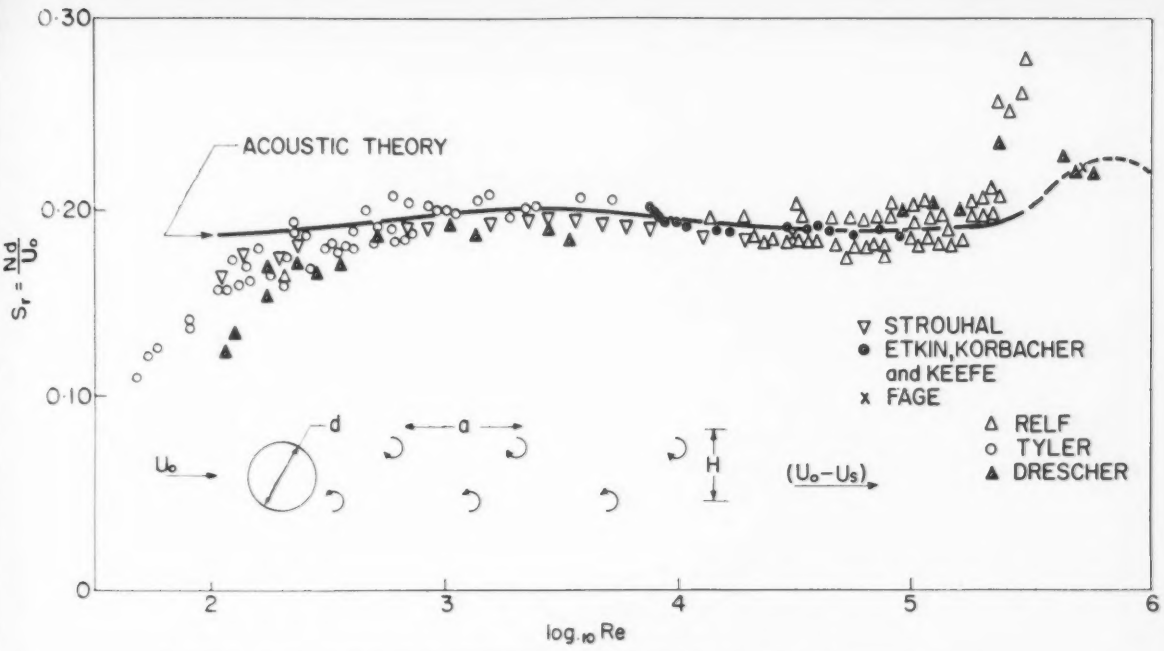

Figure 5—A comparison of experimental Strouhal Numbers with Shaw's acoustic theory.

stream side, so that the net drag force which follows from the integration of the distribution of pressure at the body surface would be zero. Kirchhoff takes a more realistic approach by dividing the flow into two regions consisting of an outer potential flow field up to the wake envelope, and the wake region itself. The two regions are separated by a shear layer which in the theory is idealized as a sheet of velocity discontinuity. The pressure distribution calculated up to the wake boundary from potential flow roughly approximates the experimentally observed one, but the Kirchhoff theory runs into difficulty in the important wake region in that it assumes the velocity in the fluid to be equal to the free stream velocity, resulting in a base pressure in the wake region which is equal to the free stream pressure. The predicted drag on the body is therefore much lower than the actual value.

The celebrated Karman vortex street theory on the other hand attempts to relate the base pressure with the building up and shedding of vortices in the wake. By doing a momentum balance through a section of the periodic wake Karman arrives at the relationship

$$R = \frac{\kappa^2 \rho}{2a\pi} + \frac{\kappa \rho h}{a}(U_o - 2U_s) \qquad (6)$$

where R is the drag force, ρ the fluid density, h the spacing between vortex rows (see Figure 5), a the distance between consecutive vortices, U_o the mean stream velocity, U_s the velocity of the vortices relative to the stream velocity and the vorticity content of each *individual* vortex, $\kappa = (K\ a)/(U_o - U_s)$. From stability considerations and by assuming ideal fluid behavior Karman deduced that $\frac{h}{a}$ can only have a value of 0.281; secondly, as a result of his momentum balance, it was assumed that κ was given by the expression $2U_s a/\tanh(\pi h/a)$ so that in effect κ was equal to $2\sqrt{2}\ aU_s$. The drag coefficient could then be found from the relationship

$$C_D = R/(1/2)\rho U_o^2 d = (a/d)[1.59(U_s/U_o) - 0.63(U_s/U_o)^2] \qquad (7)$$

Goldstein [21] points out that even if Karman's two assumptions are valid, the drag coefficient could not be evaluated unless both a and U_s were experimentally determined. In the event that the Strouhal Number were known, U_s could be evaluated from the expression

$$N = (U_o - U_s)/a \qquad (8)$$

and the vorticity per unit time K would be equal to $\kappa N = \kappa (U_o - U_s)/a$.

Important, and understandably what the author calls "disturbing" modifications to the von Karman theory have recently been proposed by Birkhoff [68]. After citing evidence that the Karman configuration of h/a = 0.281 has higher order instability, he shows that *all* h/a ratios are stable providing that *mean* values of h and a are used and that the instability present is only associated with the periodicity. For nonviscous systems h/a is proved to be invariant, whereas in a real fluid the moment hK is a constant where K—the averaged value of K—decreases downstream as vorticity is annihilated so that h must gradually increase.

In the same paper Birkhoff cites the possibility that the perplexing problem of theoretically accounting for the Strouhal Number magnitude may be associated with the characteristic flapping of the wake. By equating an approximation of the cross-force resulting from the flapping to the transverse acceleration of the wake fluid, he obtained the expression:

$$Sr = (1/2)[d/(k'l'\pi)]^{1/2} \qquad (9)$$

where l' is the average length of the wavering portion of the wake, and k' is the ratio of the loosely defined wake diameter d* (usually taken as being equivalent to h) to the cylinder diameter d. The only support available as yet for Equation (9) is that the values of k' and l' which would

have to be assumed to predict observed Strouhal Numbers are not unreasonable.

Next follow attempts to combine the Kirchhoff and Karman theories, if not to theoretically solve the drag problem to at least reduce the number of parameters which must be supplied by experiment. Heisenberg [87] assumed the Kirchhoff flow field in what at first appeared to be a successful attempt to predict the ratios U_s/U_o and a/d needed for the Karman drag coefficient. The agreement of his results with experiment have been shown to be fortuitous [21], his derivation having greatly underestimated the complexity of the flow.

In an extremely interesting discussion Jeffreys [29] points out that Kirchhoff's theory should have its wake fluid velocity corrected and Prandtl [88] and Roshko [89, 90] have attempted to do this by replacing it with a fictitious fluid velocity U_w defined by:

$$U_w^2/U_o^2 = k^2 = 1 + C_p \quad \ldots\ldots(10)$$

C_p, called the wake underpressure coefficient, is related to the drag coefficient and is calculated from the difference of the mean fluid pressure in the wake P_w, and the free stream pressure P_s in the relationship

$$P_s - P_w = C_p\,(1/2)\rho U_o^2 \quad \ldots\ldots(11)$$

Prandtl used Equation (11) in a very approximate theoretical derivation showing that

$$\lambda_s = \frac{1}{2}\,(1 + C_p) \quad \ldots\ldots(12)$$

and Birkhoff incorporated the vorticity survival fraction β into this equation so that it has the final form:

$$\lambda = \frac{1}{2}\,\beta\,(1 + C_p) \quad \ldots\ldots(13)$$

This equation would undoubtedly have to be refined before it could be considered to be theoretically significant.

Birkhoff added the above concepts to the Karman treatment, noting that the Karman formula for κ can be rewritten to give

$$\epsilon\,(1 - \epsilon) = \frac{1}{2}\,\lambda \tanh(\pi h/a) \quad \ldots\ldots(14)$$

where ϵ is the ratio (U_s/U_o) needed for the Karman formula. By substituting for λ in Equation (14) this leads to

$$\epsilon\,(1 - \epsilon) = \frac{1}{4}\,\beta\,(1 + C_p) \tanh(\pi h/a) \quad \ldots\ldots(15)$$

This expression cannot as yet be confirmed experimentally since adequate measurements of ϵ are lacking. Birkhoff also introduced a modified Strouhal Number Sr_B which uses the actual wake diameter d^* in place of the body diameter d, i.e.

$$Sr_B = Nd^*/U_o \quad \ldots\ldots(16)$$

By assuming $\beta h = d^*$, and by using the relationship $N/U_o = (1 - \epsilon)/a$, he obtains an approximate expression

$$Sr_B = \beta h\,(1 - \epsilon)/a \quad \ldots\ldots(17)$$

In a similar treatment Roshko [89, 90] rewrites Equation (14) ending up with the expression

$$\epsilon = \left(1/2\right)\left(1 \pm \sqrt{1 - (\beta k^2)/\sqrt{2}}\right) \quad \ldots\ldots(18)$$

He proposes a modified Strouhal Number Sr_R which incorporates not only the wake diameter but also the ficticious wake velocity U_w, i.e.

$$Sr_R = Nd^*/U_w \quad \ldots\ldots(19)$$

and he derives an expression for Sr_R which is in effect identical in derivation and in result to Birkhoff's Equation (17) except in that d^* is replaced by h alone rather than by βh. He then employs Equations (17), (18) and (19) in a graphical solution which amounts to a compact summary of the results of combining the Kirchhoff and Karman theories. By substituting the ϵ as given in (18) into the Karman drag Equation (7) a family of curves having C_D d/h as the ordinate, k as the abscissa and β as the varying parameter are obtained. Next, by using the empirically modified Kirchhoff theory i.e. calculating the flow up to the wake by the methods of classical hydrodynamics and by arbitrarily substituting different values of the base pressure as reflected in k and then calculating the drag coefficient from an integration of the pressure about the body, Roshko obtains a family of curves having C_D d/d* as the ordinate, k as the abscissa and the shape of the cylinder as the varying parameter, thus extending the treatment to cylinders of non-circular cross-section. If the assumption is allowed that $d^* = h$ then the points of intersection of the C_D d/h vs. k and C_D d/d* vs. k curves represent wake solutions for varying β values and what is most interesting, varying cylinder shape. This means that only β need be measured to determine C_D d/d* and k for any cylinder shape, allowing the drag coefficient to be determined from a plot of d'/d vs. k obtained from the modified Kirchhoff theory. Roshko points out that any interference in the wake in the form of other bodies or free stream turbulence would change β and therefore C_D, and he illustrates this with some initial experimental evidence.

The at times superficial treatment given to the wake by Birkhoff and Roshko seems to have exhausted that which can be done with the limited experimental results presently available. Further empirical work now in progress should allow replacement of some of the parameters employed with others which correspond more truthfully to the actual wake phenomena.

A third theory which may be useful, but which has not as yet been developed for the subsonic wakes of blunt bodies is that of momentum diffusion involved in the mixing theory for the interaction between dissipative flows and nearly isoentropic streams proposed by Crocco and Lees [86]. It considers the difference of pressure between the base of the wake and the free stream as resulting from the diffusion of momentum across the discontinuity of velocity forming the wake envelope. It cannot in itself be successful since it omits a vital part of the mechanism, as is demonstrated by Roshko, namely that of the formation of the vortices, but it can probably be incorporated into an overall solution of the wake.

The theories thus far presented are based on conventional fluid flow concepts, and it is entirely possible that the difficulties encountered are in part due to an omission of less evident but vitally important occurrences in the wake. A theory of such a nature was presented by Shaw [35, 36] in 1949, but as if by a conspiracy of silence, it has been avoided or overlooked by nearly all of the many workers in the field who have published since–this in spite of its apparent success at providing a completely theoretical derivation of the sought after ratio a/d.

In essence, Shaw argues that there are three disturbance centres in the flow about a cylinder, two strong ones at the separation points and a third weak one at the front stagnation point—a model which is in complete agreement with Piercy and Richardson's results (Figure 4). These centres emit acoustic pressure pulses which travel in the cylinder boundary layer and through the ambient flow at sonic velocities. From the time taken by the pulses to travel between disturbance points, Shaw shows their frequency to be about equal to $3C/2\pi d$ where C is the speed of sound. Moreover since a shed vortex continues to oscillate at this frequency it sends back pulses to the still attached layer at a frequency which due to the Doppler effect is reduced in the ratio $[1 - (U_o - U_s)/C]$ thereby interacting with the acoustic vibrations of the attached fluid vibrating with the original frequency, and as a consequence producing strong pulses with the beat frequency $(3C/2\pi d)[(U_o - U_s)/C]$ which in turn cause the shedding of the vortex. The shedding frequency of vortex pairs is therefore $(1/2)(3/2\pi d)(U_o - U_s)$, so that the Strouhal Number is given by

$$Sr = (3/4\pi)(1 - U_s/U_o) \quad \ldots\ldots\ldots\ldots\ldots\ldots (20)$$

This is in effect saying that

$$a = 4\pi d/3$$

a result that agrees very well with experiment and also with Birkhoff's proof that "a" in a given wake is invariant. Figure 5 shows the comparison of the theoretically predicted Strouhal Number—U_s/U_o having been obtained by inserting experimental C_D values into the Karman equation—with some of the available experimental results and the theoretical curve almost appears to have been drawn by the method of least squares. Excellent results have also been obtained for cylinders of non-circular cross section [91] by revising the passage time for the pulses as a result of the shape of the body. Comment on and criticism of Shaw's exciting theory will be awaited, particularly from those active in the *measurement* of the aerodynamic sound generated in the environment of an immersed body.

In summary, a review of the sphere wake literature shows that the comprehension of this complex region is impeded by a lack of adequate experimental substance in combination with the theoretical difficulties common to studies of flow systems in which the inertia terms are significant. There is an immediate need for a paralleling application to the sphere wake of the albeit limited and unrefined information obtained from the simpler two-dimensional cylinder system. In spite of its shortcomings, the information presented forms a foundation for the understanding of the aerodynamics of particles moving in less idealized fluid environments where complications which include the particle acceleration, shape, rotation, concentration, and the fluid turbulence become operative, and these matters will be dealt with in the forthcoming installments of this series.

Nomenclature

Any consistent set of units may be employed. Those listed are merely illustrative.

a	= distance between consecutive vortices, ft.
C_D	= drag coefficient, dimensionless
C_p	= pressure coefficient, dimensionless, Equation (11)
C	= velocity of sound, ft./sec.
d	= body diameter, ft.
d*	= wake diameter, ft.
E	= total wake energy, ft. lb./sec.
E_1	= wake energy associated with fundamental shedding frequency, ft. lb./sec.
E_2	= wake energy associated with first harmonic of shedding frequency, ft. lb./sec.
E_R	= wake energy associated with truly turbulent fluctuations, ft. lb./sec.
F	= shedding frequency of sphere wake, sec.$^{-1}$
h	= lateral spacing between vortex centres for cylinder wake, ft.
K	= vorticity passing through separated layer cross-section per unit time, ft.^{2}/sec.^{2}, Equation (2)
k	= ratio of ficticious wake velocity to fluid velocity, dimensionless.
k′	= ratio of wake diameter to cylinder diameter, dimensionless.
l′	= average length of wavering portion of wake, ft.
l'_s	= distance from rear stagnation point to vortex centre, ft.
l_s	= length of sphere wake, ft.
N	= shedding frequency of cylinder wake, sec.$^{-1}$
N_2	= first harmonic of shedding frequency, sec.$^{-1}$
P_s	= mean static pressure in free stream, lbs./ft.^{2}
P_w	= mean static pressure in wake flow, lbs./ft.^{2}
R	= fluid drag force on body, lb. force, or lbs/ft. (for two-dimentional case).
Re	= Reynolds parameter, dimensionless.
Sr	= Strouhal Number, dimensionless, Figure 5.
Sr_B	= Strouhal Number due to Birkhoff, Equation (16).
Sr_R	= Strouhal Number due to Roshko, Equation (19).
U_o	= free stream velocity, ft./sec.
U_s	= velocity of vortices relative to stream velocity, ft./sec.
U_w	= ficticious wake velocity, ft./sec., Equation (10).
u	= instantaneous fluid velocity in x direction, ft./sec.
u′	= total fluctuating component of fluid velocity in x direction, ft./sec.
u_1', u_2', u_r'	= fluctuating component of fluid velocity in x direction associated with the fundamental and first harmonic of the shedding frequency, and the truly turbulent fluctuations respectively, ft./sec.
v	= instantaneous velocity in y direction, ft./sec.
x	= co-ordinate parallel to stream direction.
y	= co-ordinate transverse to stream direction.
α	= angle between rear stagnation point and separation circle, degrees.
β	= vorticity survival fraction, dimensionless, Equation (4).
β_x	= vorticity survival fraction at point x, dimensionless.
Δ	= half-angle of wake cone, degrees, Figure 3.
ϵ	= ratio (U_s/U_o), dimensionless.
κ	= vorticity content per vortex, ft.^{2}/sec.
λ	= reduced vorticity, dimensionless, Equation (3).
λ_s	= reduced vorticity at separation point, dimensionless
λ_x	= reduced vorticity at point x, dimensionless.

Acknowledgments

The authors wish to express their appreciation for the continued assistance given to them by Librarians A. Finnemore and L. Lefebvre of the Pulp and Paper Research Institute of Canada, and P. Kier of McGill University, in obtaining the many papers reviewed in this series. L. B. Torobin is indebted to the Scientific Research Bureau, Trade and Commerce Department, Province of Quebec, for three consecutive Fellowships in support of his research program.

References

(1) Torobin, L. B., and Gauvin, W. H., Can. J. Chem. Eng., **37**, 132 (1959).
(2) Williams, D. H., Phil. Mag. **29**, 526 (1915).
(3) Nisi, H., and Porter, A. W., Phil. Mag. **46**, 754 (1923).
(4) Taneda, S., Rep. Res. Inst. Appl. Mech. Japan, **IV**, 99 (1956).
(5) Nemenyi, P., Trans. Am. Geophys. Union **21**, 633 (1940).
(6) Lunnon, R. G., Proc. Roy. Soc. (London), **118A**, 680 (1928).
(7) Schmidt, F. S., Ann. Physik, (4) **61**, 633 (1920).
(8) Lunnon, R. G., Proc. Roy. Soc. (London), **A110**, 302 (1926).
(9) Liebster, H., Ann. Physik, **82**, 541 (1927).
(10) Schmiedel, Von J., Physik. Z., **29**, 593 (1928).
(11) Winny, H. F., Aeronaut. Res. Comm. Rep. and Mem., 1531 (1932).
(12) Ermisch, H., Abh. d. Aer. Inst. Aacchen, Heft 6, 18 (1927).
(13) Karman, Th. von, Vortrage A.D. Geb. d. Hydro u. Aerodynamik, Innsbruck, 136 (1922), J. Springer, Berlin (1924).
(14) Falkenhagen, H., Handbuch der Experimental Physik, **4**, Part 1, 155 (1931).
(15) Möller, von W., Physik. Z., **39**, 57 (1938).
(16) Foch, A., and Chartier, C., Compt. Rend. **200**, 1178 (1935).
(17) Chartier, C., Publications Scientifiques et Techniques du Ministere de L'Air, No. 114 (1937).
(18) Cometta, C., Brown U., Div. Eng., T.R. WT-21 (A.F.O.S.R. T.N. 57-760 (1957).
(19) Garner, F. H., Chemistry and Industry, Feb. 25, 141 (1956).
(20) Shiller, L., and Linke, W., N.A.C.A. T.M. 715 (1933).
(21) Goldstein, S., Modern Developments in Fluid Dynamics, Vol. II, Oxford University Press (1938).
(22) Schlichting, H., Boundary layer theory, translated by J. Kestin, McGraw-Hill Book Co. Inc., New York (1955).
(23) Flachsbart, O., Bat. Advisory Comm. Aeronaut. Tech. Mem. 475 (1925).
(24) Karman, Th. von, and Rubach, W., Physik. Z. **13**, 49 (1912).
(25) Rosenhead, L., Advances in Applied Mech., III, 185 (1953).

(26) Levy, H., and Forsdyke, A. G., Proc. Roy. Soc. (London) **A114**, 594 (1927).
(27) Levy, H., and Forsdyke, A. H., Proc. Roy. Soc. (London) **A116**, 352 (1927).
(28) Rosenhead, L., Proc. Roy. Soc. (London), **A127**, 590 (1930).
(29) Jeffreys, H., Proc. Roy. Soc. (London) **A128**, 376 (1930).
(30) Levy, H., Aeronaut. Res. Comm. Rep. T 2921 (1930).
(31) Lampariello, G., Linl. Rend. (6) **15**, 432 (1932).
(32) Levy, H., and Forsdyke, A. G., Proc. Roy. Soc. (London) **A120**, 670 (1928).
(33) Stanton, T. E., and Marshall, D., Aeronaut. Res. Comm. Rept. and Mem., 1358 (1932).
(34) Evans, R. L., 4th Midwestern Conf. on Fluid Mechanics (1955).
(35) Shaw, R. A., Aeronaut. Res. Council Rep. 12, 376 (1949).
(36) Shaw, R. A., Aeronaut Res. Council F.M. 1395 (1949).
(37) Townsend, A. A., The Structure of Turbulent Shear Flow, Cambridge University Press, Cambridge (1956).
(38) Kobashi, Y., J. Phys. Soc. Japan, **12**, 533 (1957).
(39) Grant, H. L., J. Fluid Mech., **4**, 149 (1958).
(40) Ahlborn, F., Mechanismus des Hydrodynamischen Widerstandes, Hamburg (1902).
(41) Benard, H., Compt. Rend., **147**, 839, 970; **156**, 1225, (1913); **187**, 1028 (1928).
(42) Karman, Th. von, Göttinger Nachrichten, **509** (1911).
(43) Carmichel, C., and Dupin, P., J. of Rheol. **3** (1932).
(44) Fage, A., Proc. Roy. Soc. (London), **A144**, 381 (1934).
(45) Fage, A., and Johansen, F. C., Phil. Mag. (7), **5**, 417 (1928).
(46) Fage, A., and Faulkner, F. M., Aeronaut. Res. Comm. Rep. and Mem. 1369 (1931).
(47) Relf, E. F., Phil. Mag. **42**, 173 (1921).
(48) Relf, E. F., and Ower, E., Aeronaut. Res. Comm. Rep. and Mem., 825 (1923).
(49) Relf, E. F., and Simmons, L. F. G., Phil. Mag. **49**, 509 (1925).
(50) Rosenhead, L., and Schwabe, M., Proc. Roy. Soc. **A129**, 115 (1930).
(51) Richardson, E. G., Proc. Roy. Soc. (London) **36**, 153 (1923).
(52) Blenk, W., Luftfahrtforschung, **12**, 38 (1935).
(53) Link, W., Physik. Z., **32**, 900 (1931).
(54) Thom, A., Proc. Roy. Soc. **A141**, 651 (1933).
(55) Lock, C. H. N., Aeronaut. Res. Comm. Rept. and Mem. 986 (1925).
(56) Lehnert, R., Physik, **38**, 476 (1937).
(57) Kruger, F., and Lauth, A., Ann. d. Phys. **44**, 801 (1914).
(58) Tyler, E., Phil. Mag. (7) **11**, 849 (1931).
(59) Kovasznay, L. S. G., Proc. Roy. Soc. (London) **A198**, 174 (1949).
(60) Drescher, H., AVA Monographs, G.D.C. 441T, Aeronaut. Res. Council Rep. 11, 391 (1947).
(61) Etkin, B., Korbacher, G. K., and Keef, R. T., J. Acoust. Soc. Amer. **29**, 30 (1957).
(62) Roshko, A., N.A.C.A. T.R. 1194 (1954).
(63) Taneda, S., Rep. Res. Inst. App. Mech. Japan, **4**, 29 (1955).
(64) Hama, F. R., J. Aeronaut. Soc. **2**, 24 (1957).
(65) Richardson, E. G., App. Sci. Res. **A7**, 341 (1958).
(66) Piercy, N. A. V., and Richardson, E. G., Phil. Mag. **5**, 6 (1928).
(67) Fage, A., and Johansen, F. C., Proc. Roy. Soc. **A116**, 170 (1927).
(68) Birkhoff, G., J. Appl. Phys., **24**, 98 (1953).
(69) Sato, H., J. Phys. Soc. Japan, **11**, 702 (1956).
(70) Maekawa, T., and Atsumi, S., N.A.C.A. T.M. 1352 (1952).
(71) Strasberg, M., and Cooper, R. D., 9th Congr. Intern. Mecan Appl., **2**, 384 (1957).
(72) Taneda, S., J. Phys. Soc. Japan, **11**, 302 (1956).
(73) Kawaguchi, M., J. Phys. Soc. Japan **8**, 747 (1953).
(74) Richardson, E. G., J. Aeronaut, Sci., **22**, 775 (1955).
(75) Meecham, W. C., and Ford, G. W., J. Acoust. Soc. Amer., **30**, 318 (1958).
(76) Lighthill, M. J., Proc. Roy. Soc. **A211**, 564 (1952).
(77) Lighthill, M. J., Proc. Roy. Soc. **A222**, 1 (1954).
(78) Bingham, S., Weimer, M., and Griffith, W., Princeton University, Dept. of Physics Report 11-13 (1952).
(79) Gerrard, J. H., Proc. Phys. Soc. (London), **68**, 453 (1955).
(80) Phillips, O. M., J. Fluid Mech. **1**, 607 (1956).
(81) McGregor, D. M., U.T.I.A. T.N. 14 (1957).
(82) Hodgins, J. W., Hoffman, T. W., and Pei, D. C., Can. J. Chem. Eng. **35**, 18 (1957).
(83) Garber, D. I., J. Aeronaut. Sci., **25**, 275 (1958).
(84) Roshko, A., N.A.C.A. T.N. 3168 (1954).
(85) Karman, Th. von, Göttinger Nachrichten, 547 (1912).
(86) Crocco, L., and Lees, L., J. Aeronaut. Sci., **19**, 649 (1952).
(87) Heisenberg, W., N.A.C.A. T.N. 126 (1923).
(88) Prandtl, L., Physik. Z., **23**, 366 (1922).
(89) Roshko, A., N.A.C.A. T.N. 3169 (1954).
(90) Roshko, A., J. Aero. Sci., **22**, 124 (1955).
(91) Shaw, R. A., Aeronaut. Res. Council Rep. 18, 455 (1956).

★ ★ ★

Development of Design Criteria for Biological Treatment of an Industrial Effluent Containing 2,4-D Waste Water[1]

R. E. MILLS[2]

The development of design criteria for a waste water treatment plant is described. Operating results for a laboratory activated sludge unit, a Dowpac trickling filter pilot plant, and an aero-accelator activated sludge pilot plant are given. Studies with the aero-accelator pilot unit indicated that by observing certain critical nutrient and dilution requirements the industrial effluent, containing toxic 2,4-D waste water, could be satisfactorily treated by bio-oxidation. A phenol removal of 99% and a biochemical oxygen demand (B.O.D.) removal of 90% to 95% was obtained. In the full scale treatment plant, the estimated cost of operation was calculated at $0.50 per pound of phenol removed, and $0.08 per pound of B.O.D. removed.

Naugatuck Chemicals, Division of Dominion Rubber Co. Limited, manufactures a wide variety of rubber, agricultural, industrial chemicals and plastics in its plant at Elmira, Ontario. The industrial waste from these operations currently averages about 0.238 million imp. gallons per day and has a five-day biochemical oxygen demand (B.O.D.) averaging about 700 p.p.m.

The "phenolic" wastes are presently chlorinated and discharged to effluent ponds having no overflows, while the non-phenolic wastes are discharged to equalizing lagoons.

This discussion is intended to outline an investigation of a method to improve present treatment facilities of the industrial wastes shown in Table I. The investigation started in the laboratory and advanced to the pilot plant phase. Two different biological pilot units were used during the study; the trickling filter and activated sludge system. The laboratory and pilot plant trickling filter studies include the treatment of the phenolic waste waters only. The pilot plant activated sludge studies include the treatment of the principal component waste streams shown in Table 1.

The history of the approach to this problem dates from about 1950. Among the various types of industrial organic wastes produced, the most troublesome and costly from the standpoint of treatment, is a dichlorophenol (D.C.P.) containing waste resulting from the production of 2,4-dichlorophenoxyacetic acid (2,4-D). Several different methods of treating this waste water have been investigated in an attempt to improve treatment efficiency and cost of operation.

The alkaline chlorination process was adopted about 1951 and is still in operation today achieving a 95-98% destruction of the dichlorophenol content of the waste. Although the degree of treatment is considered satisfactory for the chlorination process, the treated waste still contains 20-30 p.p.m. of dichlorophenol and hence cannot be discharged to the receiving stream. The cost of treatment is about $1.00 per pound of dichlorophenol destroyed.

Laboratory Investigation

In 1954, it was decided to investigate the bio-oxidation process as a cheaper and more efficient method of treating the "phenolic" waste waters. "Phenolic" wastes are intended here to include both the phenol and 2,4-D component waste streams shown in Table 1. Laboratory studies began with the investigation of synthetic waste waters containing phenol, dichlorophenol and/or 2,4-D acid. Following this, the study advanced to an investigation of the actual plant phenolic waste streams. The laboratory units, Figure 1, were designed to permit continuous feeding of synthetic and plant wastes with continuous removal of the treated effluent. Each unit was seeded with sewage activated sludge and operated with continuous feeding and aeration, 24 hours a day, 7 days a week. Feeds were changed, samples for analysis taken, temperatures recorded, and any changes in operating procedure made at the same time each day. Feed waters and effluents were analyzed for chemical oxygen demand (C.O.D.) and where possible the individual contaminating component in the waste. Nitrogen as ammonium nitrate and phosphorous as potassium dibasic phosphate were added to the feed to give an approximate C:N ratio of 20:1 and C:P ratio of 30:1.

Based on the laboratory investigation of both synthetic and actual plant "phenolic" wastes, it was found that, like phenol, dichlorophenol and 2,4-D acid could also be oxidized by bacterial action. A summary of operation of one of the laboratory units treating 2,4-D waste water is

[1]*Manuscript received July 6, 1959.*
[2]*Naugatuck Chemicals Division of Dominion Rubber Co. Limited.*
Based on a paper presented at the 14th Purdue Industrial Waste Conference, Purdue University, Lafayette, Indiana, U.S.A. May, 1959.

TABLE 1

COMPONENT WASTE STREAMS

	Flow gal./min.	Phenol		B.O.D.	
		p.p.m.	lb./day	p.p.m.	lb./day
Aniline and nitrobenzol	4	–	–	5750	330
Phenol	11	400*	63*	1330	210
2,4-D	10	1320**	190**	2160	310
Misc. chemicals	100	–	–	350	500
Rubber chemicals	15	–	–	280	60
Polyester resins	12	–	–	1020	200
New chemical development	10	–	–	70	10
TOTAL	162		253		1620

*Phenol (Carbolic Acid).
**2,4-dichlorophenol (D.C.P.).

shown in Table 2. Based on the encouraging laboratory results, it was decided to advance to the pilot plant stage of the investigation.

Pilot Plant Trickling Filter Investigation

The pilot plant trickling filter, Figures 2 and 3, was designed as a combined trickling filter and activated sludge system employing Dowpac 10, formerly Dowpac HCS, as the filter media [1,2].

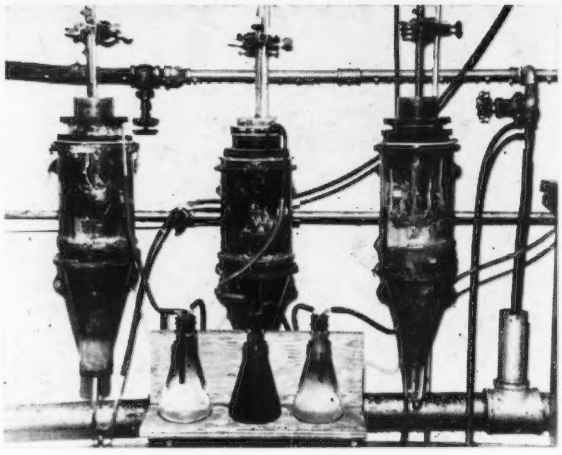

Figure 1—Laboratory biological units.

(a) Investigation of 2,4-D Waste

The pilot unit was seeded with sewage activated sludge. Using the phenol waste water as influent, the biologically active slime was established on the packing and in the activated sludge tank. After activation, the influent was gradually changed to the dichlorophenol containing 2,4-D waste water, to which had been added nitrogen and phosphorous salts to supply a minimum carbon-to-nitrogen-to-phosphorous ratio of 20:2:1. During an 8 month period an attempt was made to treat 2,4-D waste water in the unit, but without the desired success.

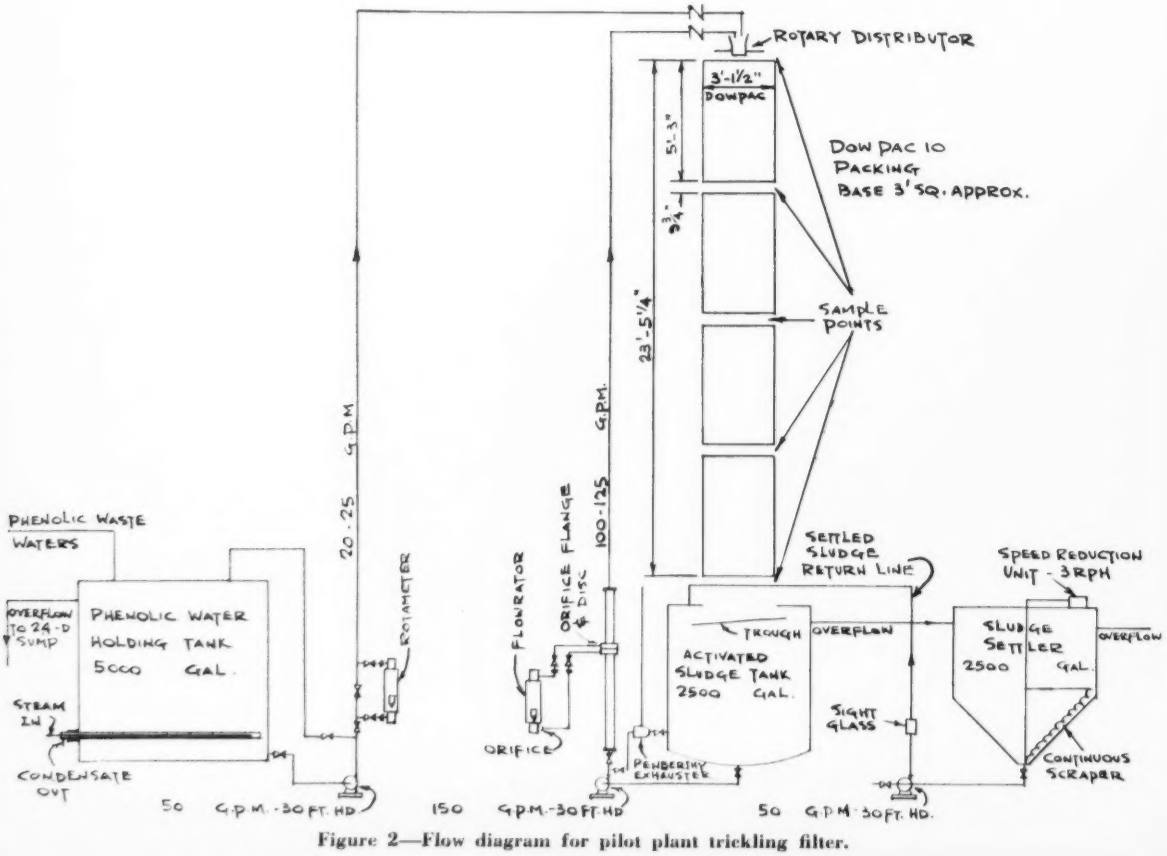

Figure 2—Flow diagram for pilot plant trickling filter.

TABLE 2

OPERATING SUMMARY — LABORATORY BIOLOGICAL UNIT
2,4-D WASTE WATER

	Influent		Effluent		% Removal
	Max.	Av.	Max.	Av.	
Flow, influent, litres/day	0.8	0.5	0.8	0.5	–
Flow, dilution, litres/day	4.8	3.0	4.8	3.0	–
Flow, pH	8.3	7.9	8.8	8.7	–
D.C.P., p.p.m. (after dilution)	148	138	9	7	–
D.C.P., removed, lb./1000 cu. ft./day	–	–	31	25	95
C.O.D., p.p.m. (after diution)	1045	970	240	195	–
C.O.D., removed lb./1000 cu. ft./day	–	–	175	150	80

	Max.	Av.
Temperature, °F	74	72
Air loading, cu. ft./(min.)(sq. ft.)	1.5	1.2
Clarification area overflow rate, gal./(min.)(sq. ft.)	0.010	0.006

When operating on 2,4-D waste alone, suspended solids could not be held in the activated sludge tank. The biological growth on the packing changed from a gelatinous material characteristic of phenol waste treatment to a rather hard pebbly slime. When any of the biological growth on the packing sloughed off, it was not replaced. At one period of operation the influent consisted of a synthetic waste water containing only dichlorophenol. The result was the same as when treating the actual dichlorophenol containing 2,4-D waste water. This study showed that dichlorophenol, although it can be classified as a "phenolic" compound can not be satisfactorily oxidized biologically under the same conditions as can phenol. The reaction of the bacteria to the dichlorophenol indicated also that the latter is a protoplasmic poison that inhibits in some way the normal metabolic processes of the bacteria. Chlorine itself is a well known bactericide and there was evidence here to indicate that the introduction of chlorine into the phenol molecule creates a compound, dichlorophenol, that is apparently toxic to the bacterial culture which existed during the study.

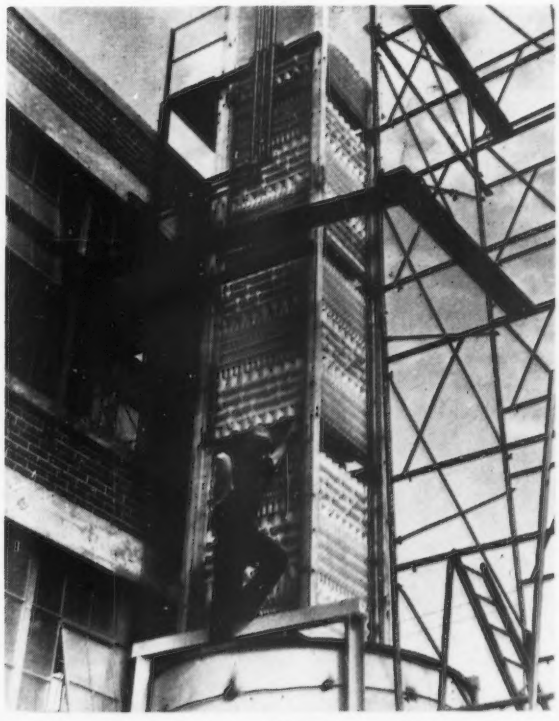

Figure 3—Pilot plant trickling filter.

Actually the pilot unit treated 400-500 gallons of 2,4-D waste water per day. Before being applied to the filter, however the waste was diluted with water. During the most efficient period of operation, an average of 7.8 lb. per day of dichlorophenol were removed at an efficiency of 86%. In addition, an average of 16.7 lb. per day of chemical oxygen demand (C.O.D.) were removed showing an average removal of 70%. A summary of the operation of the unit treating 2,4-D waste water is shown in Table 3. Although operation of the pilot unit on this waste could not be called a failure, it could not be considered commercially feasible, since the unit could neither treat a sufficiently large volume of the waste, nor could the dichlorophenol content of the effluent be reduced below that which could be achieved by chlorination.

(b) Investigation of Phenol Waste

At the end of the 2,4-D production season, a portion of the phenol (carbolic acid) waste water shown in Table 1 was very successfully treated in the unit. An average of 11.8 lb. per day of phenol were removed showing an average removal of 99.5%. In addition, an average of 30.3 lb. per day of C.O.D. was removed showing an average removal of 95.3%. A summary of this operation is shown in Table 4. Although it was not the ultimate objective,

TABLE 3
OPERATING SUMMARY — PILOT PLANT (DOWPAC 10) TRICKLING FILTER
2,4-D WASTE WATER

	Influent		Packing Effluent			Aeration Tank Effluent			Total Percent Removal
	Max.	Av.	Max.	Av.	Av. % Removal	Max.	Av.	Av. % Removal	
Flow, influent, gal./min.	0.4	0.3	0.4	0.3	–	0.4	0.3	–	–
Flow, dilution, gal./min.	4.0	3.0	4.0	3.0	–	4.0	3.0	–	–
Flow, pH	8.3	7.8	–	–	–	7.9	7.7	–	–
D.C.P., p.p.m. (after dilution)	250	205	60	30	–	60	30	–	–
D.C.P., removed, lb./1000 cu. ft./day	–	–	49	38	86	nil	nil	nil	86
C.O.D., p.p.m. (after dilution)	780	585	215	170	–	215	170	–	–
C.O.D., removed, lb./1000 cu. ft./day	–	–	142	87	70	nil	nil	nil	70

	Max.	Av.
Temperature, °F	82	80
Recirculation, gal./min.	20	20
Recirculation ratio	6.1	4.6
Clarification area overflow rate, gal./(min.)(sq. ft.)	0.07	0.05
Mixed liquor solids, ml./1000 ml	nil	nil
Mixed liquor suspended solids, p.p.m.	nil	nil
Sludge volume index, %	nil	nil

TABLE 4
OPERATING SUMMARY — PILOT PLANT (DOWPAC 10) TRICKLING FILTER
PHENOL WASTE WATER

	Influent		Packing Effluent			Aeration Tank Effluent			Total Percent Removal
	Max.	Av.	Max.	Av.	Av. % Removal	Max.	Av.	Av. % Removal	
Flow, influent, gal./min.	5.0	3.2	5.0	3.2	–	5.0	3.2	–	–
Flow, dilution, gal./min.	1.4	1.0	1.4	1.0	–	1.4	1.0	–	–
Flow, pH	10.3	8.2	–	–	–	8.2	7.3	–	–
Phenol, p.p.m. (after dilution)	500	240	20	8	–	1.2	0.8	–	–
Phenol, removed, lb./1000 cu. ft./day	–	–	110	57	97	3.1	0.9	86	99
C.O.D., p.p.m. (after dilution)	1424	730	186	102		114	57	–	–
C.O.D., removed, lb./1000 cu. ft./day	–	–	225	136	88	11	9	50	95

	Max.	Av.
Temperature, °F	83	80
Recirculation, gal./min.	20	20
Recirculation ratio	4.8	3.1
Clarification area overflow rate, gal./(min.)(sq. ft.)	0.10	0.07
Mixed liquor solids, ml./1000 m.	110	90
Mixed liquor suspended solids, p.p.m.	1200	1020
Sludge volume index, %	92	81

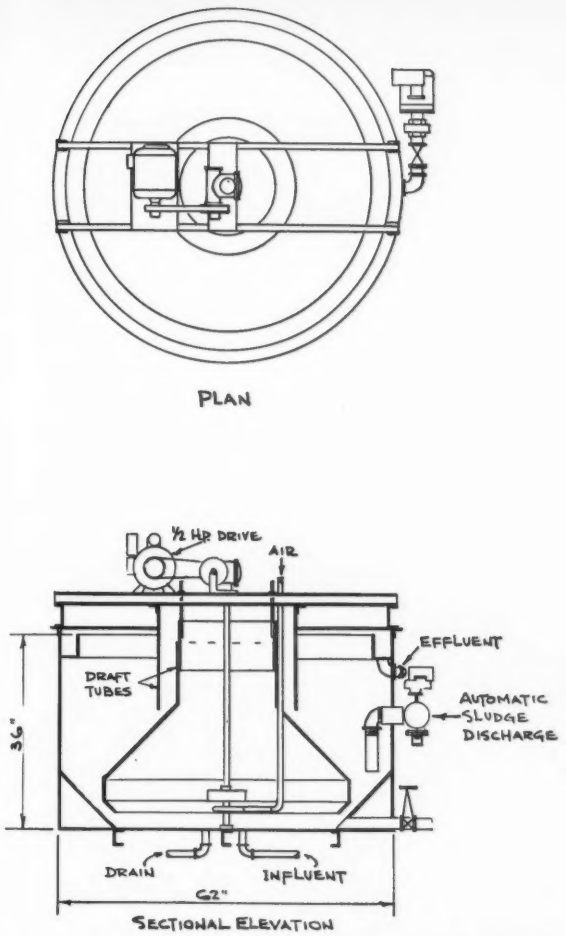

Figure 4—Aero-accelator pilot plant—17 cu. ft. aeration volume.

it was estimated that by increasing the packing capacity by a factor of 4, or by adding three additional towers, the total volume of the phenol waste water could be treated on the Dowpac pilot unit. The estimated cost of treating the total phenol waste stream in an expanded unit was calculated to be $0.26 (summer operation) to $0.34 (winter operation) per pound of phenol removed. This cost includes amortization, labor, power, steam, laboratory services and nutrients.

Pilot Plant Activated Sludge Investigation

Following the pilot plant trickling filter studies, it became apparent that improved treatment facilities were required, not only for the phenolic wastes, but also for the non-phenolic wastes presently discharged to the equalizing lagoons. It was therefore decided to further the study by investigating the activated sludge process.

In the general field of industrial waste treatment there is increasing recognition of the advantages of activated sludge treatment in a completely mixed system. Such a system can, of course, handle shock loads effectively, because feed to the system is dispersed rapidly throughout the entire mass of activated sludge. Furthermore, it is possible to operate a completely mixed system at much higher loads than have characterized the traditional activated sludge flow sheet in the past.

In November 1957 further studies were undertaken with an Aero-Accelator pilot plant. The pilot unit, Figure 4, provided a completely mixed aeration volume and clarification zone in a single basin. It was 62 in. in diameter and had an aeration volume of approximately 17 cu. ft.

A complete study program was set up and carried out under the direction of the pilot plant manufacturer [3]. The pilot work was a complex problem involving the control of temperature, air requirements, oxidation reduction potential, dissolved oxygen, nutrient addition, degree of neutralization, aeration solids, biochemical oxygen demand (5-day, 68°F.), and numerous other less important factors. The chemical and biochemical analyses carried out during this investigation were essentially those outlined in the 10th Edition of "Standard Methods" [4].

Since previous studies indicated that the dichlorophenol containing 2,4-D waste water would not in itself support a biological floc, it was decided to attempt to treat this waste in the Aero-Accelator pilot unit along with other more amenable waste waters.

The laboratory and pilot plant trickling filter studies previously discussed, deal only with the treatment of the phenolic waste waters. The pilot plant activated sludge studies discussed in the remainder of this paper, include an investigation of the treatment of the principal component waste streams shown in Table 1. For this reason there is no direct comparison between the laboratory and trickling filter, and the activated sludge studies.

Since the first four component waste streams shown in Table 1 would make up about 80% of the total organic and hydraulic loading to a full scale plant, pilot studies were limited to these four waste streams only. The waste stream from the production of polyester resins was not included in the study since this waste did not exist at the time of the pilot plant investigation. In addition, the time-honored method of investigating each individual waste stream was largely abandoned in an attempt to shorten the study period.

The Aero-Accelator pilot plant was seeded with sewage activated sludge and a satisfactory biological floc established on an influent consisting of the aniline and nitrobenzol, and phenol waste waters. After activation, the proportion of 2,4-D waste water in the feed mixture was gradually increased until the aniline and nitrobenzol, phenol and 2,4-D waste streams, to which nitrogen and phosphorous additions were made, were fed to the unit in the ratio of their respective flow rates. The Aero-Accelator pilot unit operated for about two weeks on this influent, and then for no apparent reason, the characteristics of the mixed liquor solids in the aeration zone deteriorated and the floc was lost. The unit was again seeded and operated under the same conditions as before, but again the floc was lost after a two week period of operation. Trace amounts of cobalt, manganese and ferrous salts were added to the unit and this addition appeared to have a beneficial effect on the characteristics of the mixed liquor solids. By this addition the initial period of operation was extended and the Aero-Accelator pilot unit operated for another five weeks before any further sign of floc deterioration was noticed. When this occurred the trace element addition was replaced by the daily addition of settled sewage. The affect of the sewage on the sludge characteristics is shown in Figure 5, where the settling rate is plotted both before and after the sewage addition. The mixed liquor suspended solids concentration was essentially the same for both curves. The sludge settling rates were observed in a 1000 ml. glass graduate. The pilot unit continued to operate for an additional three

weeks on the influent composed of the aniline and nitrobenzol, phenol, and 2,4-D waste waters. Operation was successful during this period due to the daily addition of settled sewage [5].

Once the problem of essential nutrient requirement was resolved, the study was able to proceed and during the next phase of the investigation the miscellaneous chemical waste stream was included in the Aero-Accelator pilot plant influent. This waste was previously excluded, since it was an unknown from a biological standpoint because no previous laboratory or pilot plant work had been carried out on it. The influent first investigated consisted of the miscellaneous chemicals, phenol, and aniline and nitrobenzol waste streams. Operation was excellent. The second influent investigated consisted of the above three waste streams, plus the 2,4-D waste. Operation was still good, but conditions of operation were slightly more critical. A summary of the operation of the Aero-Accelator pilot unit on these two influents is shown in Table 5.

From the data obtained in this last phase of the study, it was felt that the major characteristics of the activated sludge system were known and a full plant scale design could be considered.

The seven main factors which govern the design of a full scale treatment plant were calculated and are as follows:

1. The optimum temperature of the operation was found to range between 73° and 88°F. The median temperature was 85°F.
2. The B.O.D. loading of the activated sludge system was found to vary considerably with the various raw waste streams. On the typical waste-miscellaneous chemicals, phenol, aniline and nitrobenzol, and 2,4-D, a maximum B.O.D. loading of 375 lb. per 1,000 cu. ft. of aeration volume per day was obtained. Without the 2,4-D waste, a maximum loading of 790 lb. B.O.D. per 1,000 cu. ft. was possible, but this loading produced excessive sludge bulking. A successful loading (no bulking) was 200 lb. B.O.D. per 1,000 cu. ft. While this loading is somewhat higher than the average value shown under Influent No. 2 in Table 5, it is nevertheless a loading that lies within the range of satisfactory operation.
3. The air requirements for oxidation of the organics with the bacteria operating in the logarithmic growth phase, again when treating the typical waste including 2,4-D, was 1.3 lb. oxygen per lb. of B.O.D. This oxygen requirement is based on a substrate temperature of 85-87°F. and a minimum mixed liquor dissolved oxygen content of 2.0 p.p.m.
4. The hydraulic loading of the clarification unit to produce an acceptable quality effluent from the Aero-Accelator pilot plant was found to be 0.24 gal./(min.)(sq. ft.) The controlling loading of the Aero-Accelator pilot unit was, however, the B.O.D. loading, rather than clarification. The design overflow rate was selected from the sludge subsidence tests, rather than the hydraulic throughput for the pilot unit. It is believed that a slightly higher rise rate can be tolerated in the full scale unit. In this connection, it is of interest to note that the 2,4-D waste results in a considerably more dense and more rapidly settling sludge than is produced when this waste is not present in the stream being investigated.
5. Based on a total waste flow of 165 gal./min., a dilution factor of 3.4 was found necessary for the process to proceed successfully.

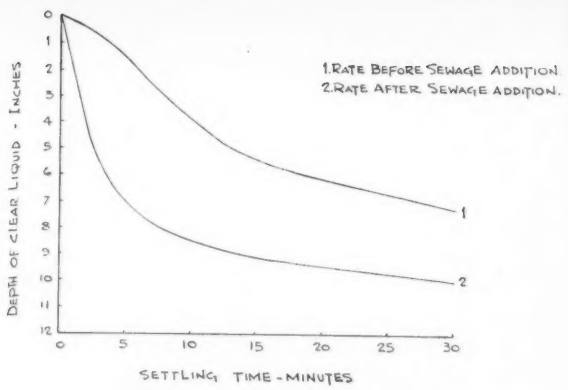

Figure 5—Sludge settling curve.

6. The levels of essential nutrients and essential metabolite supplement necessary to insure active growth in the biological system are as follows:
   (a) The B.O.D.:N ratio must be no greater than 20:1. Lesser ratios may be tolerated.
   (b) The B.O.D.:P ratio must be no greater than 100:1, and may vary to 80:1.
   (c) Essential metabolites in the form of sewage should be added in a ratio of 1:600 on a weekly basis.
7. It is estimated that the phenol content of the treated effluent will be less than 1 p.p.m. when influent concentration ranges up to 500 p.p.m., less than 1.5 p.p.m. when influent ranges up to 1,000 p.p.m., and less than 3 p.p.m. when the influent contains up to 3,000 p.p.m. phenol. B.O.D. reduction is estimated to be of the order of 90-95%.

Figure 6 shows the principle dimensions of the Aero-Accelator Type AR unit which was recommended for this

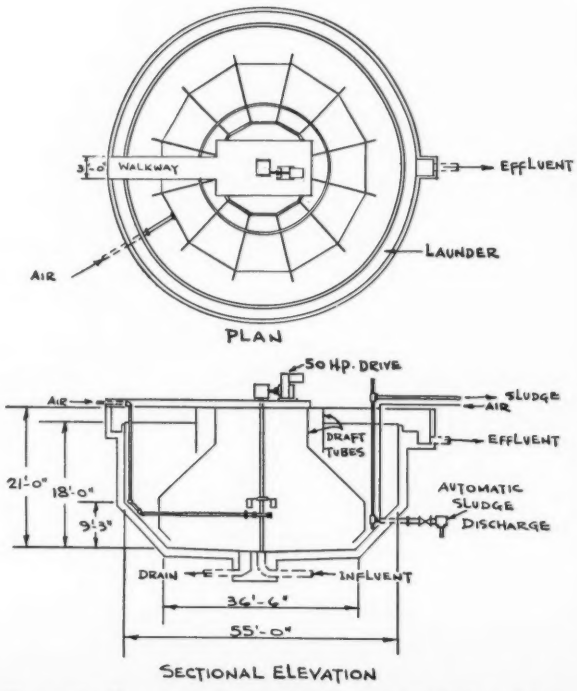

Figure 6—Proposed aero-accelator activated sludge plant.

TABLE 5

OPERATING SUMMARY — PILOT PLANT AERO ACCELATOR
GENERAL PLANT WASTE WATER

	Influent No. 1					Influent No. 2				
	Infl.		Effl.		% Removal	Infl.		Effl.		% Removal
	Max.	Av.	Max.	Av.		Max.	Av.	Max.	Av.	
Flow, influent, gal./min.	17.4	12.5	17.4	12.5	–	9.9	7.5	9.9	7.5	–
Flow, dilution, gal./min. (50% tapwater) (50% effluent)	53	37	65	37	–	37	25	34	25	–
Flow, pH	7.7	7.4	7.8	7.5	–	7.9	7.4	8.0	7.5	–
B.O.D. (5-day, 68°F.) p.p.m. (after dilution)	860	730	84	46	–	375	330	86	61	–
B.O.D., removed, lb./1000 cu. ft./day	–	–	790	350	95	–	–	375	130	88

	Influent No. 1		Influent No. 2	
	Max.	Av.	Max.	Av.
Temperature, °F	88	86	88	86
Air loading, cu. ft./(min.)(sq. ft.)	1.5	1.4	1.2	0.9
Clarification area overflow rate, gal./(min.)(sq. ft.)	0.10	0.06	0.11	0.06
D.O., aeration zone, p.p.m.	3.7	0.5	2.9	1.0
Mixed liquor solids, mil./1000 ml	810	444	600	480
Mixed liquor suspended solids, p.p.m.	8492	7566	8830	8075
Sludge volume index, %	104	59	76	60

Influent No. 1 — Misc. chem. – 100; Phenol – 11; Aniline and nitrobenzol – 4
Influent No. 2 — Misc. chem. – 100; Phenol – 11; Aniline and nitrobenzol – 4; 2,4-D – 10

application. Some extra capacity was included to provide for overloads which may inadvertently occur. Basis for the design of this unit, of course, stems from the analysis of the pilot plant study. The operational characteristics of the unit are as follows:

Flow capacity ..... 560 gal./min.
Hydraulic loading ..... 0.3 gal./(min.)(sq. ft.)
B.O.D. capacity ..... 2760 lb./day
B.O.D. loading—202 lb./1000 cu. ft. aeration volume/day
Nominal air required ..... 1300 stand. cu. ft./min.
Maximum air capacity ..... 1350 stand. cu. ft./min.
Power to drive unit ..... 50 h.p.

The 1300 stand. cu. ft./min. air is based on supplying 3580 lb. of oxygen per day, and is based on a 12% oxygen transfer efficiency.

Conclusion

From the laboratory and pilot plant investigations described, design criteria was ultimately developed for biological treatment of an industrial effluent containing toxic 2,4-D waste water. The following significant facts were established during this study:

1. The trickling filter design, employing Dowpac 10 as the filter media, is a satisfactory device for oxidizing phenol (carbolic acid). An average phenol removal of 99.5% and a chemical oxygen demand (C.O.D.) removal of 95.3% was obtained.
2. Dichlorophenol, although a phenolic compound, cannot be satisfactorily oxidized by bacterial action under the same conditions as can phenol. However, by treating the dichlorophenol containing 2,4-D waste water along with other more amenable waste streams, the phenolic content of the waste can be satisfactorily oxidized, providing certain critical nutrient and dilution requirements are observed.
3. In a preliminary assessment of the operation of the full scale Aero-Accelator waste treatment plant, it was calculated that the total industrial effluent, including the 2,4-D waste water, could be treated for the same total yearly cost as is currently experienced for the treatment of the 2,4-D waste alone.

References

(1) Bryan, E. H., Molded Polystyrene Media for Trickling Filters, Industrial Wastes, 1, 2, 80 (Nov.-Dec. 1955).
(2) Plastics Technical Service Bulletin, "Dowpac NF-90 and Dowpac HCS", The Dow Chemical Company, (1955).
(3) Technical Service Bulletin, 0-65-2-2A, Infilco Inc., (1954).
(4) "Standard Methods for the Examination of Water, Sewage, and Industrial Wastes", 10 Edition, APHA; AWWA; FSIWA (1955).
(5) Oginsky, E. L., Umbrait, W. W., "An Introduction to Bacterial Physiology", W. H. Freeman & Company, San Francisco, (1954).

★ ★ ★

An Analysis of Air and Solid Flow in a Spouted Wheat Bed[1]

B. THORLEY[2], *J. B. SAUNBY*[3], *K. B. MATHUR*[4] *and G. L. OSBERG*[5]

Detailed studies of the air and solid flow patterns in a spouted wheat bed have been made in column sizes up to 2 ft. in diameter. Orifice size, cone angle, bed height and air flow were varied so as to establish their effect on these flow patterns. Air flow within the bed was obtained from pressure drop gradients, and solid flow was obtained from particle velocity measurements taken at the wall. Pressure drop, air flow distribution between spout and annulus, solid circulation rate and flow line data are summarized. A correlation is proposed which relates pressure drop and particle velocity at the top of the bed with superficial air velocity at air flows above minimum spouting. Particle velocity measurements in the spout were made from photographs, and were calculated approximately from the drag equation for a single particle.

THE contacting of fluids and granular solids in a spouted bed has received special study in these laboratories in recent years. Early work by Mathur and Gishler [1] described the mechanism of spouting, and produced an empirical correlation for predicting the minimum air required for spouting a variety of materials. Publications have appeared on heat transfer [2] and on potential applications to the drying of wheat and wood chips [3,4,5]. Recent studies have been made of the flow patterns of air and solid within the spouted bed with the object of developing rational correlations for predicting spouted bed behavior.

The general flow of wheat particles in a spouted bed is illustrated in Figure 1. Wheat particles are lifted as a dilute suspension through the central core, 1, by a high velocity air stream. At the top of the bed, 2, where the central stream velocity is suddenly reduced, the wheat particles fall back onto the bed. These then flow, as a slowly moving packed bed, 3, downward and toward the spout. The air enters the column through an orifice, 4, flows up the spout and up through the void space in the moving packed bed.

This paper summarizes the observations made on column sizes up to 2 ft. I.D. Pressure drop, minimum air flow, and the effect of design variables on air and solid flow patterns were measured, the design variables studied being bed depth, inlet diameter, cone angle and column size.

EXPERIMENTAL

Data were obtained from three columns: 0.5 ft. I.D. x 4 ft. glass, 1 ft. I.D. x 7 ft. steel column fitted with plexiglass windows and a 2 ft. I.D. x 8 ft. plexiglass column: 0.5 ft. and 2 ft. I.D. semicircular columns with plexiglass fronts were also used. Cone angles and orifice sizes were changed by insertions between flanges provided for this purpose. Straightening vanes were placed in the approach pipe to the column. The air was filtered and then metered with a calibrated orifice.

Air and solid flow rates within the spouted bed were measured as before [1] except that the static pressure measurements were made with a Betz Manometer sensitive to 0.01 mm. of water.

Pressure Drop Across a Spouted Bed

The relationship between pressure drop and air flow is shown in Figure 2 for wheat spouting in a 2 ft. I.D. column, at 24 in. and 70 1/2 in. bed depths. The section, AB on the curve corresponds to the pressure drop through a fixed bed plus the additional pressure required to form an internal spout within the bed. Wheat particles must be pushed upward against the weight of the bed. Void volume in the packed bed surrounding the cavity is reduced and so pressure drop is increased. As the internal spout moves up the cone, a point is reached where the pressure drop decreases, (section BC), due to the decreasing length of packed bed between the internal spout and the top of the bed. Further increases in flow result in a sharp drop in pressure drop at D, where the internal spout breaks through the surface of the bed. Point E is defined as incipient spouting. At flows beyond E, pressure drop remains approximately constant.

When the air flow is reduced, pressure drop follows the path EE′, D′. At E′, the spout suddenly collapses.

[1]*Manuscript received July 2, 1959.*
[2]*NRC Post-doctoral Fellow, 1953-55. Present address: Cabot Carbon Limited, England.*
[3]*NRC Post-doctoral Fellow, 1957-59. Present address: Union Carbide Chemicals Company, South Charleston 3, W. Va., U.S.A.*
[4]*Junior research officer 1954-55. Present address: Imperial Chemical Industries (India), 34 Chowringhee, Calcutta 16, India.*
[5]*Division of Applied Chemistry, NRC, Ottawa, Ont.*
Based on a paper presented to the C.I.C. Chemical Engineering Conference, Sarnia, Ont. March 1956. Contribution from the Division of Applied Chemistry, National Research Council. Issued as No. 5311.

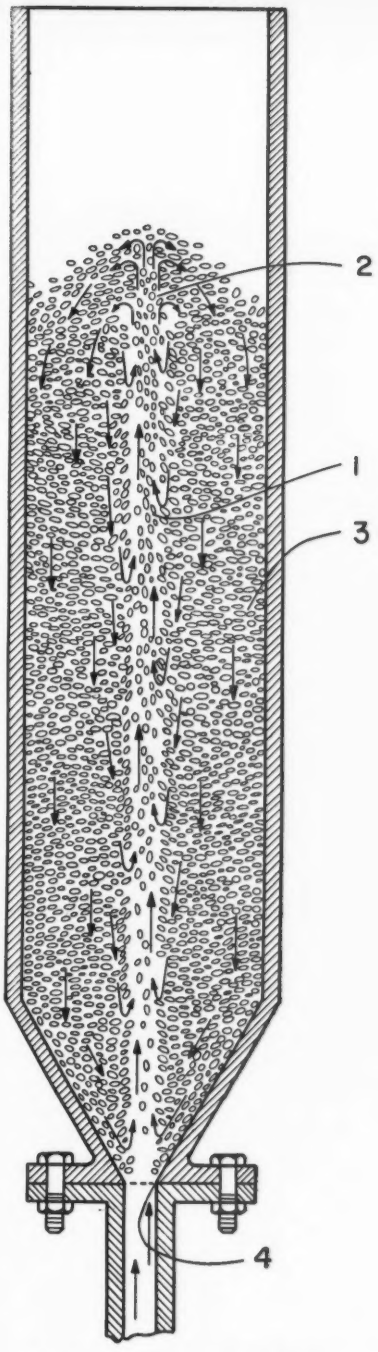

Figure 1—Spouted wheat bed.

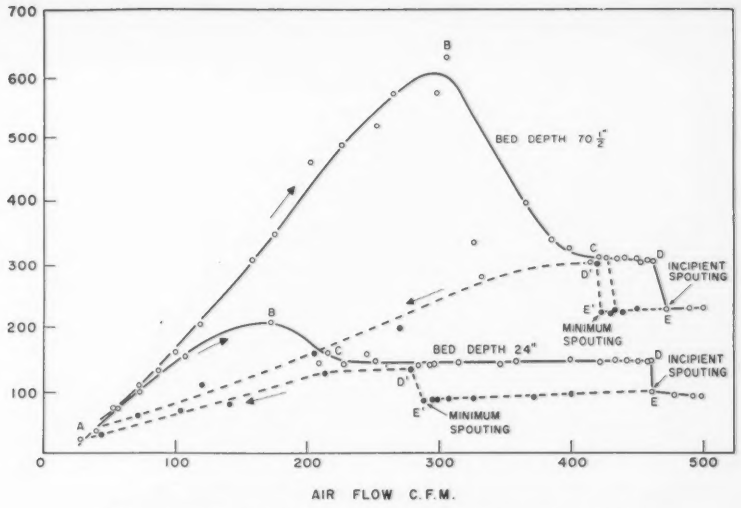

Figure 2—Pressure drop vs. air flow. $D_c = 2$ ft.; $D_i = 2$ in.; $L = 2$ & 5.9 ft.; cone 45°.

The air flow corresponding to E′ is defined as minimum spouting flow, and is selected for correlation purposes because it can be reproduced reliably. The section D′A corresponds to the pressure drop flow relationship for the packed bed of wheat. The data for this section can be predicted by the Ergun equation for packed beds [6].

The data for the two bed heights are shown to illustrate the magnitude of the hysteresis loop, and to show that the difference between incipient and minimum spouting air flow decreases as bed height is increased. The maximum pressure corresponding to B is not readily correlated since it depends on packing and compressive effects which are variable.

The location of pressure taps in the orifice region introduces variable effects. A negative pressure was noted in the cone just above the orifice presumably due to a Venturi effect. The data used in Figure 2 were obtained from pressure taps located in the entrance pipe and at the top of the bed. The empty column value was subtracted from the full column value to give the net pressure drop across the bed. When the pressure tap was located in the cone (1/3 of cone height), the pressure drop data obtained showed close agreement with the Ergun equation for packed beds. The hysteresis loop was also smaller. The pressure drop data reported in the Tables were obtained with pressure taps located in the cone and at the top of the bed.

Attempts to correlate observed spouted bed pressure drop data with packed bed properties were not successful probably because the pressure drop is largely determined by the pressure drop across the spout. The pressure drop gradient is low near the orifice, and increases to an approximately constant value at the top of the bed. This changing gradient is due to air flowing out of the spout into the bed and wheat flowing into the spout, which causes a change in density of the wheat-air mixture in the spout with bed height. At low bed depths the pressure drop data in Table 1 expressed as $\Delta P/L\rho_p$ has a value between 0.25 and 0.3, but, when $L/D > 2$ values range from 0.35 - 0.45 with an average value of 0.4.

The maximum pressure drop across an unrestrained bed is equal to the weight of the bed

$$\Delta P = L\rho_p(1 - \epsilon_b) \quad \ldots\ldots\ldots\ldots\ldots\ldots\ldots\ldots (1)$$

For wheat ϵ_b is equal to 0.4 and hence $\Delta P/L\rho_p = 0.6$. The pressure drop across a spouted bed is therefore approximately equal to 2/3 the pressure due to the weight of the bed.

When the pressure drop across a bed of wheat is equal to the weight of the bed, spouting no longer occurs. The bed height at which this occurs is just above the maximum spoutable bed height. The corresponding gas velocity may be calculated by substituting for $\Delta P/L$ from Equation (1) in the Ergun equation

TABLE 1

SUMMARY OF PRESSURE DROP AND SOLID FLOW DATA AT VARYING AIR FLOW RATES AND BED HEIGHTS

D_c ft.	L ft.	°Cone	D_i in.	U_c ft./sec.	ΔP lb./ft.^{2}	h_s ft.	k ft./sec./ ft.	V_o ft./sec.
0.5	1.0	60	0.5	2.58	20.3	1.25	–	–
				2.66	20.5	1.29	0.0	.088
				2.95	19.9	1.5	0.0	.100
				3.21	19.2	1.75	0.0	.117
				3.51	18.8	2.0	0.0	.129
				3.77	18.4	2.25	0.0	.139
	1.5	60	0.5	3.10	44.4	1.75	–	–
				3.13	47.3	1.75	0.074	.165
				3.59	44.5	2.05	0.073	.168
				4.02	44.3	2.30	0.078	.194
	2.0	60	0.5	3.47	64.0	2.17		
				3.61	66.5	2.30	0.090	.228
				3.69	66.1	2.34	0.091	.235
				4.06	65.7	2.54	0.096	.262
				4.23	66.2	2.66	0.100	.283
1.0	2.0	60	1.0	1.81	41.7	3.08		
				2.01	40.7	3.08	0.005	.064
				2.20	37.8	3.83	0.008	.076
				2.36	34.4	4.5	0.007	.082
				2.52	31.7	5.0	0.007	.086
1.0	4.0	60	1.0	2.52	118	4.58		
				2.58	112	4.66	.015	.123
				2.65	112	4.92	.017	.129
				2.72	116	5.08	.019	.135
				2.83	107	5.75	.026	.158
				2.95	106	6.08	.027	.168
				3.04	110	6.58	.030	.175
				3.12	103	6.82	.033	.180
	6.0	60	1.0	2.58	214	6.3	0	
				2.83	211	6.5	.027	.202
				2.93	212	6.65	.031	.218
				3.06	214	7.15	.040	.248
				3.13	215	7.4	.045	.267
				3.20	211	7.65	.051	.289
2.0	3.0	60	2.0	1.51	59.8	6.55	0	.028
2.0	4.0	60	2.0	1.80	90.5	7.32	0	.036
				1.85	97.0	8.0	0.0007	.039
				1.91	98.0	8.25	0.0008	.040
				1.97	99	8.75	0.001	.043
				2.02	99	9.34	0.0011	.044
				2.08	101	10.0	0.0014	.045
				2.15	111	10.8	0.0013	.047
				2.22	121	11.8		
2.0	5.0	60	2.0	2.06	130	8.5	.0011	.045
2.0	6.0	60	2.0					
				2.21	183	9.1	.0036	.060
				2.25	182	9.7	.0037	.062
				2.30	185	10.1	.0039	.063
				2.36	185	11.1	.0042	.066
				2.39	187	11.7	–	–

$$g\frac{\Delta P}{L} = \frac{150}{D_p^2}\mu_f\frac{(1-\epsilon_b)^2}{\epsilon_b^3}U_m + 1.75\frac{(1-\epsilon_b)}{\epsilon_b^3}\rho_f\frac{U_m^2}{D_p} \quad \ldots\ldots(2)$$

giving

$$1.75\rho_f D_p.\ U^2_m + 150\mu_f(1-\epsilon_b).\ U_m - D^2_p\epsilon^3_b\rho_p g = 0$$

The maximum spoutable bed depth can now be calculated by equating the value for U_m, obtained by solving the above quadratic, to the standard spouted bed Equation (3). Figure 3 shows the agreement between calculated and experimental values for a variety of materials reported earlier [1].

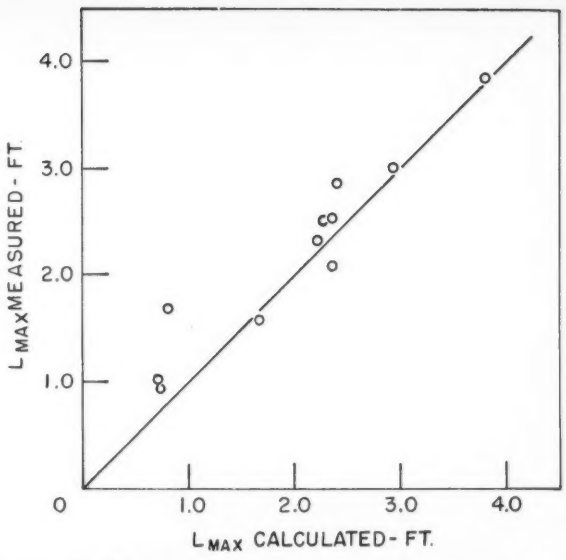

Figure 3—Measured vs. calculated maximum spoutable bed depth.

Minimum Spouting Velocity

Previous work [1] on 6, 9, and 12 in. I.D. columns resulted in an empirical equation for minimum spouting velocity

$$U_m = (D_p/D_c)(D_i/D_c)^{1/3}\,2gL\left(\frac{\rho_p-\rho_f}{\rho_f}\right)^{1/2} \quad \ldots\ldots(3)$$

Minimum air flows were measured for the 2 ft. I.D. column using three different orifices and three different cone angles. The data are summarized in Table 2. For varying orifices the air flow required for minimum spouting increased slightly with orifice diameter. A two fold change in D_i, (1-7/8 in. to 4 in.), caused about 10% increase in minimum air required for spouting. This change is in agreement with previous data [1].

The effect of cone angle on minimum spouting velocity is not large. The minimum spouting velocity was similar for 45° and 60° cones but about 10% higher with the 85° cone. This difference is larger than the experimental error, but is not sufficient to justify any change in Equation (3). The calculated values based on Equation (3) are shown in Table 2. These are about 10% lower than the observed values.

TABLE 2

MINIMUM INCIPIENT AIR VELOCITIES FOR SPOUTING WHEAT IN 2 FT. COLUMN

Cone Angle°	Di in.	L ft.	U_I ft./sec.	U_m ft./sec.	U_m (calc)
45	4	5.9	2.51	2.24	2.16
		5.0	2.45	2.15	1.99
		4.1	2.41	1.95	1.80
		3.0	2.60	1.67	1.55
60	4	6.0		2.16	2.18
		5.0		2.05	1.99
		4.0		1.88	1.78
85	4	6.1		2.48	2.20
		5.2		2.33	2.03
		4.1		2.17	1.80

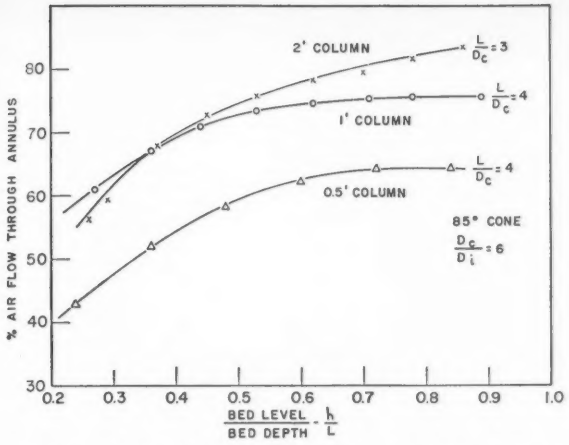

Figure 4—Effect of column diameter on air flow pattern.

AIR FLOW PATTERN

Air Flow in the Annulus

The distribution of air between spout and annulus is important in assessing the effectiveness of the gas-solid contact. Previous work [1] with the 0.5 ft. I.D. column has shown that up to 70% of the total gas flowing passes through the annulus. The distribution in a 2 ft. column was therefore examined under various conditions.

Air flow was estimated from pressure drop measurements at different bed levels. A relationship between pressure gradient and air flow was first established empirically using a packed bed. Measurements were also made of pressure drop per foot of bed height in a moving packed bed in which air and solid flow was maintained at the same value as in the annulus of a spouted bed. The pressure drop per foot vs. air flow curves were similar in magnitude and shape in both cases. Pressure drop profiles measured in the annulus of a spouted bed were converted to velocities using these curves and hence volume flows were obtained.

Radial pressure gradients were small compared with the vertical pressure gradient so that the horizontal component of flow was neglected. The error introduced in neglecting horizontal air flow is significant only when L/r_0 ratios are small ($L/r_0 < 1$). It is also assumed that the void fraction in the moving annular bed is the same as the void fraction in the stationary packed bed. This is a reasonable assumption in the main body of the bed, but is not justified in the cone region, or at the top of the bed. In the cone particles tend to a preferred orientation as they are deflected into the spout. At the top of the bed, near the spout, the bed is expanded and a higher voidage results.

Effect of Design Variables on Air Flow Pattern

Air distribution within the annulus was measured under varying conditions in several different columns. Figure 4 shows the percentage of the total air flowing through the annulus at various fractional bed levels. The annular air flow increases with column diameter. Flow data are not recorded for the cone region or at the top of the bed because of the changes in void volume in these regions.

In Table 3, the ratio Q_a/Q, for the 2 ft. column, is tabulated at several fractional bed levels. In the first group of data, the cone angle and orifice size are constant, the bed depth varying from 3-6 ft. As bed height is increased, air flow required for spouting also increases,

TABLE 3

AIR FLOW DISTRIBUTION IN ANNULUS OF 2 FT. I.D. COLUMN

Cone Angle°	Di in.	Q s.c.f.m.	L ft.	Q_a/Q at 2 ft. Level	3.3 ft. Level	4.2 ft. Level	5.0 ft. Level	5.8 ft. Level
60	2	234	3	1.02				
60	2	286	4	.75	.90			
60	2	337	5	.56	.67	.80	.90	
60	2	370	6	.48	.59	.71	.80	.88
60	2	370	6	.48	.59	.71	.80	
60	3	427	6	.59	.68	.78	.83	
60	4	448	6	.62	.71	.79	.83	
45	2	382	6	.58	.65	.74	.82	.89
60	2	374	6	.48	.59	.71	.81	.88
85	2	363	6	.40	.53	.66	.77	.87
85	2	340	6	.47	.61	.74	.83	
85	2	371	6	.41	.55	.68	.75	
85	2	402	6	.36	.49	.61	.70	

but at the same level of bed approximately the same volume of air flows through the annulus section. At the 3.3 ft. level the volume of air flowing through the annulus in 4, 5, and 6 ft. beds was 257, 226, and 218 c.f.m. respectively. In the second group of data, bed height, and cone angle are constant, and orifice size varies. The ratio Q_a/Q increases with increasing orifice size, particularly in the lower half of the bed. In the third group, bed height and orifice size are constant, but cone angle is varied. These data show that more air flows into the annulus particularly to the lower section, when the cone angle is small. In the last group of data, air flow was increased from 110 to 120% and 130% of minimum spouting flow. As air flow increased, the annular flow remained essentially constant. At the 4.2 ft. level for example, the volumetric flows were 252, 252 and 245 c.f.m. respectively, indicating that the excess air passed through the spout.

This data on annular air flow suggests that the most effective contact between gas and solids occurs when column diameter and orifice diameter are at a maximum, and total air flow and cone angle are at a minimum.

Air Flow Through Spout

Air flow through the spout at different bed levels is obtained from the difference between the total air flow and that calculated as flowing through the annulus. The linear velocity is obtained from a knowledge of the spout diameter. The effect of design variables on the air flow in the spout may therefore be deduced from the preceding discussion on annular air flow.

Spout Diameter

The spout diameter was measured from photographs of the vertical section through the spout in a semi circular column. It is assumed that the spout was not significantly affected by the wall and thus that any changes in spout shape or size were directly related to changes in design variables. Data are summarized in Table 4 where spout diameters are tabulated at several bed levels for a variety of conditions. These data were taken from smooth curves drawn through the experimental points.

Several general observations may be made. For the 2 ft. I.D. column with $D_i = 4$ in., the spout width decreased to about 2.5 in. immediately above the orifice, then flared out to a maximum at about 0.4L, and finally contracted again toward the top. For smaller orifices, the spout profiles were similar, except that the constriction noted for the 4 in. orifice was absent when the 2 and 3 in.

TABLE 4

SPOUT DIAMETER DATA FROM 0.5 AND 2 FT. I.D. SEMI CIRCULAR COLUMNS

D_c ft.	Cone Angle°	D_i in.	Q s.c.f.m.	L ft.	D_s – in.			
					0.3L	0.5L	0.7L	0.9L
2	60	2	207	6	3.4	3.3	3.0	2.8
		3	223	6	3.4	3.3	3.0	2.8
		4	257	6	3.5	3.4	3.1	3.0
	60	2	211	5	3.3	3.1	2.8	2.6
		2	232	5	3.4	3.3	3.1	2.9
		2	253	5	3.8	3.6	3.4	3.3
	60	2	150	3	2.5	2.6	2.6	2.4
		2	161	4	2.8	2.9	2.6	2.4
		2	189	5	3.0	3.0	2.7	2.5
0.5	85	¾	23.0	2	1.5	1.6	1.6	1.8
			25.3	2	1.6	1.7	1.7	1.8
			27.6	2	1.7	1.7	1.8	1.8
	85	¾	20.2	1.5	1.4	1.4	1.4	1.4
			18.4	1	1.2	1.3	1.3	1.3
	85	⅜	22.5	2	1.5	1.6	1.6	1.7

orifices were used. Thus, the orifice diameter had no direct effect on spout diameter. Data from the 0.5 ft. I.D. column supported this observation. Of the variables such as column diameter, bed height, and air flow which were examined, only air flow had an easily discernible effect. Spout diameter was approximately proportional to the flow rate above minimum required for spouting, a 20% increase in flow rate causing roughly the same increase in spout diameter.

Particle Flow Pattern

The circulation of solids within a spouted bed followed a regular, and easily studied pattern. Particle velocity measurements at the wall were used to estimate solid circulation rate. Typical data are given in Figure 5 in which particle velocities measured at the circumference of the column are plotted against fractional bed depth for the 0.5 ft. and 2 ft. I.D. column. Particle velocity increased linearly with bed level, and so particle velocity at the wall may be represented by a linear equation having an initial value V_o at $h/L = 1$, and a slope, k, which is a measure of the cross flow of wheat into the spout.

Flow Line Correlations

Measurement of particle velocity and direction of motion at the transparent face of a sectional column enables flow lines for particles starting at various radii to be constructed. Several flow lines for the 2 ft. column obtained in this way are shown in Figure 6. In the top half of the bed, the flow lines are approximately parabolic, the equation of which can be developed in the following way.

Assume the origin to be at the wall, and at the top of the bed. The radius of a segment is then $(r_o\text{-}r)$ at a distance y from the top of the bed. Assume also cylindrical symmetry in flow lines, and uniform bulk density throughout the bed. Then a material balance on a cylindrical element of volume, $2\pi(r_o\text{-}r)dr.dy$ with wheat flow in the top, out of the bottom, and in from the wall and out toward the spout, will result in the differential equation

$$-\frac{dV}{dy} - \frac{dX}{dr} + \frac{X}{r_o - r} = 0 \qquad \ldots\ldots\ldots\ldots\ldots\ldots (4)$$

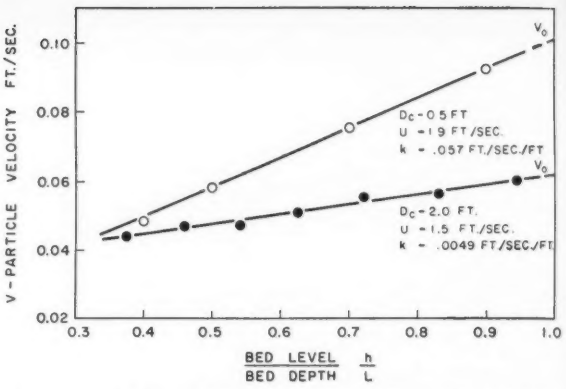

Figure 5—Wall particle velocity at different bed levels. $D_c/D_i = 6$; $L/D_c = 3$; 60° cone.

at

$$r = 0,\ V = V_o,\ \frac{dV}{dy} = -k.$$

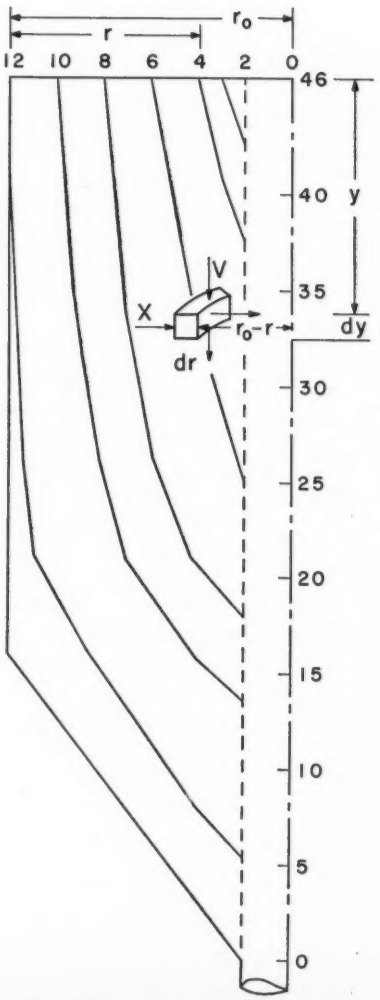

Figure 6—Wheat flow lines in annulus section D_c= 2 ft.; D_i = 4 in.; Q = 252 c.f.m.; cone 60°.

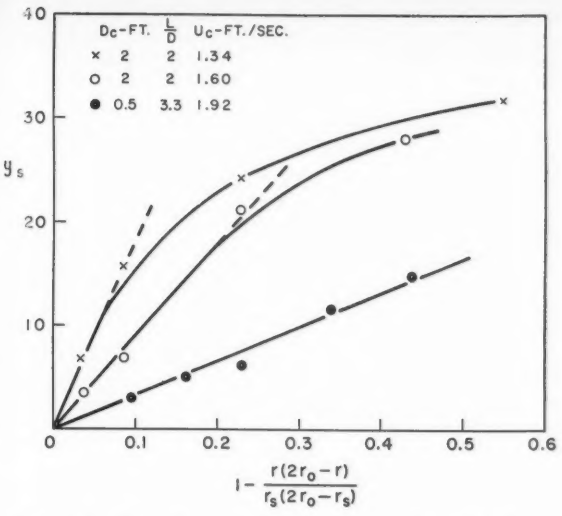

Figure 7—Flow line correlation for annular solid flow.

Integrating with respect to y at the wall

$$V = V_o - ky \quad \ldots\ldots(5)$$

Integrating with respect to r at constant y

$$k - \frac{dX}{dr} + \frac{X}{r_o - r} = 0 \quad \ldots\ldots(6)$$

$$X = \frac{k}{2}\left[\frac{r_o^2 - (r_o - r)^2}{r_o - r}\right] \quad \ldots\ldots(7)$$

By definition

$$X = \frac{dr}{dt}, \quad V = \frac{dy}{dt}.$$

Integration of Equations (5) and (7) leads to

$$\ln\left(\frac{V_o - ky}{V_o}\right) = -kt \quad \ldots\ldots(8)$$

and

$$\ln\left[\frac{r}{r_s}\left(\frac{2r_o - r}{2r_o - r_s}\right)\right] = k(t - t_s) \quad \ldots\ldots(9)$$

where $(r_o\text{-}r_s)$ is the radius of the spout, and $(t\text{-}t_s)$ is the time required for a particle starting at (r,y,t) to reach the spout wall at r_s. Since the particle requires the same time to fall the distance y to y_s, Equations (8) and (9) may be equated, and rearranged to give

$$y_s = \frac{V_o}{k}\left(1 - \frac{r(2r_o - r)}{r_s(2r_o - r_s)}\right) \quad \ldots\ldots(10)$$

where y_s is the vertical distance in inches from the top of the bed to the point at which the particle enters the spout, and $(r_o\text{-}r)$ and $(r_o\text{-}r_s)$ are the starting radius and spout radius in inches, respectively.

Three sets of flow line data are available to test this equation. In Figure 7, y_s is plotted against a function of r given by Equation (10). The 0.5 ft. I.D. column data were obtained by a photographic method [7], and these plot as a linear relationship. The 2 ft. I.D. column data at the higher flow of 252 c.f.m. also show a linear relationship to about the 2 ft. level, but at 210 c.f.m. i.e. slightly above minimum spouting flow, the linear relationship holds to only 15 inches from the top. A comparison of

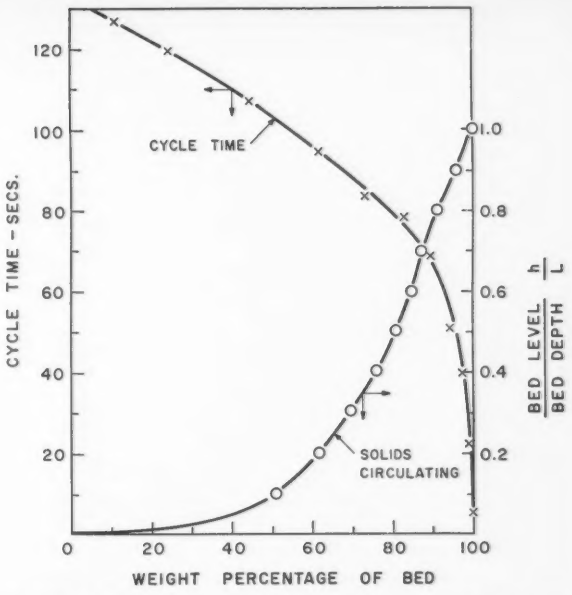

Figure 8—Weight distribution vs. cycle time and per cent of total solids passing each bed level. $D_c = 2$ ft.; $L = 4$ ft.; $U_c = 1.6$ ft./sec.

TABLE 5

COMPARISON OF CALCULATED AND OBSERVED SLOPES FOR CORRELATION OF PARTICLE FLOW IN ANNULUS

D_c ft.	U_c ft./sec.	k ft./sec./in.	V_o ft./sec.	V_o/k in.	Slope in.
2	1.34	.00021	.028	135	182
2	1.60	.00039	.041	105	91
0.5		.00057	.192	34	32

the slopes of these lines with V_o/k ratio is shown in Table 5. The approximate agreement indicates that particle velocity data at the wall does reflect, at least in the top section of the bed, the solid flow pattern within the annulus. In the bottom half of the 2 ft. column, the effect of the cone on flow lines is dominant so that the simple model postulated could not be expected to apply.

From the flow line data in Figure 6, the time required for particles to make one cycle can be estimated. The distribution of cycle times for one run is shown in Figure 8. Although some short circuiting of wheat occurred at the top of the bed, the major portion of the wheat (> 90%) took 60 seconds or longer to make one cycle. Also shown on the same figure is the fraction of total solids flowing through the spout at various levels of the bed. About two-thirds of the wheat entered the spout in the cone region. Study of a 2 ft. bed of wheat in a 0.5 I.D. column showed a similar solid flow versus height distribution plot.

Effect of Design Variables on Annular Solid Flow

The effects of changing variables such as orifice size, cone angle, column diameter, bed height, and air flow on solid flow pattern were evaluated in terms of particle velocity V_o at $h/L = 1$, and cross flow k. Data have been summarized in Tables 1 and 6.

The first group of data in Table 6 show the results of varying inlet diameter. Orifices from 3/8 in. to 1-1/4 in. diameter were used in the 0.5 ft. I.D. column. Total air

TABLE 6

EFFECT OF ORIFICE SIZE, CONE ANGLE ON ANNULAR SOLID FLOW

D_c ft.	L ft.	Cone Angle°	Di in.	U_c ft./sec.	k ft./sec./ft.	V_o ft./sec.	Cross* Flow lb./sec./in.	Total* Flow lb./sec.
0.5	2	60	0.375	3.30	.037	.139	.031	1.4
			0.50	3.30	.040	.139	.034	1.4
			0.75	3.30	.053	.139	.044	1.4
			1.0	3.30	.061	.139	.051	1.4
			1.25	3.30	.052	.134	.044	1.4
2.0	4	45	1.875	1.96	–	.042	–	7.2
			3.0	2.21	–	.040		6.9
			4.0	2.24	–	.037		6.3
0.5	2	45	0.50	3.24	.048	.145	.04	1.5
		60	0.50	3.30	.040	.139	.034	1.4
		85	0.50	3.17	.040	.139	.034	1.4
2.0	4	45	4.0	2.24	–	.037	–	6.3
		60	4.0	2.08	.00013	.030	.023	5.2
		85	4.0	2.17	.00058	.036	0.10	6.2

*Cross Flow $= \frac{\pi}{4}(D_c^2 - D_s^2)\rho_b \cdot k$. $D_c = 2.0$ ft., $D_s = 3.0$ in.

*Total Flow $= \frac{\pi}{4}(D_c^2 - D_s^2)\rho_b V_o$. $D_c = 0.5$ ft., $D_s = 1.75$ in., $\rho_b = 56$ lb./ft.^{3}

flow was constant. There was no significant change in the total amount of solids circulating but there was an increase in the cross flow rate as the orifice diameter was increased. Thus, more solids entered the core from the cone region as inlet air velocity was increased. A similar series of runs in the 2 ft. I.D. column did not show such a definite trend. Inlet orifices from 1-7/8 in. to 4 in. diameter were used, but total flow could not be held constant because larger air flows were required to maintain spouting as inlet diameter was increased. These data show that overall circulation rate increased with increasing inlet velocity, i.e. with decreasing orifice size.

The second group of data show the effect of cone angle on solid circulation pattern. Three cone angles 45°, 60°, 85° were used in 0.5 ft. and 2 ft. I.D. column. In the 0.5 ft. column the total flow and cross flow were the same for the 60° and 85° cone, and both a little less than was observed with the 45° cone. In the 2 ft. column, the total solid flow was about the same for the 45 and 85° cone but lower for the 60° cone. Cross flow into the spout appeared to increase with increasing cone angle.

Data in Table 1 show the effect of varying bed height and air flow rate on solid circulation rate. Since wheat does flow into the spout at all levels of bed, circulation rate would be expected to depend on bed height. The gas flow required for spouting also increases with bed height and so these two variables are not independent hence the effect of bed height is not clearly shown. The dominating variable affecting solid circulation rate is the gas flow rate. An examination of data in Table 1, shows that an increase in total air flow results in a corresponding increase in particle velocity.

Air and Solid Flow Correlation

The relationship between air flow and solid circulation rate can be developed in the following way if it is assumed that the pressure drop across a spouted bed is determined by the density of the wheat-air mixture in the spout

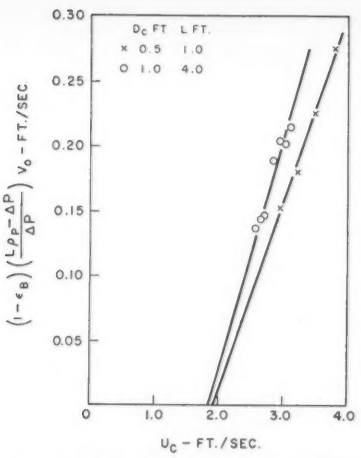

Figure 9—Relationship between particle velocity and superficial air velocity.

$$\Delta P = (1 - \epsilon_s)\rho_p L$$

or

$$\epsilon_s = 1 - \Delta P/\rho_p L \quad \ldots\ldots(11)$$

Spout void fraction, ϵ_s, can also be expressed as

$$\epsilon_s = \frac{Q_s}{Q_s + W/\rho_p} \quad \ldots\ldots(12)$$

Equating (11) and (12) and rearranging

$$W = \frac{\Delta P \rho_p}{\rho_p L - \Delta P} \cdot Q_s \quad \ldots\ldots(13)$$

Expressing air and solid flow rates in terms of superficial velocity, putting $Q_s = Q_c - Q_a$ and taking the area of the annulus equal to the area of the column, Equation (13) becomes

$$(1 - \epsilon_b)\left(\frac{\rho_p L - \Delta P}{\Delta P}\right) V_o = U_c - U_b \quad \ldots\ldots(14)$$

This indicates a linear relationship between superficial column velocity and the function of V_o given by the left hand side of the equation. Figure 9, in which typical data for 0.5 ft. and 1 ft. columns is plotted, shows that a linear relationship is obtained. Although the 2 ft. column data available also show a linear relationship, slope and intercept vary considerably from the other column size data. Values of slope and intercept, the latter expressed in terms of U_m, increase slightly with increasing bed depth and with decreasing column diameter. Using average values for slope and intercept, the following equation relating U, V_o and ΔP is obtained which fits the 0.5 ft. and 1 ft. column data within ± 15%

$$(1 - \epsilon_b)\left(\frac{\rho_p L - \Delta P}{\Delta P}\right) V_o = 0.17(U_c - 0.75U_m) \quad \ldots\ldots(15)$$

Under minimum spouting conditions

$$\frac{L\rho_p}{\Delta P} = 1 + \left(\frac{c}{1 - \epsilon_b}\right) \cdot \frac{U_m}{V_o} \quad \ldots\ldots(16)$$

Plotting $L\rho_p/\Delta P$ vs U_m/V_o results in a straight line (Figure 10) with a slope of 0.14 and an intercept of 1.0 confirming the linear relationship between solid circulation rate and air flow and hence the assumption that the pressure drop

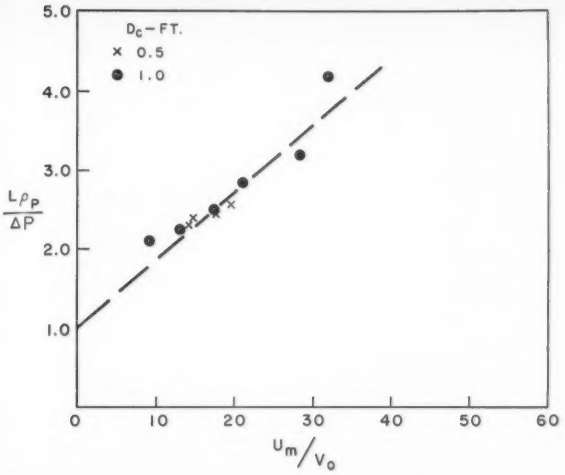

Figure 10—Relationship between pressure drop and air: solid flow ratio at minimum spouting.

across a spouted bed is determined by the wheat-air mixture in the spout. Use of Equation (15) or (16) along with the fact that the pressure drop across the bed is approximately two-thirds the pressure due to the weight of the bed enables particle velocity V_o and hence total solid flow rate to be calculated for the 0.5 and 1.0 ft. column.

Particle Flow in the Spout

The movement of particles up the spout was clearly visible at the flat face of the semi circular column, and was recorded on film with a 16 mm. Western Fastax cine camera using a film speed of 2000 frames per second. These photographs showed that in the cone region the walls of the cone were constantly collapsing and the particles were being swept up by the high velocity jet. Above the cone region, particles entering the spout appear to do so as the result of collisions of the ascending particles with particles in the wall of the spout. In the central region of the core, however, wheat particles move in streamline paths with few interparticle collisions.

Particle velocity at different bed levels was estimated from the photographs and one set of data, at minimum spouting velocity, is shown in Figure 11. This is based on particles in the centre of core, and no attempt was made to determine a velocity distribution across the cone.

The main forces affecting particle motion are: (a) accelerating force due to frictional drag on the particle by the air stream, (b) decelerating force due to gravity, (c) decelerating force due to collision of particles with the wall. This latter force is presumably proportional to the density of particles in the spout, which varies with bed height. As a first approximation, in estimating particle velocity, this term will be neglected. Using the first two forces, the following equation may be derived from the usual drag Equation (8)

$$\frac{dV_p}{dt} = 3/4\ C_d/D_p\ \rho_f/\rho_p\ (U_s - V_p)^2 - \left(\frac{\rho_p - \rho_f}{\rho_p}\right) g \quad \ldots(17)$$

Both U_s and V_p are functions of the bed height. From the air distribution measurements described earlier, V_s can be estimated, and for the data shown in Figure 11, it is 24 ft./sec. at the top of the bed. The air velocity at the orifice is 80.6 ft./sec. If the change in spout velocity is assumed to be linear with bed height, the relationship for data in Figure 11 is given by

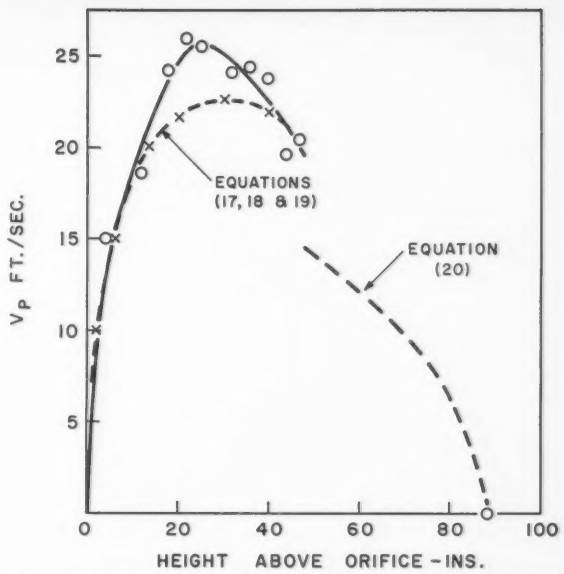

Figure 11—Particle velocity in the spout $D_c = 2$ ft.; $D_i = 4$ ins.; $L = 4$ ft.; $Q = 210$ c.f.m.

$$U_s = 80.6 - 14.15L \quad \ldots(18)$$

With Equations (17) and (18), and the third relationship that

$$\frac{dL}{dt} = V_p \quad \ldots(19)$$

particle velocity at various heights can be calculated by a successive approximation method.

The calculated particle velocity curve is shown in Figure 11. The agreement with the observed curve is fair in view of the assumptions made. The maximum velocity is about 10% low, and the curve also predicts the maximum to be somewhat higher up in the bed. The assumption of linear relationship of Equation (18) is satisfactory for the upper half of the bed, but there is no supporting data for the cone region where the accelerating force is dominant. In fact in this region, U_s might be higher than predicted by Equation (18) because a necking down of the spout to 3 in. was observed. This would of course increase the magnitude of the drag term.

The velocity of the particle as it leaves the bed can be estimated from the spout height by the equation

$$V_p = \left[2.\left(\frac{\rho_p - \rho_f}{\rho_p}\right) \cdot g(h_s - L)\right]^{1/2} \quad \ldots(20)$$

The curve based on Equation (20) is shown in Figure 11. The particle velocity falls substantially below the observed velocity at the top of the bed. A similar calculation for the same bed at air flow 252 c.f.m. showed close agreement with the observed value. The cause of the discrepancy at 210 c.f.m. is not known.

On the basis of these limited data, particle motion can be estimated approximately by utilizing the frictional drag and gravitational forces only, indicating that the deceleration due to interparticle collision is small and can be neglected.

Conclusions

The minimum spouting velocity in a 2 ft. I.D. column can be estimated within a 15% accuracy from the previously proposed Equation (1) which was based on 0.5 to 1 ft. I.D. columns.

No suitable general correlation based on packed bed properties was found for predicting pressure drop across a spouted bed. Pressure drop was however approximately two-thirds the pressure due to the weight of the bed. The pressure drop across a spouted bed is determined by the density of wheat-air mixture in the spout.

The maximum spoutable bed height can be estimated from the air velocity through a wheat bed which produces a pressure drop equal to the weight of the bed. The Ergun equation can be used for estimating the air velocity, and Equation (3) relating minimum spouting velocity and bed height can be used to estimate the bed height.

The maximum proportion of air passing through the annulus is obtained with large column diameter, large orifice size, and small cone angle, and when the spouted bed is operated near minimum spouting velocity.

The main variables affecting spout size for a bed of wheat are total air flow and column size. Orifice size has little direct effect.

The flow of wheat in the annulus can be estimated from particle velocity measurements taken at the wall of the column. Particle velocity data show that about two-thirds of the wheat enters the spout in the cone region, and about one-third along the spout. The flow line data within the upper half of the annulus follows a parabolic path which can be derived from a simple model. Analysis of the flow line data also yields data on distribution of cycle times within the bed.

Column variables such as cone angle and orifice size affect mainly the rate of cross flow of solids into the spout.

The main variable affecting solid turnover rate is total air flow. A relationship between air flow, solid flow and pressure drop can be derived.

The principal forces determining particle motion up the spout are frictional drag and gravitational forces. The decelerating force due to interparticle collision is small. The particle velocity can therefore be estimated from an equation based only on drag and gravitational terms.

Nomenclature

D = Diameter, ft.
C_d = Drag Coefficient — assumed equal to unity
c = Constant
g = Gravitation constant, ft./sec.^{2}
h = Level in bed, ft.
k = Cross flow velocity gradient, ft./sec./ft.
L = Bed height above orifice, ft.
ΔP = Pressure drop, lb./ft.^{2}
Q = Volume air flow rate, s.c.f.m., 32F°., 1 a.t.m.
r_o = Radius of column, ft.
t = Time, secs.
U = Linear air flow rate, ft./sec.
V = Vertical component of particle velocity, ft./sec.
W = Mass flow of solids, lb./sec.
X = Horizontal component of particle velocity, ft./sec.
y = Bed depth measured from top of the bed, ft.
z = Distance above orifice, ft.
ρ = Density, lbs./ft.^{3}
ϵ = Void fraction
μ = Viscosity, lb./ft. sec.

Subscripts

a = annulus
b = packed bed
c = column
f = fluid (air)
I = incipient
i = inlet
m = minimum
o = wall
p = particle
s = spout

Acknowledgments

The authors wish to acknowledge the generous assistance given by P. E. Gishler and J. Klassen to the early stages of this project, and to note also the valuable contributions to construction and operation of apparatus by the technical staff of the Chemical Engineering Section.

References

(1) Mathur, K. B., Gishler, P. E.; A.I.Ch.E. Journal 1, 157 (1955).
(2) Klassen, J., Gishler, P. E.; C.J.Ch.E., 36, 12 (1958).
(3) Mathur, K. B., Gishler, P. E.; J. App. Chem. 5, 624 (1955).
(4) Cowan, C. B., Peterson, W. S., Osberg, G. L.; Pulp and Paper Mag. (Dec.) 139 (1957).
(5) Cowan, C. B., Peterson, W. S., Osberg, G. L.; The Engineering Journal 41, 60 (1958).
(6) Ergun, Sabri; Chem. Eng. Prog. 48, 89 (1952).
(7) Madonna, L. A.; N.R.C. report, not published.
(8) Brown, G. G. Unit Operations, p. 73, J. Wiley & Sons.

★ ★ ★

Heats of Mixing and Vapor-Liquid Equilibrium Calculations[1]

BENJAMIN C.-Y. LU[2]

In the literature, when the available integrated forms of the Gibbs-Duhem equation are employed for extrapolating vapor-liquid equilibrium data at isobaric conditions, the relative partial molal enthalpies at constant liquid compositions, L, are assumed either to be zero or to be independent of temperature. An investigation of the temperature effect on heats of mixing for non-ideal solutions reveals that these assumptions are invalid and that the quantity L varies linearly with temperature. Therefore the liquid activity coefficients at constant compositions should involve three temperature terms of the form a + (b/T) + c log T for extrapolating purposes. As a result, more general equations are proposed.

THE successful application of various distillation methods in chemical industries and the design of fractional distillation apparatus depend upon the knowledge of vapor-liquid equilibria of the mixture encountered. For this reason, most investigations on vapor-liquid equilibria are made at constant pressure conditions. When these data are reported, their thermodynamic consistency has usually been checked by the authors. The purposes of testing the thermodynamic consistency are to indicate that the data are self consistent and to smooth the data for interpolating and extrapolating purposes. One of the test methods usually employed is to fit the data by means of some algebraic equations with the condition that the Gibbs-Duhem equation of the form

$$\left(\frac{\partial \ln \gamma_1}{\partial \ln x_1}\right)_{T,p} = \left(\frac{\partial \ln \gamma_2}{\partial \ln x_2}\right)_{T,p} \quad \ldots\ldots\ldots\ldots\ldots\ldots (1)$$

be satisfied. The frequently used equations in the literature are the equations of van Laar and Margules as rearranged by Carlson and Colburn [1]; the van Laar equation as proposed by White [2], Li and Coull [3], Robinson and Gilliland [4] and Yu and Coull [5]; and other equations such as presented by Wohl [6], Redlich and Kister [7], and Benedict, Johnson, Solomon and Rubins [8].

The applications of these equations for extrapolating vapor-liquid equilibrium data from one isobaric condition to another should, however, be made with reservations. For example, Yang and van Winkle [9] measured the vapor-liquid equilibrium data for the system octane-ethyl benzene at various total pressures. They found that their data can be represented by the van Laar equations, proposed by Robinson and Gilliland [4].

$$T \ln \gamma_1 = \frac{B}{\left(1 + A\frac{x_1}{x_2}\right)^2} \quad \ldots\ldots\ldots\ldots\ldots\ldots (2a)$$

$$T \ln \gamma_2 = \frac{AB}{\left(A + \frac{x_2}{x_1}\right)^2} \quad \ldots\ldots\ldots\ldots\ldots\ldots (2b)$$

at each of the total pressures. The constants A and B of Equation (2) are supposed to be independent of temperature. However, they observed that for the system investigated, the values of A and B increase with increasing pressure, therefore, the values also increase with increasing temperature). Eduljee, Kumarkrishnarao and Rao [10] correlated the vapor-liquid equilibrium data for the system acetone-water, using a form of the van Laar equation given by Li and Coull [3] and White [2].

$$T \ln \gamma_1 = \frac{A}{\left(1 + \frac{A\,x_1}{B\,x_2}\right)^2} \quad \ldots\ldots\ldots\ldots\ldots\ldots (3a)$$

$$T \ln \gamma_2 = \frac{B}{\left(1 + \frac{B\,x_2}{A\,x_1}\right)^2} \quad \ldots\ldots\ldots\ldots\ldots\ldots (3b)$$

The constants are found to be functions of temperature, while they are supposed to be independent of temperature. There are many other similar observations in the literature, indicating that equations such as Equations (2) and (3) may be used for representing the data over the temperature range at a certain total pressure, but they are not good enough for extrapolating purposes.

Yu and Coull [5] pointed out that if Equations (2) and (3) were true, a plot of ln γ vs. 1/T at constant composition would yield a straight line passing through the origin. They studied the change of activity coefficients with temperature for the systems ethanol-water, chloroform-ethanol and n-propanol-water over a short temperature range and found that when ln γ is plotted against 1/T at constant composition, a straight line is obtained over

[1] *Manuscript received June 17, 1959.*
[2] *Assistant Professor of Chemical Engineering, University of Ottawa, Ottawa, Ont.*
Based on a paper presented at the 42nd Annual Conference, The Chemical Institute of Canada, Halifax, N.S., May 25-27, 1959.

the range under consideration, but not passing through the origin. They obtained

$$(\ln \gamma)_x = a'' + \frac{b''}{T} \quad \ldots\ldots(4)$$

and suggested the following form of the isobaric equation

$$T \ln \gamma_1 = \frac{a + b\,T}{\left[1 + \frac{(a + b\,T)\,x_1}{(c + d\,T)\,x_2}\right]^2} \quad \ldots\ldots(5a)$$

$$T \ln \gamma_2 = \frac{c + d\,T}{\left[1 + \frac{(c + d\,T)\,x_2}{(a + b\,T)\,x_1}\right]^2} \quad \ldots\ldots(5b)$$

for calculating the activity coefficients of a solution over its boiling point range at low pressure. Should Equation (4) be employed for extrapolating purpose for the system ethanol-water, using the constants obtained by Yu and Coull [5], the activity coefficients of ethanol at infinite dilution as represented by Equation (6),

$$(\ln \gamma_1)_{x1=0} = 3.22 - 576/T \quad \ldots\ldots(6)$$

would always increase with increasing temperature. Otsuki and Williams [11] determined the vapor-liquid equilibrium data for this system at various total pressures from 1 atm. to 300 p.s.i.a. They observed that the activity coefficients of ethanol at infinite dilution decrease with increasing temperature.

The van Laar equations as rearranged by Carlson and Colburn [1]

$$\log \gamma_1 = \frac{A}{\left(1 + \frac{A\,x_1}{B\,x_2}\right)^2} \quad \ldots\ldots(7a)$$

$$\log \gamma_2 = \frac{B}{\left(1 + \frac{B\,x_2}{A\,x_1}\right)^2} \quad \ldots\ldots(7b)$$

represent well the data on many binary systems and appear to be the simplest in application. Nord [12] suggested that Equation (7) is as good or perhaps slightly better than Equations (3) and (5). It is known, however, that there are many systems which can not be represented at all by means of Equation (7). This applies even to binary hydrocarbon mixtures, whose activity coefficients are found to be functions of temperature [13, 14]. Since Equation (7) does not take into account the variation of activity coefficients with temperature, any extrapolation using the constants obtained at one isobaric condition to another wou'd be erroneous most likely.

Other equations, which involve similar assumptions as in Equations (2), (3), (5) and (7), are usually not adequate enough for extrapolating isobaric vapor-liquid equilibrium data either. The constants obtained at one condition may not be used for other conditions.

It seems clear, therefore, that all the integrated forms of the Gibbs-Durhem equation proposed in the literature, when they are employed for isobaric equilibrium data, are not general enough for extrapolating purposes. The purposes of this investigation are to determine the temperature effect on activity coefficients, using the correlated results on heats of mixing data, and to develop more general equations for representing and extrapolating binary vapor-liquid equilibrium data at isobaric conditions.

Temperature Effect on Liquid Activity Coefficients

The activity of a component, say component 1, in a non-ideal solution is defined by

$$d\,\mu_1 = R\,T\,d \ln a_1^* \text{ (at constant T, p)} \quad \ldots\ldots(8)$$

where μ_1 is the chemical potential of component 1. Integrating this equation,

$$\mu_1 = (G_{T,p})_1 + R\,T \ln a_1^* \text{ (at constant T, p)} \quad \ldots\ldots(9)$$

where $(G_{T,p})_1$ refers to the molar free energy of pure component 1 as liquid at the T,p of the solution. Substituting the activity coefficient which is defined by

$$\gamma_1 = \frac{a_1^*}{x_1}$$

into Equation (9), and dividing both sides of the resulting equation by T, we obtain

$$\frac{\mu_1}{T} = \frac{(G_{T,p})_1}{T} + R \ln x_1 + R \ln \gamma_1 \quad \ldots\ldots(10)$$

Partial differentiation of this equation with respect to temperature at constant pressure and constant composition gives

$$\frac{\partial(\mu_1/T)}{\partial T} = \frac{\partial[(G_{T,p})_1/T]}{\partial T} + R\left(\frac{\partial \ln \gamma_1}{\partial T}\right) \text{ (at constant P, composition)} \quad \ldots\ldots(11)$$

or

$$-\frac{\bar{H}_1}{T^2} = -\frac{(H_{T,p})_1}{T^2} + R\left(\frac{\partial \ln \gamma_1}{\partial T}\right) \text{ (at constant P, composition)}$$

Rearranging,

$$\frac{\partial \ln \gamma_1}{\partial T} = \frac{(H_{T,p})_1 - \bar{H}_1}{R\,T^2} = -\frac{L_1}{R\,T^2} \text{ (at constant P, composition)} \quad \ldots\ldots(12)$$

This is the expression for the temperature dependence of the activity coefficients, in which $(H_{T,p})_1$ = molal enthalpy of pure component 1, and $\bar{H}_1$ = partial molal enthalpy of component 1 in the solution at the same temperature. Similar equation may be derived for component 2. For simplicity, the dependence of activity coefficients on pressure is neglected in the following discussion.

The quantity L_1 may be defined as the relative partial molal enthalpy of component 1. It is the heat absorbed per mole of component 1 at constant T,p when the pure component is dissolved in a large quantity of the solution without changing the composition of the solution.

It is seen from Equation (12) that L is a positive quantity, (heat is absorbed) activity coefficient decreases with temperature. On the other hand, when L is a negative quantity (heat is evolved), activity coefficient increases with temperature. The magnitude of variation of activity coefficients with temperature depends on the quantity L. Carlson and Colburn [1] inspected the values of L at infinite dilution calculated from heats of mixing liquid in the International Critical Tables, and reported values as high as 2000 calories per mole for organic liquid mixtures, and 5000 calories per mole for mixtures of alcohols and water.

In the literature, the integrated forms of the Gibbs-Duhem equation may be separated into two groups. One of which considers L =0, that is, there is negligible or no heat effect on mixing liquids. Therefore, the activity coefficients are assumed to be independent of temperature. The application of the integrated forms of Equation (1),

which are limited to isothermal and isobaric conditions, to isobaric vapor-liquid equilibrium data involves automatically this assumption.

The other group considers L = constant, at constant liquid composition. Substituting this expression into Equation (12), and integrating, yields Equation (4).

In Equations (2) and (3), the change of activity coefficient with temperature at constant composition is considered to be

$$(\ln \gamma)_x = \frac{\text{constant}}{T} \quad \ldots\ldots\ldots\ldots\ldots\ldots (13)$$

In other words, the integration constant a″ of Equation (4) is assumed to be zero. It is seen that Equation (13) is only a special case of Equation (4), which offers a better approximation than all the other cases considered.

Should Equation (4) be an exact representation of the variation of activity coefficients with temperature, the experimental procedure for the determination of vapor-liquid equilibrium data would be very much simplified. It is very unfortunate that there is much experimental evidence indicating the inadequacy of Equation (4). First, Equation (4) does not permit the value of activity coefficient at constant composition to be a maximum or a minimum at any temperature, and second, there are indications that L changes rather rapidly with temperatures.

Correlation of Heats of Mixing Data

The term heat of mixing as used in this paper is defined as the amount of heat absorbed by the system when n_1 moles of pure component 1 and n_2 moles of pure component 2 are mixed at constant temperature and pressure, ΔH_N^M, or as the amount of heat absorbed per mole of mixture when the pure components are mixed at constant temperature and pressure, ΔH^M. Hence

$$\Delta H_N^M = h_{soln} - n_1 \cdot (H_{T,p})_1 - n_2 \cdot (H_{T,p})_2 \quad \ldots\ldots (14)$$

where h_{soln} is the enthalpy of the solution. Partial differentiation of Equation (14) with respect to n_1 and n_2 gives

$$\frac{\partial(\Delta H_N^M)}{\partial n_1} = \bar{H}_1 - (H_{T,p})_1 = L_1 \quad \ldots\ldots (15a)$$

$$\frac{\partial(\Delta H_N^M)}{\partial n_2} = \bar{H}_2 - (H_{T,p})_2 = L_2 \quad \ldots\ldots (15b)$$

In order to correlate the relative partial molar enthalpies L_1 and L_2 with temperature and therefore to determine the variation of activity coefficient with temperature, the knowledge of heats of mixing is essential. The quantity ΔH_N^M may be expressed as a function of temperature in the following manner,

$$\Delta H_N^M = a(n_1, n_2) + b(n_1, n_2)\, T + c(n, n_2)\, T^2 + \ldots (16)$$

where $a(n_1,n_2)$, $b(n_1,n_2)$ and $c(n_1,n_2)$ are functions of n_1 and n_2 only. Differentiating Equation (16) with respect to n_1,

$$\frac{\partial(\Delta H_N^M)}{\partial n_1} = a'(n_1, n_2) + b'(n_1, n_2)\, T + c'(n_1, n_2)\, T^2 + \ldots (17)$$
$$= L_1$$

It is seen therefore the quantities L_1 and L_2 have the same temperature terms as the quantity ΔH_N^M. The simplest four temperature functions for ΔH_N^M are discussed here. For simplicity, only L_1 will be considered in cases 2 to 4.

Case 1. $\Delta H_N^M = 0$, therefore $L_1 = L_2 = 0$, and

$$\frac{\partial \ln \gamma_1}{\partial T} = \frac{\partial \ln \gamma_2}{\partial T} = 0$$

The activity coefficients are independent of temperature.

Case 2. At constant composition, ΔH_N^M = constant. Therefore L_1 = constant and

$$(\ln \gamma_1)_x = a'' + \frac{b''}{T} \quad \ldots\ldots\ldots\ldots (4)$$

This is the equation proposed by Yu and Coull [22]. If a″ = 0, Equation (4) represents the condition proposed by White [18], Li and Coull [11] and Robinson and Gilliland [16].

Case 3. At constant composition, ΔH_N^M is a linear function of temperature.

$$\Delta H_N^M = a + b\, T \quad \ldots\ldots\ldots\ldots\ldots\ldots (18)$$

Therefore

$$L_1 = a' + b'\, T \quad \ldots\ldots\ldots\ldots\ldots\ldots (19)$$

and

$$\ln \gamma_1 = a'' + \frac{b''}{T} + c'' (\ln T) \quad \ldots\ldots\ldots\ldots (20)$$

Case 4. At constant composition

$$\Delta H_N^M = a + b\, T + c\, T^2 \quad \ldots\ldots\ldots\ldots\ldots (21)$$

Therefore

$$L_1 = a' + b'\, T + c'\, T^2 \quad \ldots\ldots\ldots\ldots\ldots (22)$$

and

$$\ln \gamma_1 = a'' + \frac{b''}{T} + c'' (\ln T) + d''\, T \quad \ldots\ldots\ldots (23)$$

It should be pointed out, in passing, that the constants involved in Equations (18-23) may either be positive or negative. Therefore, only plus signs are employed in these equations.

An attempt has been made to correlate the quantity $\Delta H_N^M/N = \Delta H^M$, the heat of mixing per mole of mixture, wtih temperature, using the available data in the literature. It is found that most of the existing data are limited to a single temperature, making an extensive correlation impossible. However, from the available data for non-ideal solutions and some of the near ideal solutions, the correlated results indicate that the assumptions

$$\Delta H^M = 0 \qquad \text{(at constant composition)}$$

$$\Delta H^M = \text{constant (at constant composition)}$$

as involved in Equations (1-5) and (7) are too simple to describe the situation. This explains the inadequacy of these equations for extrapolating purposes.

A part of the investigation may be presented here:

1. The heat of mixing data of Bosjnakovic and Grumbt [15] for the system ethanol-water (0°-100°C.) are recalculated and shown in Figure 1. It is found that at low alcohol concentration (10-50 wt. % alc. or 4.2-28.1 mole % alc.), ΔH^M can be represented very well by means of Equation (18), i.e., it varies linearly with temperature at constant compositions. However, at higher alcohol concentrations, the temperature effect on ΔH^M is apparently more complicated at high temperatures. This may be caused by errors due to evaporation or condensation, which have large heat effects.

2. When the relative partial molal enthalpies at infinite dilution, L_1° and L_2°, (L_1 and L_2 at $x_1 = 0$ and $x_2 = 0$ respectively) for the systems: ethanol-water (0°-100°C.), using the calculated values of Jones, Schoenborn and Colburn [16]; methanol-water (4-42.4°C.), n-propanol-

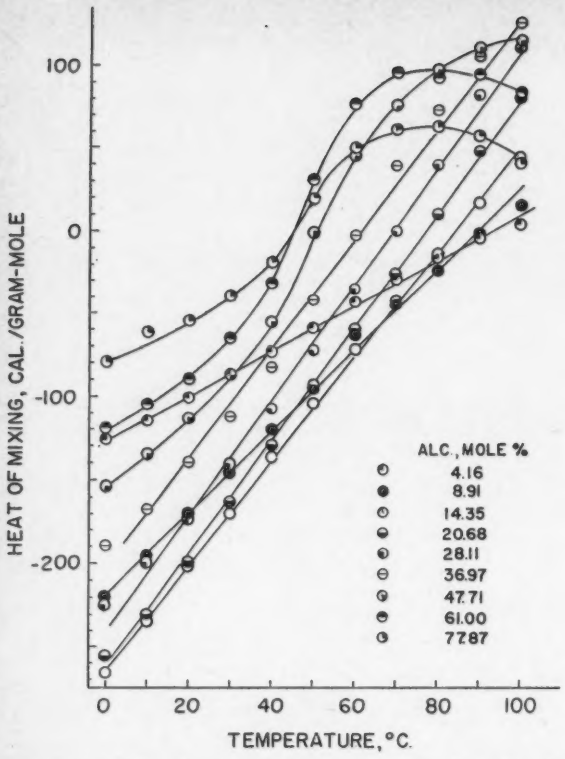

Figure 1—Heat of mixing data for the system ethanol-water [15].

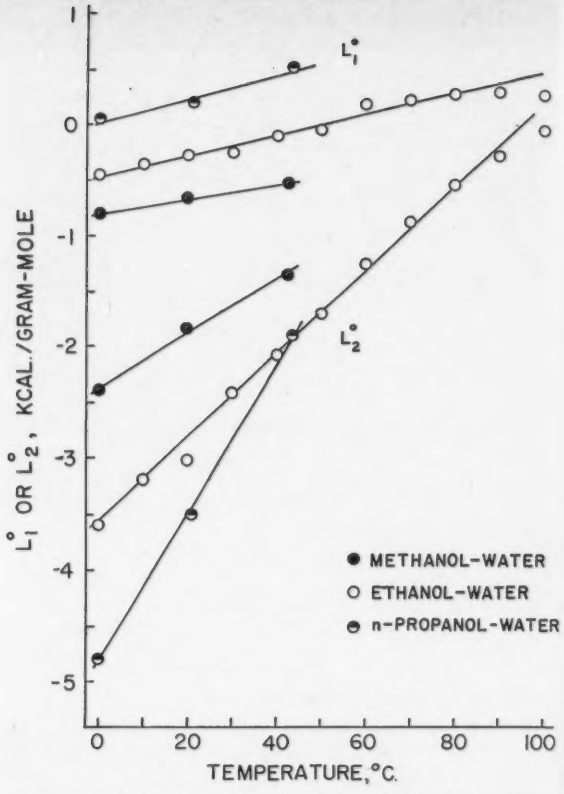

Figure 2—Variation of partial molal enthalpies at infinite dilutions with temperature.

water (0-43.4°C.), carbon disulphide-ethanol (0-15.5°C.), ethanol-benzene (0-15°C.) and ethyl ether-chloroform (3-24°C.), using the calculated values of Colburn and Pigford [17] are plotted against T, straight lines are obtained indicating that they are linear functions of temperature. A part of these results is shown in Figure 2.

3. Cheeseman and Ladner [18] investigated the variation of the heat of mixing with temperature for the three nearly ideal mixtures: benzene-toluene (6.3°-64.5°C.), toluene-para-xylene (14.7°-50.3°C.), benzene-para-xylene (14.7°-53.3°C.), and observed that the heat of mixing varies almost linearly with temperature.

There is other evidence in the literature supporting the applicability of Equation (18).

1. Scatchard and Ticknor [19] expressed the Scatchard excess free energy ΔG^E, cal./g-mole, for the systems methanol-carbon tetrachloride (25-55°C.) and methanol-benzene (25-55°C.) by means of the following expression

$$\Delta G^E = x_1 x_2 [- e - f T \ln T + g T - (h - i T)(x_1 - x_2) + j T(x_1 - x_2)^2 - (k - l T)(x_1 - x_2)^3 + (m - r T)(x_1 - x_2)^4] \quad \ldots\ldots(24)$$

It can be readily shown that Equation (24) is a direct support of Equation (18). The Scatchard excess free energy may be expressed by

$$\Delta G^E = \Delta H^E + T\left(\frac{\partial \Delta G^E}{\partial T}\right) \text{(at constant x)} \quad \ldots\ldots(25)$$

Since the heat of mixing for an ideal solution is zero, the excess enthalpy of mixing ΔH^E is equivalent to the heat of mixing ΔH^M. Therefore,

$$\Delta H^E = \Delta H^M$$

$$\Delta G^E = \Delta H^M + T\left(\frac{\partial \Delta G^E}{\partial T}\right) \text{(at constant x)} \quad \ldots\ldots(26)$$

Differentiating Equation (26) with T at constant x, one obtains,

$$\frac{\partial \Delta H^M}{\partial T} = - T\left(\frac{\partial^2 \Delta G^E}{\partial T^2}\right) \text{(at constant x)} \quad \ldots\ldots(27)$$

If ΔH^M is a linear function of T, i.e. $\Delta H^M = a + b T$,

$$\frac{\partial^2 \Delta G^E}{\partial T^2} = - \frac{b}{T} \text{(at constant x)} \quad \ldots\ldots(28)$$

or

$$\frac{\partial \Delta G^E}{\partial T} = c - b \ln T \text{ (at constant x)} \quad \ldots\ldots(29)$$

where c is the integration constant. Therefore

$$\Delta G^E = a + (b + c) T - b T \ln T \text{ (at constant x)} \quad \ldots(30)$$

This agrees with the expression of Equation (24).

2. Adcock and McGlashan [20] measured the heats of mixing for the systems carbon tetrachloride-cyclohexane (10-55°C.) and benzene-diphenyl (10°-60°C.). Their results agree with the temperature terms of Equation (24) and therefore support Equation (18).

Proposed Equation

It is seen from the above discussion that over a moderate range of temperature and at constant liquid compositions, the relationship that the quantity L is a linear function of temperature (Equation (19)) provides a much

closer approximation than the other relationships proposed in the literature, namely, L = 0 and L = constant. Therefore, the activity coefficient for a component at constant composition should follow the temperature terms as indicated in Equation (20). The following forms of the isobaric equation may be used for calculating the liquid activity coefficient of a solution over a larger temperature range than the previously suggested equations in the literature.

1. Redlich and Kister [7] proposed the following equation for representing the liquid activity coefficients at isothermal conditions,

$$\log \gamma_1 = (1 - x_1)^2 [B + C(4x_1 - 1) + D(2x_1 - 1)(6x_1 - 1)] \quad \ldots\ldots(31a)$$

$$\log \gamma_2 = x_1^2 [B + C(4x_1 - 3) + D(2x_1 - 1)(6x_1 - 5)] \quad \ldots\ldots(31b)$$

They have developed these equations by expanding the function $Q = \left(\frac{\Delta G^E}{2.3\ R\ T}\right)$ into a power series at constant temperature. The quantities B, C and D of Equation (31) may be modified for representing isobaric data by including the temperature terms as expressed by Equation (20),

$$\begin{aligned} B &= a + b/T + c \log T \\ C &= a' + b'/T + c' \log T \\ D &= a'' + b''/T + c'' \log T \end{aligned} \quad \ldots\ldots(32)$$

Therefore

$$\log \gamma_1 = (1 - x_1)^2 \left[a + \frac{b}{T} + c \log T + \left(a' + \frac{b'}{T} + c' \log T \right) \times (4x_1 - 1) + \left(a'' + \frac{b''}{T} + c'' \log T \right) (2x_1 - 1)(6x_1 - 1) \right] \quad \ldots\ldots(33a)$$

$$\log \gamma_2 = x_1^2 \left[a + \frac{b}{T} + c \log T + \left(a' + \frac{b'}{T} + c' \log T \right) \times (4x_1 - 3) + \left(a'' + \frac{b''}{T} + c'' \log T \right) (2x_1 - 1)(6x_1 - 5) \right] \quad \ldots\ldots(33b)$$

Equation (33) is an exact representation of Equation (20).

2. For systems which can be fitted by the van Laar type equation at constant temperature, the following equation may be employed.

$$\log \gamma_1 = \frac{a + b/T + c \log T}{\left(1 + \frac{a + b/T + c \log T}{a' + b'/T + c' \log T} \cdot \frac{x_1}{x_2} \right)^2} \quad \ldots\ldots(34a)$$

$$\log \gamma_2 = \frac{a' + b'/T + c' \log T}{\left(1 + \frac{a' + b'/T + c' \log T}{a + b/T + c \log T} \cdot \frac{x_2}{x_1} \right)^2} \quad \ldots\ldots(34b)$$

This equation is somewhat different from Equation (20). It may be seen from actual calculations, however, that a slight variation of the ratio

$$\left(\frac{a + b/T + c \log T}{a' + b'/T + c' \log T} \right)$$

does not affect materially the value of γ. The advantage of Equation (34) is that it only requires three accurately determined experimental points (T-x-y). The necessity for accurate data, however, cannot be over-emphasized.

Other equations such as those proposed by Wohl [6] and Benedict et al. [8] may be modified in a similar manner by introducing Equation (20).

Although the foregoing discussion is limited to binary systems, the temperature correction terms can be readily extended into the calculations of ternary activity coefficients. For example, the equations proposed by Redlich and Kister [7] for ternary systems at constant temperature can be modified in the same manner as the modification of Equation (31), and be employed for representing isobaric ternary data. The proposed expression for representing liquid activity coefficients as a function of temperature (Equation 20) may also prove to be useful in the liquid-liquid equilibrium calculations.

Sample Calculation

The extrapolation of the vapor-liquid equilibrium data for the system ethanol-water illustrates the calculation. The vapor-liquid equilibrium data for the system at 74.79°C. [21] and the heats of mixing data for the system over the temperature range 0-100°C. [15] are employed for determining the temperature effect on activity coefficients. First of all, the thermodynamic consistency of the isothermal data is tested by means of the Redlich-Kister relationship [7].

$$\int_{x_1=0}^{x_1=1} \log \left(\frac{\gamma_1}{\gamma_2} \right) dx_1 = 0 \quad \ldots\ldots(35)$$

It is observed that the area represented by the integral of Equation (35) equals 0.0081, instead of zero. The data are then adjusted by means of a procedure similar to that proposed by Broughton and Brearley [22]. The observed relative volatility is corrected using the relationship

$$\alpha_{corrected} = \alpha_{observed}^{1/S} \quad \ldots\ldots(36)$$

The quantity S is determined by

$$S = \frac{0.0081 + \log (p_1^\circ/p_2^\circ)}{\log (p_1^\circ/p_2^\circ)} = 1.0227 \quad \ldots\ldots(37)$$

The corrected activity coefficients are then calculated.

At isothermal conditions, the van Laar equations (Equations (7a) and (7b)) may be rearranged to give

$$(\log \gamma_1)^{0.5} = A^{0.5} - (A/B)^{0.5} (\log \gamma_2)^{0.5} \quad \ldots\ldots(38)$$

by eliminating x_1 and x_2 from these equations. If the data can be fitted by means of the van Laar equation, a straight line will result by plotting $(\log \gamma_1)^{0.5}$ vs. $(\log \gamma_2)^{0.5}$. It will be seen from Figure 3 that the isothermal data can not be very well represented by means of the van Laar equations. Equation (31) is then used to fit the activity coefficients. The values of the constants

$$\begin{aligned} B &= 0.5311 \\ C &= -0.1650 \\ D &= 0.0441 \end{aligned}$$

are obtained following the procedure outlined by Redlich and Kister [7]. Hence, at 74.79°C.,

$$(\log \gamma_1)_{x_1=0} = B - C + D = 0.740 \quad \ldots\ldots(39)$$

$$(\log \gamma_2)_{x_1=1} = B + C + D = 0.410 \quad \ldots\ldots(40)$$

and

$$\log (\gamma_1/\gamma_2)_{x_1=0.2113} = 0.5773(B - D/3) = 0.298 \quad \ldots\ldots(41)$$

The heats of mixing data of Bosjnakovic and Grumbt [15] are used to obtain the following expressions of relative partial molal enthalpies,

$$L_1^\circ = (L_1)_{x_1=0} = -13726 + 38.188\ T \quad \ldots\ldots(42)$$

$$L_2^\circ = (L_2)_{x_1=1} = -3050 + 9.288\ T \quad \ldots\ldots(43)$$

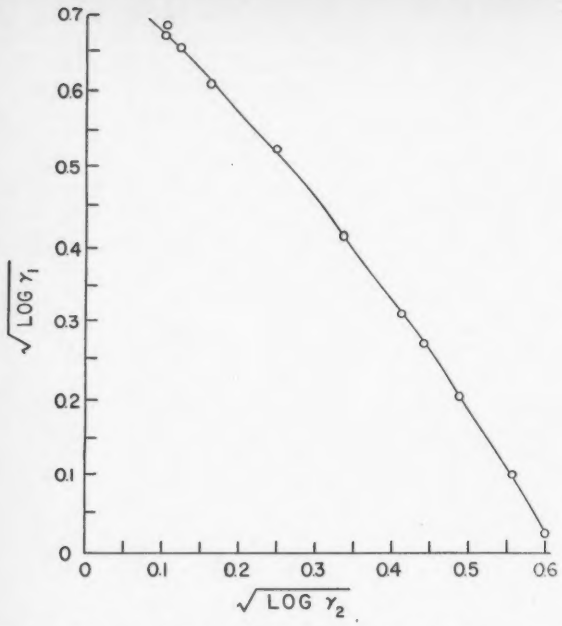

Figure 3—Plot of $(\log \gamma_1)^{0.5}$ vs. $(\log \gamma_2)^{0.5}$ for the system ethanol-water at 74.79°C. [21].

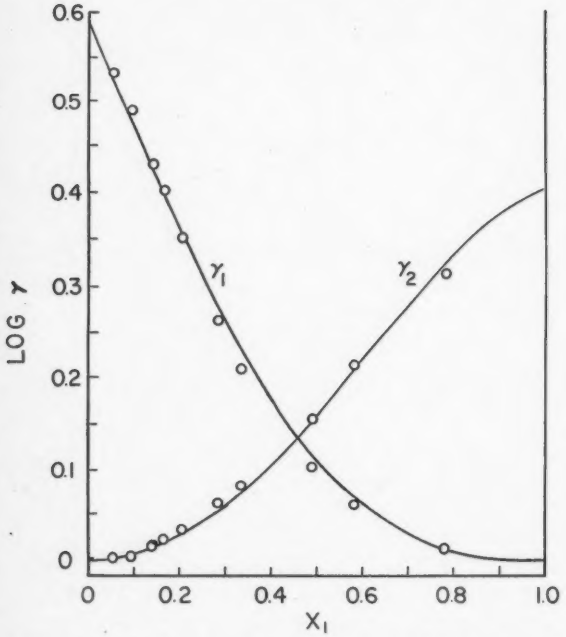

Figure 5—Calculated activity coefficients and experimental values for the system ethanol-water at 25°C.
O experimental [23]
Calculated

$$(L_1)_{x_1=0.2113} = -859.8 + 2.950\,T \quad \ldots\ldots(44)$$

$$(L_2)_{x_1=0.2113} = -1238.7 + 3.400\,T \quad \ldots\ldots(45)$$

It should be mentioned that these expressions are obtained by giving emphasis to low temperature values.

Substituting Equation (42) into Equation (12) and integrating

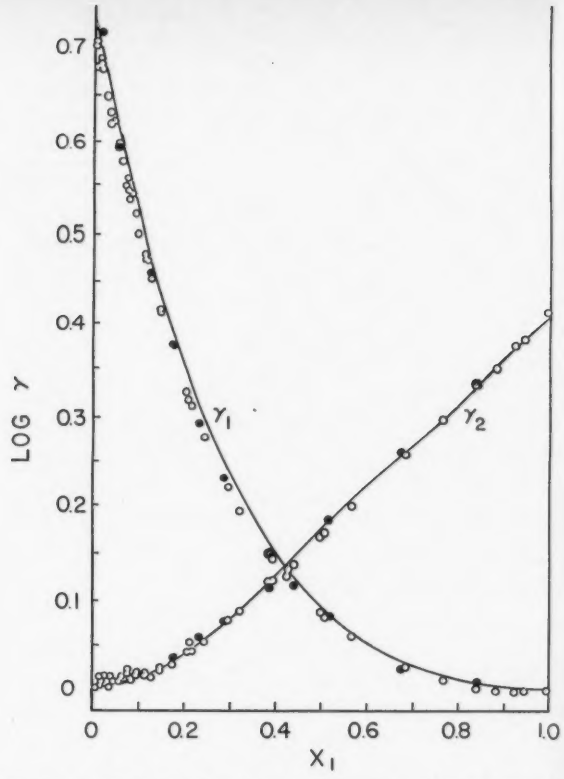

Figure 4—Calculated activity coefficients and experimental values for the system ethanol-water at 1 atm.
— Calculated
O experimental [11]
● experimental [16]

$$(\log \gamma_1)_{x_1=0} = B - C + D = 58.198 - 2999.3/T - 19.217 \log T \quad \ldots\ldots(46)$$

the integration constant is determined from Equation (39). Similarly,

$$(\log \gamma_2)_{x_1=1} = B + C + D = 14.204 - 666.4/T - 4.674 \log T \quad \ldots\ldots(47)$$

and

$$\log (\gamma_1/\gamma_2)_{x_1=0.2113} = 0.5773\,(B - D/3) = -0.4925 + 74.935/T + 0.2264 \log T \quad \ldots\ldots(48)$$

The quantities B, C and D, as expressed by Equation (32), may be determined from these expressions. Therefore,

$$\log \gamma_1 = (1 - x_1^2)\,[8.410 - 360.9/T - 2.692 \log T + (-22.00 + 1166.4/T + 7.272 \log T)\,(4x_1 - 1) + (27.79 - 1472.0/T - 9.253 \log T)\,(2x_1 - 1)\,(6x_1 - 1)] \quad \ldots\ldots(49a)$$

and

$$\log \gamma_2 = x_1^2\,[8.410 - 360.9/T - 2.692 \log T + (-22.00 + 1166.4/T + 7.272 \log T)\,(4x_1 - 3) + (27.79 - 1472.0/T - 9.253 \log T)\,(2x_1 - 1)\,(6x_1 - 5)] \quad \ldots\ldots(49b)$$

Equation (49) is used to calculate the liquid activity coefficients for the system ethanol-water at 1 atm. and 25°C. The calculated values are compared with the experimental data in Figures 4 and 5. In both cases, good agreement is obtained.

Nomenclature

A, B = van Laar constants (Equations 2, 3, 7 and 38)
B, C, D = constants of the Redlich-Kister equation (Equations 31, 32, 39, 40, 41, 46, 47 and 48)
a^* = activity of a component (Equation 8)
a, b, c, d, e, f, g, h, i, j, k, l, m, r = constants
a′, b′, c′ = constants
a″, b″, c″, d″ = constants
$a(n_1, n_2)$, $b(n_1, n_2)$, $c(n_1, n_2)$ = functions of n_1 and n_2 only (Equation 16)
$a'(n_1, n_2)$, $b'(n_1, n_2)$, $c'(n_1, n_2)$ = functions of n_1 and n_2 only (Equation 17)
G = molal free energy of pure component
ΔG^E = excess free energy, calories per gram mole
h_{soln} = enthalpy of solution
H = molal enthalpy of pure component
$\overline{H}$ = partial molal enthalpy
ΔH^E = excess enthalpy of mixing, calories per gram mole
ΔH^M = heat of mixing, calories per gram mole
ΔH_N^M = heat of mixing for N moles of mixture
L = relative partial molar enthalpy, calories per gram mole
L° = relative partial molar enthalpy at infinite dilution, calories per gram mole
n = number of moles (Equations 14 - 17)
p = total pressure
p° = vapor pressure of pure component
R = gas constant
T = absolute temperature
x = liquid phase composition, mole fraction
α = relative volatility = $y_1 x_2 / y_2 x_1$
μ = chemical potential
γ = liquid activity coefficient
Subscripts 1, 2 = low and high boiling components, respectively.

Acknowledgment

The author is indebted to the National Research Council of Canada for financial support.

References

(1) Carlson, H. C., and Colburn, A. P., Ind. Eng. Chem. **34**, 581 (1942).
(2) White, R. R., Trans. A.I.Ch.E., **41**, 539 (1945).
(3) Li, Y.-M., and Coull, James, J. Inst. Petroleum **34**, 692 (1948).
(4) Robinson, C. S., and Gilliland, E. R., "Elements of fractional distillation", 4th ed. pp. 58-59, McGraw-Hill, New York, 1950.
(5) Yu, K. T., and Coull, James, Chem. Eng. Progress, Symposium Series **48**, No. 2, 38 (1952).
(6) Wohl, K., Trans. A.I.Ch.E., **42**, 215 (1946).
(7) Redlich, Otto and Kister, A. T., Ind. Eng. Chem. **40**, 345 (1948).
(8) Benedict, M., Johnson, C. A., Solomon, E., and Rubin, S., Trans. A.I.Ch.E., **41**, 371 (1945).
(9) Yang, C. P., and van Winkle, Matthew, Ind. Eng. Chem. **47**, 293 (1955).
(10) Eduljee, H. E., Kumarkrishnarao, V. N., and Rao, M. N., Ind. Eng. Chem. Data Series **3**, 44 (1958).
(11) Otsuki, Henry, and Williams, F. C., Chem. Eng. Progress, Symposium Series **49**, No. 6, 55 (1953.
(12) Nord, Melvin; Chem. Eng. Progress, Symposium Series **48**, No. 3, 55 (1952).
(13) Hipkin, Howard, and Myers, H. S., Ind. Eng. Chem. **46**, 2524 (1954).
(14) Myers, H. S., Ind. Eng. Chem. **47**, 2215 (1955); **48**, 1104 (1956).
(15) Bosjnakovic, F., and Grumbt, J. A., Forsch. Gebiete Ingenieurw., **2**, 421 (1931).
(16) Jones, C. A., Schoenborn, E. M., and Colburn, A. P., Ind. Eng. Chem. **35**, 666 (1943).
(17) Colburn, A. P., and Pigford, R. L., Appeared in Perry, J.H. (ed.): "Chemical Engineers' Handbook" 3rd ed. pp. 530-1, McGraw-Hill, New York, 1950.
(18) Cheesman, G. H., and Ladner, W. R., Proc. Roy. Soc. (London) **A229**, 387 (1955).
(19) Scatchard, George, and Ticknor, L. B., J. Am. Chem. Soc. **74**, 3724 (1952).
(20) Adcock, D. S., and McGlashan, M. L., Proc. Roy. Soc. (London) **A226**, 266 (1954).
(21) Wrewski, M. S., J. Russ. Phys. Chem. Soc. **42**, 1 (1910) Experimental data are taken from compilation of Chu, J. C. et al. "Vapor-Liquid Equilibrium Data", p. 277, J. W. Edwards, Publisher, Inc. Ann Arbor, Michigan (1956).
(22) Broughton, D. B., and Brearley, C. S., Ind. Eng. Chem. **47**, 838 (1955).
(23) Dobson, H. J. E., J. Chem. Soc. **127**, 2866 (1925).

* * *

Removal of a Mist in a Fluidized Bed[1]

D. S. SCOTT[2] and D. A. GUTHRIE[3]

The removal of droplets from a dioctyl phthalate mist by a fluidized bed of silica gel was studied. The mist used had a narrow range of droplet diameters, which averaged 0.87 microns in size. Silica gel particles were in the range of −150 mesh to +200 mesh.

It was found that removal efficiencies were only slightly affected by a 50% change in inlet mist concentration, or by a 300% variation in depth of the fluidized bed. Collection efficiencies varied from about 90% at low superficial gas velocities to 70% at high velocities.

It is shown from these results that collection is primarily by particle diffusion. Results can be correlated in terms of equations for mass transfer in fluidized beds. The possible uses of a fluidized bed as a collecting device are discussed.

THE use of a fluidized bed to remove droplets from mists has been reported only once in the literature (1). Meissner and Mickley in this work used such a bed to remove droplets in the size range of 2-10 microns diameter from a sulphuric acid mist. Over the range of conditions used, it was found that the removal efficiency was independent of mist concentration, and increased somewhat as bed weight increased. Efficiencies increased with increased superficial velocity through the bed. Preliminary work with ammonium nitrate dust was also reported, and the above results were confirmed with the exception of the effect of velocity on the degree of removal.

From the results obtained by Meissner and Mickley, the fluidized bed seems to offer a number of advantages as an aerosol collection device. It would have a nearly constant pressure drop, independent of the age of the bed. Collection efficiencies can be well over 90%, and these have also been found to be independent of bed age. Variations in inlet mist concentrations seem to have no effect on collection performance over wide ranges, and variations in the level of solids in the bed are of minor importance also.

Fluidized beds of porous solids (for example, spent cracking catalyst, activated alumina, and silica gel) have been found to be capable of absorbing up to 5% of their own weight of a liquid before bed agglomeration due to saturation causes any effect on collection efficiency. This was also true of the collection of ammonium nitrate dust.

[1]*Manuscript received May 30, 1959.*
[2]*Associate Professor, Dept. of Chemical Engineering, The University of British Columbia, Vancouver, B.C.*
[3]*Hooker Electrochemical Limited, North Vancouver, B.C.*
Contribution from the Department of Chemical Engineering, The University of British Columbia, Vancouver, B.C.

Such a bed has no limitations with respect to temperature. It could be operated continuously, and the bed solids regenerated and the aerosol material recovered or destroyed in an auxiliary unit.

The most serious limitation would seem to be that this device is primarily suitable for mists, although it appears that it could be expected to perform equally as well for some dusts. Pressure drops through the bed are about 6-8 inches of water, which is no greater than that through other devices of comparable efficiency.

In the present work, the performance of a fluidized bed of silica gel particles was investigated for the removal of a homogeneous dioctyl phthalate mist. The average droplet diameter in all runs was 0.87 microns, with all particles in the size range of 0.5 to 1.1 microns.

A sensitive colorimetric method was developed for the analysis of dioctyl phthalate. This was necessary because it was found that traces of silica gel dust in samples were sufficient to cause erratic results when analysis by ultraviolet absorption was attempted.

Theory

The mechanism of collection in a fluidized bed could be easily visualized as occurring either by impingement due to inertial effects, or by droplet diffusion, or a combination of both. The ranges of conditions in which these mechanisms give an effective contribution to the collection efficiency have been investigated by Albrecht (2), Langmuir (3), Ramskill and Anderson (4) and Gillespie (5), in connection with the theory of aerosol filtration. It has been shown by Ramskill and Anderson (4), that there is a certain particle size for each set of filtration conditions which will result in a minimum collection efficiency; this efficiency increases as particle size is either increased or decreased. For many combinations of filter characteristics this "most difficult" size lies in the range of 0.2-2.0 microns diameter. Gillespie(5), shows further that correlation of collection efficiencies with filter characteristics is made much more difficult by the fact that many interceptions of aerosol particles by collecting surfaces are non-effective, particularly at high velocities.

Meissner and Mickley believed the major collection mechanism in their work was due to collision effects, although the small effect of bed depth could not be adequately explained on that basis. Their results were represented by an equation of the form

$$-\log \frac{C_2}{C_1} = kV_oW^n \qquad (1)$$

where n varied from 0.16 to 0.34. This equation indicates the dependence of collection efficiency on gas velocity,

and on the number of collecting particles. A sulphuric acid mist was used in this work, having an average droplet diameter from 2-6 microns. The collecting solids were of various size distributions.

The inertial effect has been shown to be proportional to Dm^2 Vo/Dp, or alternatively, the separation number U_t Vo/g Dp can be used to describe a "target efficiency" [2,3]. An estimate of this value for the results of Meissner and Mickley indicates that for all the bed solids used the inertial effect is large, and therefore should constitute the primary collection mechanism. The increase in collection efficiency with increased gas velocity and decreased size of collecting particle, which was observed in this work, also confirms this assumption.

If collection occurred by a diffusion mechanism, the simplest approach would be to represent the process by an equation of the same type as those applied to mass transfer operations. For uniformly sized droplets, the decrease in mass concentration would be proportional to the number of droplets collected. The driving force for droplet diffusion would be the mass concentration, inasmuch as the process is not reversible. The mass transfer equation could then be written

$$-\,dc = \frac{k_p}{V_o} A_p \,.\, Cdz$$

where A_p is the collecting surface per unit volume of bed solids, and k_p is a "mass transfer" coefficient for particle diffusion. The incremental bed depth dz can be expressed as $dW/\rho_B S$, where ρ_B is the bulk density of the bed, and S its cross sectional area. Further, A_p/ρ_B can be expressed as Am, the collecting surface per unit weight of solids. Making these substitutions:

$$-\,dc = \frac{k_p A_m}{V_o} CdW.$$

Integrating

$$\ln \frac{C_1}{C_2} = \int \frac{k_p Am}{V_o} dW \qquad (2)$$

The dependence of the mass transfer coefficient and effective collecting surface on bed depth, as well as on variations in the degree of fluidization are difficult to estimate. If the usual assumption is made that the mass transfer coefficient depends primarily on the flow rate for a given system then the above equation can be integrated. It is interesting to note that if a diffusional process is the principal collecting mechanism, the collection efficiency should decrease as the flow rate through the bed is increased. This feature has been discussed by Ramskill and Anderson [4].

Experimental Apparatus

The mist used was generated in a Lamer-Sinclair homogeneous aerosol generator, shown in Figure 1, using dioctyl phthalate as the liquid. A portion of dry filtered air was metered and passed through a nucleation chamber, A, where nuclei were supplied from a heated coil freshly coated with pure sodium chloride. The bulk of the air was metered, passed through a preheater, B, and into the vaporizer, C, containing the dioctyl phthalate. The mixed vapor and nuclei entered the reheater, D, and then were slowly cooled in the double walled chimney, E.

A portion of the mist laden air stream could be bled off at F, or dilution air could be added at G before the mist entered the fluidized bed, H. The fluidized bed used was constructed of a 2-inch inside diameter glass tube fitted with an outlet cyclone and collector for dust removal. Bed solids used were −150 + 200 mesh silica gel supported on a 200 mesh screen.

Sampling of the inlet or outlet mist was done by passing the entire flow for a suitable period of time through a filter holder and wet test meter. The filter used was a Millipore MF aerosol filter.

A negligible amount of mist was collected in the upper empty part of the column and the cyclone. One filter was found to be adequate to collect all the mist in a sample of air.

Particle size of the aerosol generated was determined periodically by collection of samples on coated slides, and microscopic examination.

Analaysis of Dioctyl Phthalate.

The analytical method was based on the reaction between organic esters and hydroxylamine in alkaline solutions to form a hydroxamic acid. The hydroxamic acids give colored complexes with metals, notably with iron compounds. This method was first proposed as a quantitative method by Hill [6,7], for esters of fatty acids, and was applied in the present work to aromatic esters. Subsequent to this work a more detailed investigation of the reaction was published by Goddu, LeBlanc and Wright [8].

An aerosol sample giving 0.1 to 1.5 mg. of dioctyl phthalate was collected on a Millipore filter. This was extracted with 10 ml. of petroleum ether, to the solution was added 0.3 ml. of a 2.5% solution of NaOH in 95% ethanol. The mixture was evaporated to dryness on a water bath at 67°C., removed and cooled to 25°C., and 10 ml. of a solution of ferric perchlorate and perchloric acid in ethanol added. After standing for a few minutes, the transmittancy was compared to a blank at 540 mμ.

Amounts of dioctyl phthalate could be determined with an accuracy of better than ±0.02 mg. by this method. Typical calibration charts for three organic esters are shown in Figure 2.

Results and Discussion

The mist used in all runs had an average particle diameter of 0.87 microns, with about 95% of all particles lying in the range of 0.60 to 1.1 microns. Experimental efficiencies were measured by averaging several determinations of both inlet and outlet concentrations.

In Figure 3 the effect of inlet mist concentration on removal efficiency is shown. Although the range of concentrations is not wide, it is apparent that a 50% change in inlet mist loading has no effect on the collection efficiency observed. This agrees with the results reported previously [1].

The variation of collection efficiency with superficial velocity is shown in two typical plots in Figures 4 and 5, the bed depth used in one case being double that in the other. Examination of these data shows that the effect of bed weight on mist removal is small, and in this work was less than the experimental error in determining efficiencies. Therefore, the dependence of the efficiency, C_2/C_1, on bed depth indicated in either Equations (1) or (2) does not appear to be present, again in agreement with previous work [1]. Several tests at varying velocities were carried out with the inlet screen in place but with the bed empty. About 15% to 20% of the mist was collected in passage through the inlet section and screen. However, as these are integral parts of the fluidized bed, no attempt was made to correct efficiencies by this amount.

It can be seen from Figures 4 and 5 that the removal efficiency decreases slowly as the superficial gas velocity in the bed increases. The opposite effect was found by Meissner and Mickley. If collection was primarily by a collision mechanism due to inertial forces, it would be

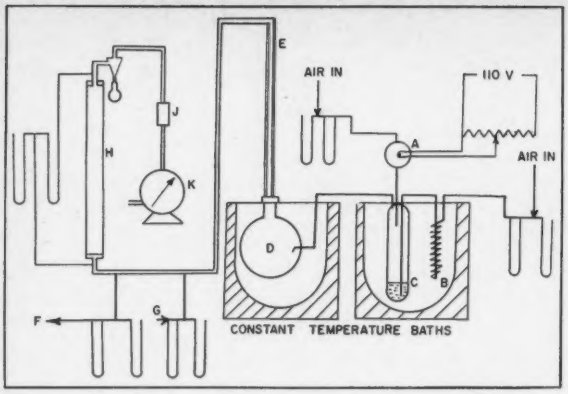

Figure 1—Sketch of the apparatus. A. nucleation coil. B. preheater. C. vaporizer. D. reheater. E. cooling chimney. F. bleed-off line. G. dilution line. H. fluidized bed. J. mist samples. K. gas meter.

expected that efficiencies should improve with an increase in the gas velocity through the bed. However, if collection is by a diffusional mechanism due to Brownian motion, then the observed effect of velocity is to be expected.

An estimate of the relative importance of inertial collection can be found by calculating the "separation number", $U_t Vo/gD_p$, for the droplets and bed particles used, and determining the "target efficiency" which might be expected for a single bed particle by use of the chart prepared by Langmuir and Blodgett [3]. The value of the separation number for the work presented here can be expressed as 0.00028 Vo. It is apparent that for the range of values of Vo given that the separation number is well below the value of about 0.04, the theoretical limit below which collection by impingement on a single sphere would be zero. Even allowing for the dissimilarity in behavior between single spheres and a fluidized bed of spheres, it is indicated that collection by inertial methods cannot be the major mechanism, and is unlikely to contribute even a significant fraction to the total collected. A comparison of the magnitude of the separation numbers shows that inertial effects in the work of Meissner and Mickley were of the order of 200-500 times as great as in these experiments.

In considering a diffusional mechanism, as expressed by Equation (2), the dependence of the mass transfer coefficient, kp, on the gas mass velocity can be estimated from correlations for fluidized beds. Use of the equations proposed by Chu, Kalil and Wetteroth [9] would indicate that kp should be proportional to $Vo^{0.22}$ for the range of Reynolds numbers covered in these tests.

This would imply that the ratio, ln C_1/C_2, should vary as $1/V^{0.78}$. The results given in Figure 4 are plotted in this way in Figure 6 to show the degree of correlation obtained. While the resulting plot is satisfactory, the data are not sufficiently extensive to confirm a value of 0.78 as the most suitable exponent. The point where fluidization is developed is shown very clearly by a plot of this type. Further results have indicated a similar transition at high superficial velocities when "slugging" occurs in the bed.

Venturi Collector—As a matter of interest, and to check the ability to predict collection mechanism by use of the relations for inertial effect, another type of device was used in which inertial effects would be expected to be much more significant. This consisted of a small glass venturi tube set over the inlet pipe of the fluidized bed so that all the gas flow was through the venturi, which

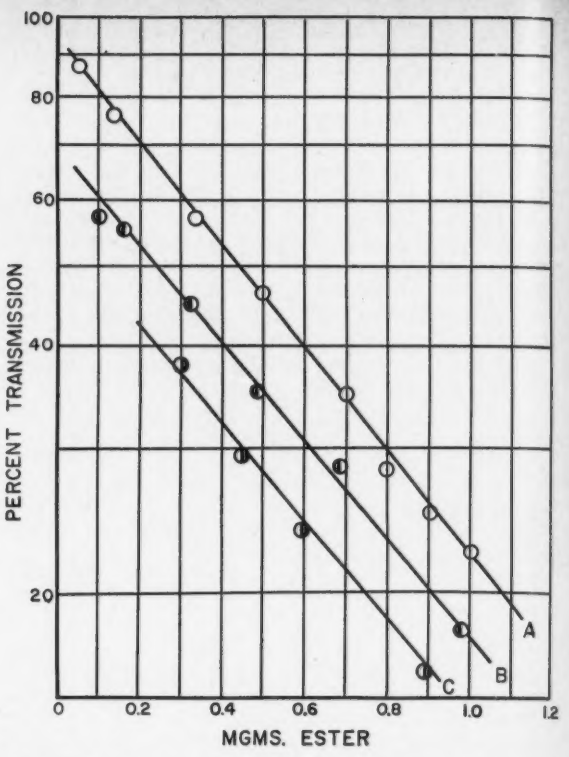

Figure 2 — Analysis of mist concentrations. A. dioctyl phthalate. B. n-butyl phthalate. C. ethyl benzoate.

was in turn surrounded by the bed of silica gel particles. Two holes were made in the throat of the venturi through which bed solids were aspirated. The gas-solid mixture left the venturi above the solids level so that the solids fell back to the bed. In such a device, a high relative velocity between mist droplets and solid collecting particles can be obtained at the throat of the venturi.

Throat velocities were varied from about 300 cm./sec. to 3000 cm./sec. Solids aspiration was such that about 10^3 mist droplets were present for each solid collecting particle, except at the highest velocities. Over the above range of velocities the collection efficiency increased slightly with throat velocity, from about 37% to 42%. According to Langmuir [3], collection on a single sphere over this range should vary from about 10% to 58%. In view of the assumptions in the theory, and its application to this case, the agreement is surprisingly good, and illustrates the point that one can predict qualitatively the nature of the collection mechanism in any particular device by this means.

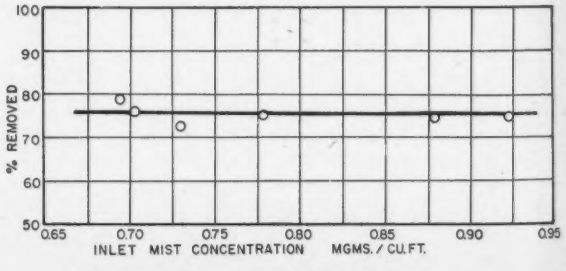

Figure 3—Effect of inlet mist concentration.

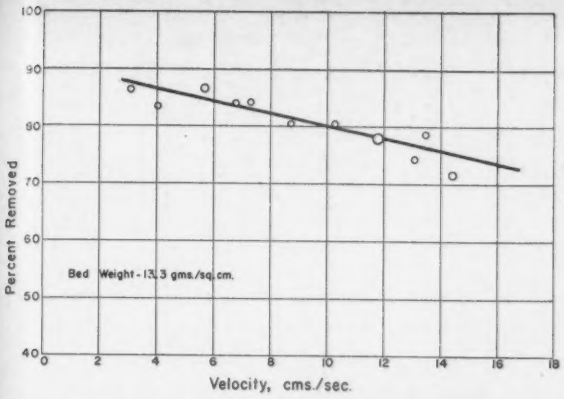

Figure 4—Variation of removal efficiency with superficial gas velocity through bed.

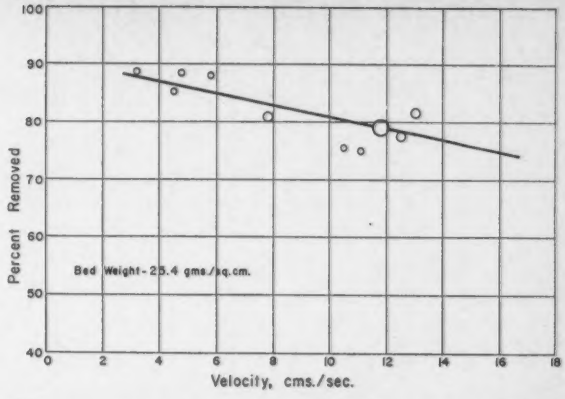

Figure 5—Variation of removal efficiency with superficial gas velocity through bed.

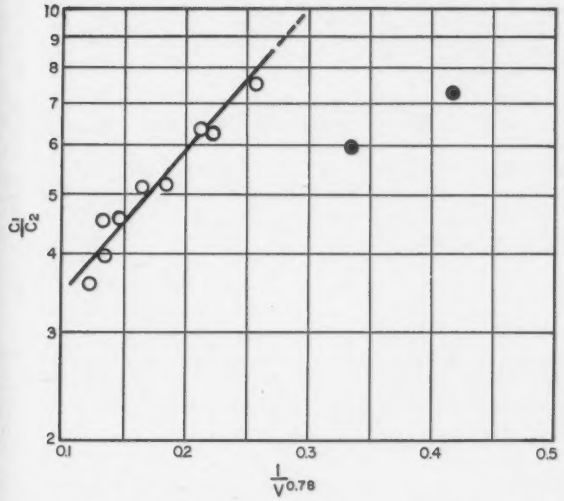

Figure 6—Correlation of removal efficiencies and superficial velocities, bed wt. 13.3 gm./sq.cm. O fluidized bed. ● packed bed.

Summary

A fluidized bed is a fairly efficient device for removing mist droplets in a size range which usually presents serious collection difficulties, that is from 0.5 to 1.5 microns diameter. The collection mechanism appears to be primarily due to diffusional effects. Collection efficiencies are not affected seriously by variations in inlet mist loadings, bed age, or the amount of bed solids, within fairly wide limits.

It is possible to predict qualitatively from theory, collection behavior of a fluidized bed as gas flow increases. Additional data would make this prediction quantitative.

It is very possible that fluidized beds could have applications as mist or dust collecting devices, particularly for those droplet sizes usually considered to form the most stable aerosols.

Nomenclature

A_m = collecting surface per unit weight of fluidized solids.
A_p = collecting surface per unit volume of fluidized solids.
C = Mist concentration, weight per unit volume.
D_m = Diameter of Mist droplet.
D_p = Diameter of the collecting solid.
g = gravitational constant.
k, k_p = constants.
S = cross sectional area of fluidized bed.
U_t = terminal velocity of a mist droplet.
V_o = superficial gas velocity in a fluidized bed.
W = weight of bed solids per unit cross sectional area of bed.
Z = depth of fluid bed.
ρ_B = bulk density of bed solids.
ρ = density of mist droplet.

Acknowledgments

The authors are grateful for the assistance of R. Rye in developing the analytical methods described. This investigation was supported by grants of the Defense Research Board, and their assistance is gratefully acknowledged. Dr. Guthrie also wishes to thank the Consolidated Mining and Smelting Company for the grant of a scholarship.

References

(1) Meissner, H. P., and Mickley, H. S., Ind. Eng. Chem. **41**, 1238 (1949).
(2) Albrecht, Physik Z., **32**, 48 (1931).
(3) Langmuir, I., and Blodgett, K. B., U.S. Department of Commerce, Office Tech. Services PB27565.
(4) Ramskill, E. A., and Anderson, W. L., J. Coll. Science, **6**, 416 (1951).
(5) Gillespie, T., J. Coll. Science, **10**, 266 (1955).
(6) Hill, U. T., Ind. Eng. Chem., Anal. Ed. **18**, 317 (1946).
(7) Hill, U. T., Ind. Eng. Chem., Anal. Ed. **19**, 932 (1947).
(8) Goddu, R. F., LeBlanc, N. F., and Wright, C. M., Anal. Chem. **27**, 1251 (1955).
(9) Chu, J. C., Kalil, J., and Wetteroth, W. A., Chem.)ng. Prog. **49**, 141 (1953).

★ ★ ★

NOTE TO THE EDITOR

Fluidization in Beds of Rice and Wheat

LIANG-TSENG FAN and CHARLES J. SWARTZ

Engineering Experiment Station, Kansas State University, Manhattan, Kansas.

When a fluid flowing upward is admitted into the bottom of a bed of a granular material, a pressure drop through the bed will result. This pressure drop will increase with increase in fluid rate until a point of equilibrium is reached at which the pressure drop through the bed multiplied by the cross-sectional area of the column is equal to the weight of the bed and at which the fluid-like motion of the bed commences [1,2]. The fluid velocity corresponding to this point is defined as onset or minimum fluidization velocity of the bed.

A new generalized correlation, which relates such factors as fluid viscosity, fluid density, particle density, shape factor of particle and void fraction at onset point to the onset velocity of fluidization, was recently proposed by Leva et al [1]. The data used in formulating this correlation were mostly obtained from experiments using metallic or mineral solid particles with small diameters. The validity of the correlation on fluidization of cereal grains, which mostly consist of relatively coarse granules with characteristics quite different from metallic and mineral particles, has never been tested. It is, however, known that when heat is being transferred from the column wall into the bed, fluidization onset is accompanied by a sharp increase in heat transfer coefficients [3]. Klassen and Gishler [4] recently published the results of their fluidization heat transfer study which includes such cereals as rice and wheat. Since their data include runs made during the packed range, the plot of heat transfer coefficients against the flow rate should show a breaking point at the onset of fluidization. Application of the generalized correlation of Leva, et al [1] to the fluidization conditions of Klassen and Gishler [4] yields the fluidization onset velocities of 490 lb./ft.²–hr. and 700 lb./ft.²–hr. for rice and wheat respectively.

In adapting the generalized correlation to beds of particles with irregular shape, it is necessary to have some means of determining an average diameter of the particles. The recommended procedure [1,3] for finding the diameter of narrow cut solids is to take the geometrical average of adjacent sieve openings d_1 and d_2 [1]. However, the sizes of relatively large grains such as rice and wheat are generally defined and measured in terms of three dimensions, i.e. length, width and thickness [5]. Comparison of the results of calculations using the square root of the product of two smallest dimensions ($\sqrt{\text{width x thickness}}$) gave results which are mentioned above and are closest to the experimental results of approximately 500 lb./ft.²-hr. for rice and approximately 700 lb./ft. for wheat.

To further verify the generality of the finding, several sets of experiments were conducted using pyrex glass pipes of various sizes as the fluidizing columns. The conditions and results of the experiments are summarized in Table 1 and Table 2 respectively. In no cases did the deviation of the calculated values–using the geometrical mean of width and thickness of the grains as the mean diameter of the grains–from the experimental data exceed 5%.

The results of the present work clearly indicate that the generalized correlation proposed by Leva, et al. [1], for the onset velocity of fluidization may be applied to fluidization of rice and wheat by gas when the proper dimensions of the grain (square root of product of two dimensions, i.e. width and thickness) are used in estimating the mean diameter of the particle.

TABLE 1

CONDITIONS OF EXPERIMENTS

Run No.	Temp. °F	Press. atm.	Fluid	Particle	Particle Density lb./ft.³	Particle Size in. x in. x in.	Column Diameter in.
1	70.0	1.0	air	rice	91.4	0.205 x 0.0900 x 0.0660	4
2	76.0	1.8	air	wheat	77.4	0.241 x 0.100 x 0.105	1
3	73.1	2.2	air	wheat	77.4	0.241 x 0.100 x 0.105	1
4	70.0	2.2	air	wheat	74.3	0.229 x 0.0958 x 0.0924	1
5	70.0	2.5	air	wheat	74.3	0.229 x 0.0958 x 0.0924	1

TABLE 2

RESULTS OF EXPERIMENTS

ONSET VELOCITY

Run No.	Calculated lb./hr.-ft.²	Observed lb./hr.-ft.²	Deviation %
1	627	646	+3.03
2	900	870	−3.33
3	935	920	−1.60
4	930	890	−4.30
5	925	900	−2.70

References

(1) Leva, M., Shirai, T., and Wen, C. Y., Genie Chimique, **73**, 33 (1956).
(2) Wen, C. Y., and Fan, L. T., Chemical Engineering, **64**, No. 7, 254 (1957).
(3) Leva, M., Weintraub, M., Grammer, M., Pollchik, M., and Storch, H. H., U.S. Bureau of Mines, Bulletin 504, p. 59 (1951).
(4) Klassen, J., and Gishler, P. E., Can. J. of Chemical Eng. **35**, 12 (1957).
(5) Jolly, L. J., and Stanton, J. E., J. App. Chem. **2**, 262 (1952).

★ ★ ★

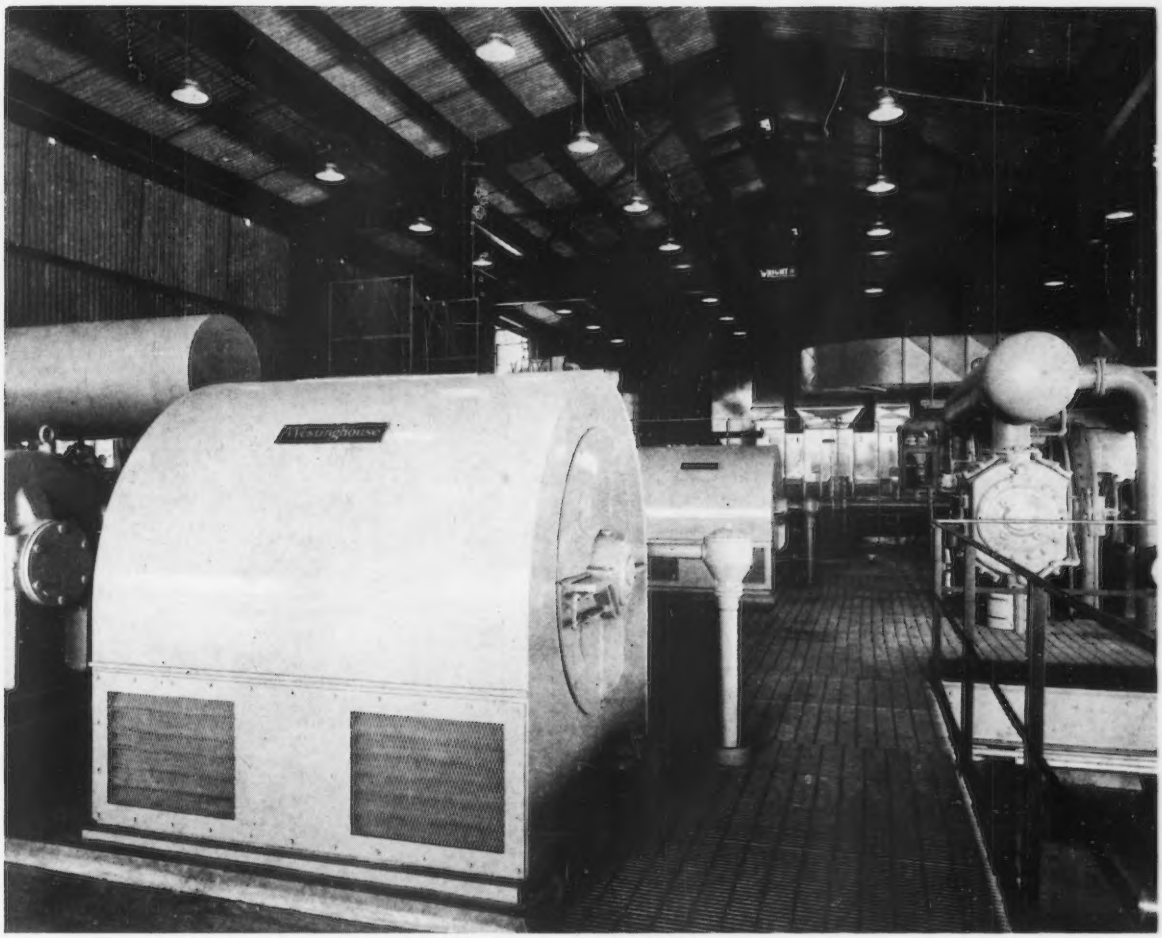

MADE IN CANADA

With the opening of Imperial Oil's new Petrochemical Plant in Sarnia a number of chemicals now imported will be made in Canada.

Here, as in noteworthy engineering works everywhere in Canada, electrical equipment bearing the Westinghouse name is found.

For instance, the largest high speed bracket type machine ever built, a 7500 horsepower induction motor was built by Canadian Westinghouse for Canadian Bechtel Limited, to drive a refrigeration compressor at Imperial Oil's Sarnia Petrochemical Plant.

A similar 6,000 horsepower Westinghouse unit drives a gas compressor at this plant to liquefy product gases from the cracking operation.

Whether your requirements are large and complicated electrical systems or standard units from stock, the engineering and the service behind the name of Westinghouse add meaning to the phrase "Buy Canadian and Buy Quality".

CANADIAN WESTINGHOUSE COMPANY LIMITED, HAMILTON

YOU CAN BE SURE... IF IT'S Westinghouse

58D150

"Cigarette foil and bridge railings. Everyone's using aluminum. Why not in our products?"

Foil packaging that is flexible, lightproof and moisture-proof. Bridge railings that are strong, rustproof and corrosion-resistant. There seems no end to the ways advantage is being taken of aluminum's remarkable combination of qualities. Its uses continue to grow with the development of new alloys, improved fabricating and welding techniques and a growing consumer demand.

PERHAPS ALCAN ALUMINUM AND ALCAN "KNOW HOW" CAN HELP YOU IN YOUR BUSINESS . . .

ALCAN are the people to see about everything concerning aluminum. They are leaders in its development and set its standards of quality. ALCAN has over fifty years' experience in aluminum and is the major source in Canada for sheet, wire, rod, bar, foil, extrusion, castings, and ingot.

ALUMINUM COMPANY OF CANADA, LIMITED

An ALUMINIUM LIMITED Company

Quebec • Montreal • Ottawa • Toronto • Hamilton • Windsor • Winnipeg • Calgary • Vancouver

ALCAN

NOTE TO THE EDITOR

Fluidization in Beds of Rice and Wheat

LIANG-TSENG FAN and CHARLES J. SWARTZ

Engineering Experiment Station, Kansas State University, Manhattan, Kansas.

When a fluid flowing upward is admitted into the bottom of a bed of a granular material, a pressure drop through the bed will result. This pressure drop will increase with increase in fluid rate until a point of equilibrium is reached at which the pressure drop through the bed multiplied by the cross-sectional area of the column is equal to the weight of the bed and at which the fluid-like motion of the bed commences [1,2]. The fluid velocity corresponding to this point is defined as onset or minimum fluidization velocity of the bed.

A new generalized correlation, which relates such factors as fluid viscosity, fluid density, particle density, shape factor of particle and void fraction at onset point to the onset velocity of fluidization, was recently proposed by Leva et al [1]. The data used in formulating this correlation were mostly obtained from experiments using metallic or mineral solid particles with small diameters. The validity of the correlation on fluidization of cereal grains, which mostly consist of relatively coarse granules with characteristics quite different from metallic and mineral particles, has never been tested. It is, however, known that when heat is being transferred from the column wall into the bed, fluidization onset is accompanied by a sharp increase in heat transfer coefficients [3]. Klassen and Gishler [4] recently published the results of their fluidization heat transfer study which includes such cereals as rice and wheat. Since their data include runs made during the packed range, the plot of heat transfer coefficients against the flow rate should show a breaking point at the onset of fluidization. Application of the generalized correlation of Leva, et al [1] to the fluidization conditions of Klassen and Gishler [4] yields the fluidization onset velocities of 490 lb./ft.^{2}–hr. and 700 lb./ft.^{2}–hr. for rice and wheat respectively.

In adapting the generalized correlation to beds of particles with irregular shape, it is necessary to have some means of determining an average diameter of the particles. The recommended procedure [1,3] for finding the diameter of narrow cut solids is to take the geometrical average of adjacent sieve openings d_1 and d_2 [1]. However, the sizes of relatively large grains such as rice and wheat are generally defined and measured in terms of three dimensions, i.e. length, width and thickness [5]. Comparison of the results of calculations using the square root of the product of two smallest dimensions ($\sqrt{\text{width} \times \text{thickness}}$) gave results which are mentioned above and are closest to the experimental results of approximately 500 lb./ft.^{2}-hr. for rice and approximately 700 lb./ft. for wheat.

To further verify the generality of the finding, several sets of experiments were conducted using pyrex glass pipes of various sizes as the fluidizing columns. The conditions and results of the experiments are summarized in Table 1 and Table 2 respectively. In no cases did the deviation of the calculated values—using the geometrical mean of width and thickness of the grains as the mean diameter of the grains—from the experimental data exceed 5%.

The results of the present work clearly indicate that the generalized correlation proposed by Leva, et al. [1], for the onset velocity of fluidization may be applied to fluidization of rice and wheat by gas when the proper dimensions of the grain (square root of product of two dimensions, i.e. width and thickness) are used in estimating the mean diameter of the particle.

TABLE 1

CONDITIONS OF EXPERIMENTS

Run No.	Temp. °F	Press. atm.	Fluid	Particle	Particle Density lb./ft.^{3}	Particle Size in. x in. x in.	Column Diameter in.
1	70.0	1.0	air	rice	91.4	0.205 x 0.0900 x 0.0660	4
2	76.0	1.8	air	wheat	77.4	0.241 x 0.100 x 0.105	1
3	73.1	2.2	air	wheat	77.4	0.241 x 0.100 x 0.105	1
4	70.0	2.2	air	wheat	74.3	0.229 x 0.0958 x 0.0924	1
5	70.0	2.5	air	wheat	74.3	0.229 x 0.0958 x 0.0924	1

TABLE 2

RESULTS OF EXPERIMENTS

ONSET VELOCITY

Run No.	Calculated lb./hr.-ft.^{2}	Observed lb./hr.-ft.^{2}	Deviation %
1	627	646	+3.03
2	900	870	−3.33
3	935	920	−1.60
4	930	890	−4.30
5	925	900	−2.70

References

(1) Leva, M., Shirai, T., and Wen, C. Y., Genie Chimique, **73**, 33 (1956).
(2) Wen, C. Y., and Fan, L. T., Chemical Engineering, **64**, No. 7, 254 (1957).
(3) Leva, M., Weintraub, M., Grammer, M., Pollchik, M., and Storch, H. H., U.S. Bureau of Mines, Bulletin 504, p. 59 (1951).
(4) Klassen, J., and Gishler, P. E., Can. J. of Chemical Eng. **35**, 12 (1957).
(5) Jolly, L. J., and Stanton, J. E., J. App. Chem. **2**, 262 (1952).

★ ★ ★